



**Anamet, inc** *Materials Engineering & Laboratory Testing*  
26102 EDEN LANDING ROAD, SUITE 3 • HAYWARD, CALIFORNIA 94545 • (510) 887-8811 • FAX (510) 887-8427

Report No. 5005.3434 C

November 6, 2018

**LABORATORY EVALUATION OF SAMPLES FROM THE  
BRAZED ALUMINUM PLATE-FIN HEAT EXCHANGER H-3059 INVOLVED IN  
THE JULY 27, 2016 FIRE AT ENTERPRISE PRODUCTS OPERATIONS,  
MOSS POINT, MS**

Customer Authorization: CSB-16-0030

Report To: U.S. Chemical Safety & Hazard Investigation  
Board  
Attn: William Hougland  
P.O. Box 25465  
Lakewood, CO 80205

---



**This report shall not be reproduced, except in full, without the written approval of Anamet.**



## CONTENTS

1.	INTRODUCTION .....	3
2.	SUMMARY OF RESULTS .....	8
3.	EVALUATION.....	9
3.1.	B Stream Inlet Nozzle Visual Examination .....	9
3.2.	B Stream Inlet Header Visual Examination.....	15
3.3.	B Stream Inlet Header Scanning Electron Microscopy (SEM) .....	15
3.4.	B Stream Inlet Header Metallography .....	15
3.5.	ACSR Sample S042-C Visual Examination.....	31
3.6.	ACSR Sample S042-C Metallography .....	31
3.7.	ACSR S042-B Visual Examination.....	47
3.8.	ACSR S042-B Scanning Electron Microscopy (SEM) .....	47
3.9.	ACSR Sample S042-B Metallography .....	48
3.10.	ACSR S042-D1 Visual Examination.....	61
3.11.	ACSR Sample S042-D1 Scanning Electron Microscopy (SEM) .....	62
3.12.	ACSR Sample S042-D1 Metallography .....	62
3.13.	ACSR Sample S042-D3 Visual Examination.....	80
3.14.	ACSR Sample S042-D3 Metallography .....	80
4.	DISCUSSION.....	85
5.	CONCLUSIONS.....	86



## 1. INTRODUCTION

Metallurgical evaluation was performed on samples of the A train cold side reboiler (ACSR) H-3059, from Enterprise Products Operations, LLC, Moss Point, MS. The subject brazed aluminum plate-fin heat exchanger was involved in the July 27, 2016 fire at the Enterprise gas processing plant. Visual examination of the site indicated heat damage was centered on the north side of the ACSR. Laboratory evaluations took place at Anamet, Inc. with participation by representatives of the CSB and interested parties. The samples examined included the B stream inlet nozzle and header, and portions of the ACSR stack that had been cut from the reboiler by Wagstaff, Inc. Work by Wagstaff was witnessed by the CSB and representatives of interested parties. The purpose of this metallurgical evaluation was to look for evidence of the initial breach in the ACSR pressure boundary and identify service related degradation that could provide information useful to service life assessment of brazed aluminum plate-fin heat exchangers.

Brazed aluminum plate-fin heat exchangers are used extensively in low-temperature applications such as the natural gas processing performed at the Enterprise facility. The components of a generalized brazed aluminum plate-fin heat exchanger are shown in Figure 1. Alternating layers of corrugated fins and parting sheets are joined by brazing; the outermost layers of fins are brazed to cap sheets. The edges of the fin and sheet stack (core) are sealed by brazed side bars and end bars. Heat is exchanged through the fins and parting sheets that separate two or more process streams directed through different layers of the exchanger. In addition to conducting heat, the fins are structural members of the core, serving to carry loads developed from the process pressure. The end bar and side bar configuration of each layer determines where the process stream of that layer enters or exits the stack. Semi-cylindrical headers welded over intentional gaps in the side bars or end bars direct process flow to and from the stack through nozzles that connect to process piping. Structural supports are welded to attachment plates that are welded to the cap sheets.

A photograph of the subject ACSR taken after the fire is shown in Figure 2, and a simplified drawing of the subject is shown in Figure 3. The ACSR was a two stream, single pass design built in 1998 by Altec International, now Chart Industries, in accordance with ASME Section XIII. The A stream (pass) entered the exchanger at the top and exited at the bottom. The B pass entered the exchanger at the bottom and exited at the top. As-built drawings of the ACSR indicated that fins, parting sheets, cap sheets, side bars, and end bars were 3003 aluminum alloy. The parting sheets and cap sheets were clad with 4004 aluminum braze alloy, and the entire 99 layer stack was vacuum brazed. The layer sequence, identified by pass, was: B, A, B, B, A, ... B, B, A, B, with layers numbered 1 through 99. Headers, nozzles, and attachment plates were 5083 aluminum alloy, joined by welding. Altec indicated the typical operating, design, and test pressures and temperatures listed in Table 1 applied to the ACSR.



Table 1  
Reported Temperatures and Pressures

		A Pass		B Pass	
		Inlet	Outlet	Inlet	Outlet
Typical Operating Pressure <sup>A</sup>	(psia)	957	952	477	476
Typical Operating Temperature <sup>A</sup>	(°F)	-36	-112.6	-112.6	-83.0
Design Temperature, max/min	(°F)	150/-200		150/-200	
Design Pressure, max	(psig)	1200		570	
Hydro Test Pressure	(psig)	1800		1200	
Leak Test Pressure	(psig)	1200		570	

<sup>A</sup> Ethane recovery case, representative of typical operation

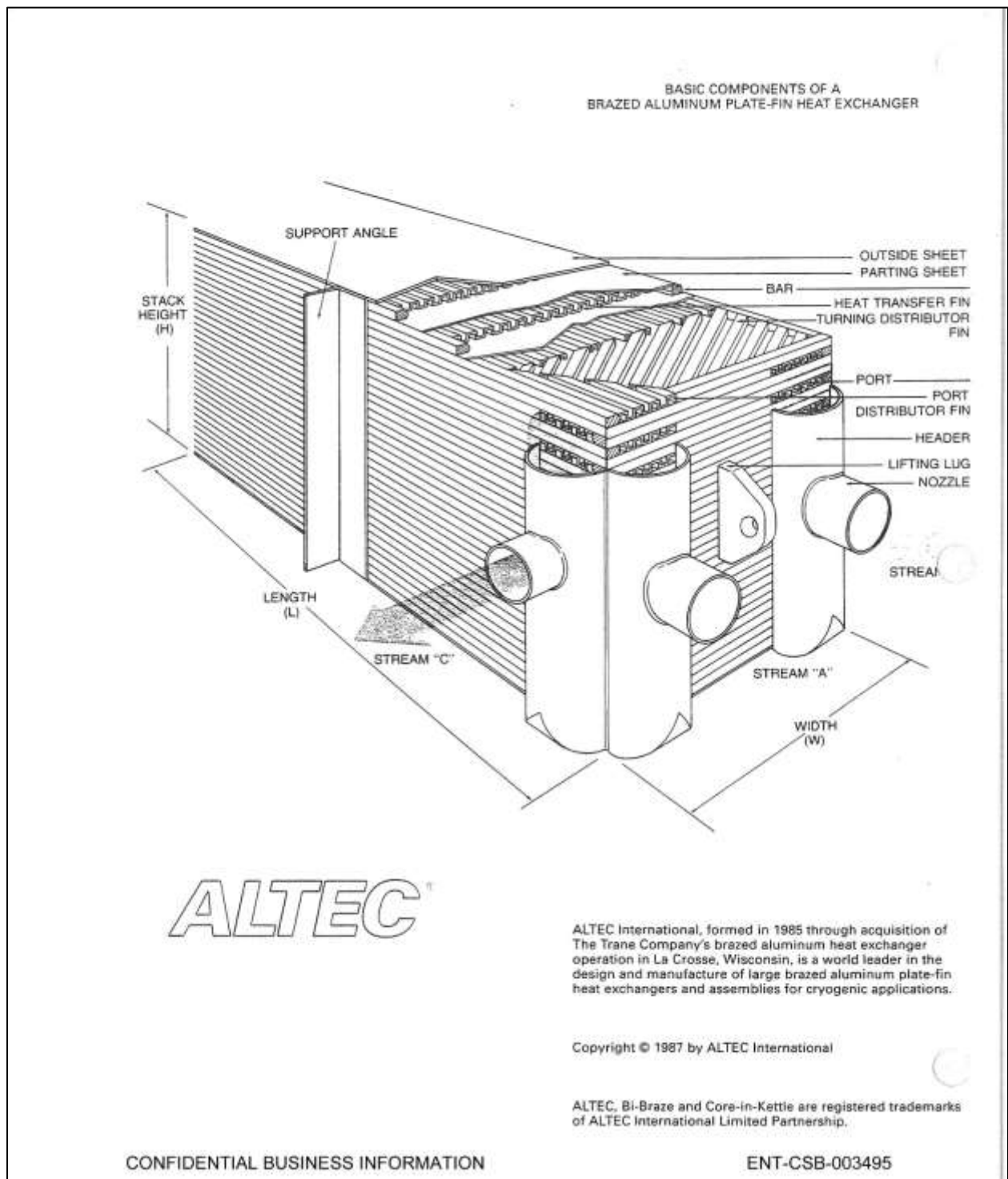


Figure 1 Components of a generalized brazed plate-fin heat exchanger. Provided courtesy of the CSB. In this schematic, the longitudinal axis of the exchanger is horizontal. The longitudinal axis of the subject ACSR was vertical, with headers located at the top and bottom.



Figure 2 Photograph of the ACSR, viewed from the south west.

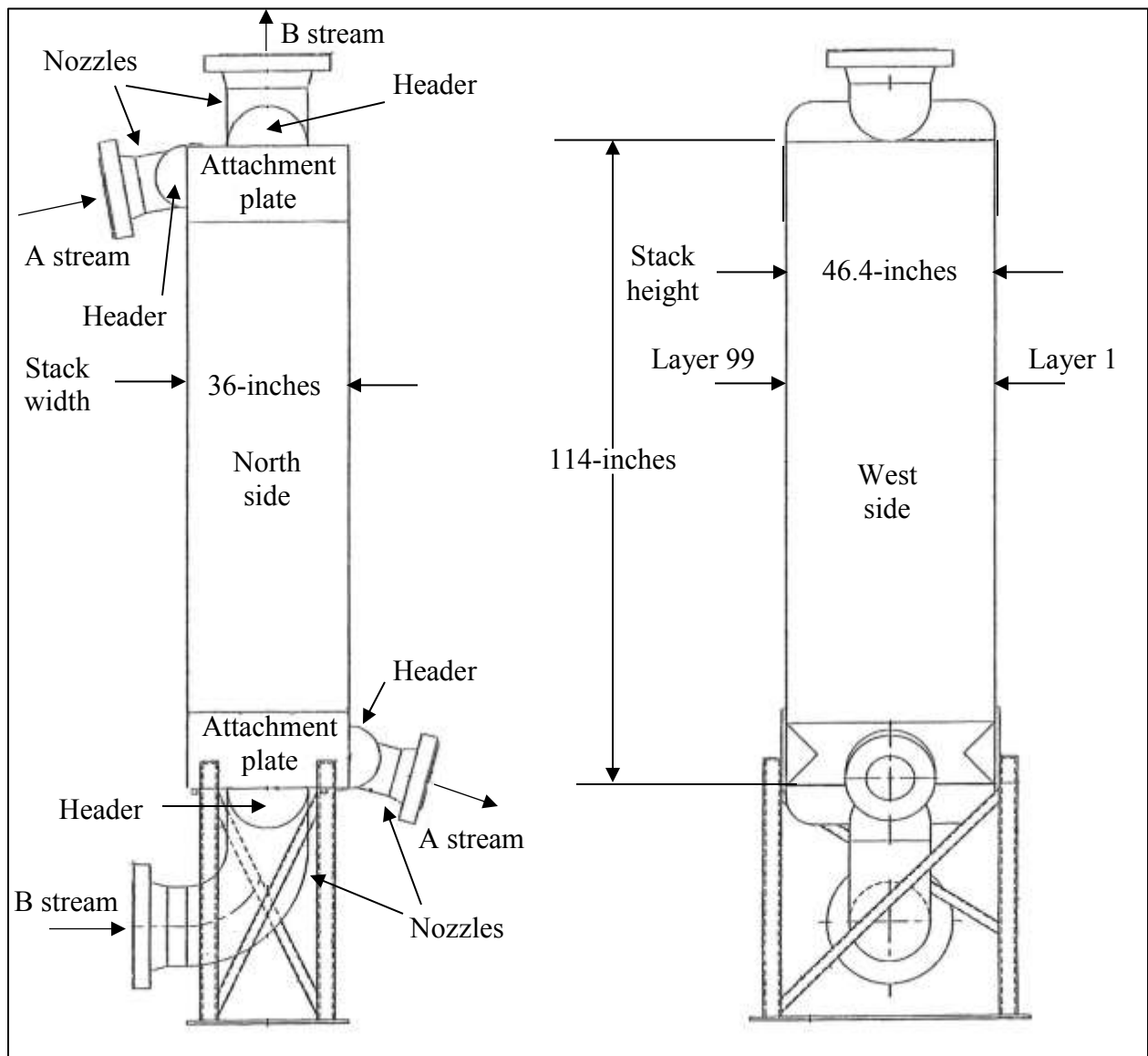


Figure 3 Drawing of the ACSR. Adapted from Altec drawing 13899A Rev. D, provided courtesy of the CSB.



---

## 2. SUMMARY OF RESULTS

During the incident fire, extensive melting and partial melting of the B stream inlet nozzle and header, the north side reinforcing pads, north side cap sheet, and layers 99-96 occurred. The fire damage destroyed evidence of a pressure boundary breach that might have occurred in these areas prior to the fire.

Fatigue cracks were found in the following regions. On the north side under the top reinforcing pad, a through-wall fatigue crack was found in the cap sheet, and fatigue cracks were found in parting sheets between layers 99 and 98, and between layers 98 and 97. On the south side under the top reinforcing pad, fatigue cracks were found in the cap sheet and through the thickness of the parting sheet between layers 1 and 2. On the south side under the bottom reinforcing pad, a fatigue crack was found in the cap sheet.

Examination of crack surfaces by scanning electron microscopy (SEM) and analysis by energy dispersive x-ray spectroscopy, indicated that an aluminum oxide layer had formed on the crack surfaces during the fire. The oxide degraded the SEM image quality and likely destroyed fine details of the cracking mechanism. However, the macroscopic and microscopic morphologies clearly indicated the cracks initiated and propagated by fatigue. Clear evidence of multiple fatigue initiation sites and fatigue progression marks were present. Fatigue striations were visible, although degraded in detail by the oxide layer. It is possible that the finest striations were destroyed by the oxide.

Metallography revealed cracks in the cap sheets and parting sheets had been blunted by plastic deformation. This is consistent with visual detection of depressions on the outside surface of the cap sheets in the vicinity of cracks. The through-wall crack in the north side cap sheet under the reinforcing pad was open enough to allow pressurized air introduced into layer 99 to escape freely. In contrast, examples of small cracks next to larger cracks and secondary cracks that branched from larger cracks were closed, with little or no significant distance between crack faces. These smaller cracks represent the general condition of fatigue cracks prior to the large thermal stresses caused by the fire.

Liquid metal embrittlement (LME) by mercury and mercury corrosion are recognized potential degradation mechanisms of brazed aluminum heat exchangers.<sup>1</sup> However, no branched, predominantly intergranular cracks characteristic of mercury LME were found, and no corrosion product indicative of mercury corrosion was found.

---

<sup>1</sup> ALPEMA, Standards of the Brazed Aluminum Plate-Fin Heat Exchanger Manufacturer's Association, Third Edition, 2010, p.63-64.



### 3. EVALUATION

#### 3.1. B Stream Inlet Nozzle Visual Examination

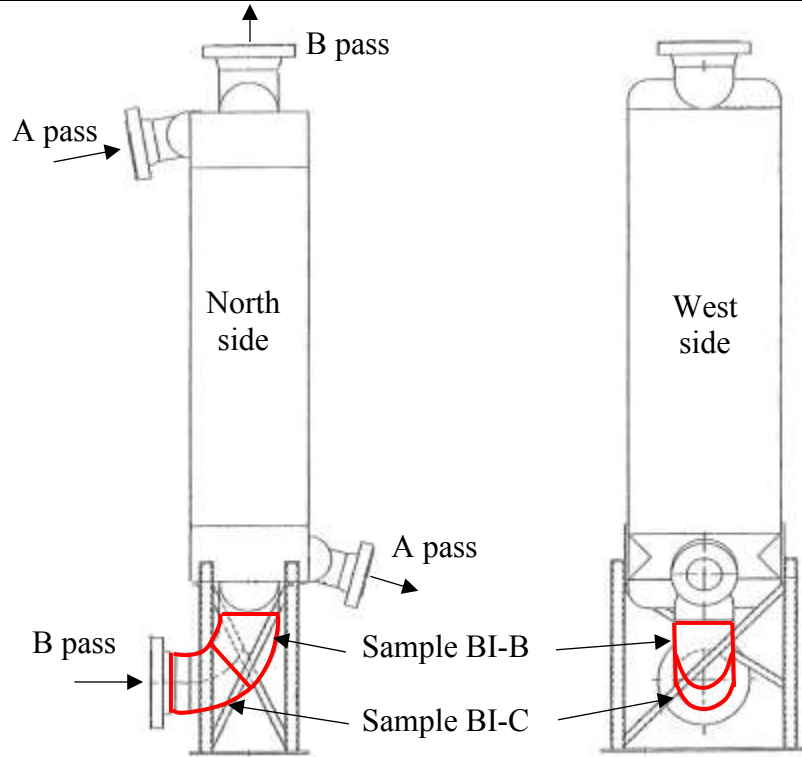
A photograph of the B stream inlet nozzle and header taken after the fire with the ACSR in place is shown in Figure 4. After removal from site, the nozzle and header were cut along the dashed lines shown in the figure. The resulting header and nozzle samples were labeled H-3059 BI-A, BI-B, and BI-C, as indicated. Laboratory evaluation of the header sample BI-A is described in the next section.

The north sides of nozzle samples BI-B and BI-C are shown in Figure 5. A large hole was present in section BI-C. Evidence of melting and partial melting during the fire included out-of-round sections, solidified drips, sag lines in the nozzle wall and weld, and dull grey oxide on the edges of the hole. Similar evidence of partial melting was present on the north side of sample BI-B. Cracks along the girth weld toe, cracks between weld passes, and transverse weld bead cracks also indicated partial melting of the nozzle. Examples of these features are shown in Figure 6 and Figure 7. If a pressure boundary breach had formed in this region of the nozzle prior to the fire, evidence of that breach was destroyed by melting, partial melting, and oxidation. The south side of the nozzle, shown in Figure 8, appeared to be in good condition.

Alloy 5083 melts approximately between 1065 °F and 1180 °F.<sup>2</sup> Common weld filler metals used with 5083 aluminum include alloys 4043 and 5183, which have similar melting ranges. Therefore, the north side of the B inlet nozzle reached temperatures near 1180 °F during the fire.

---

<sup>2</sup> ASM Specialty Handbook Aluminum and Aluminum Alloys, ASM International, p 376, 1993

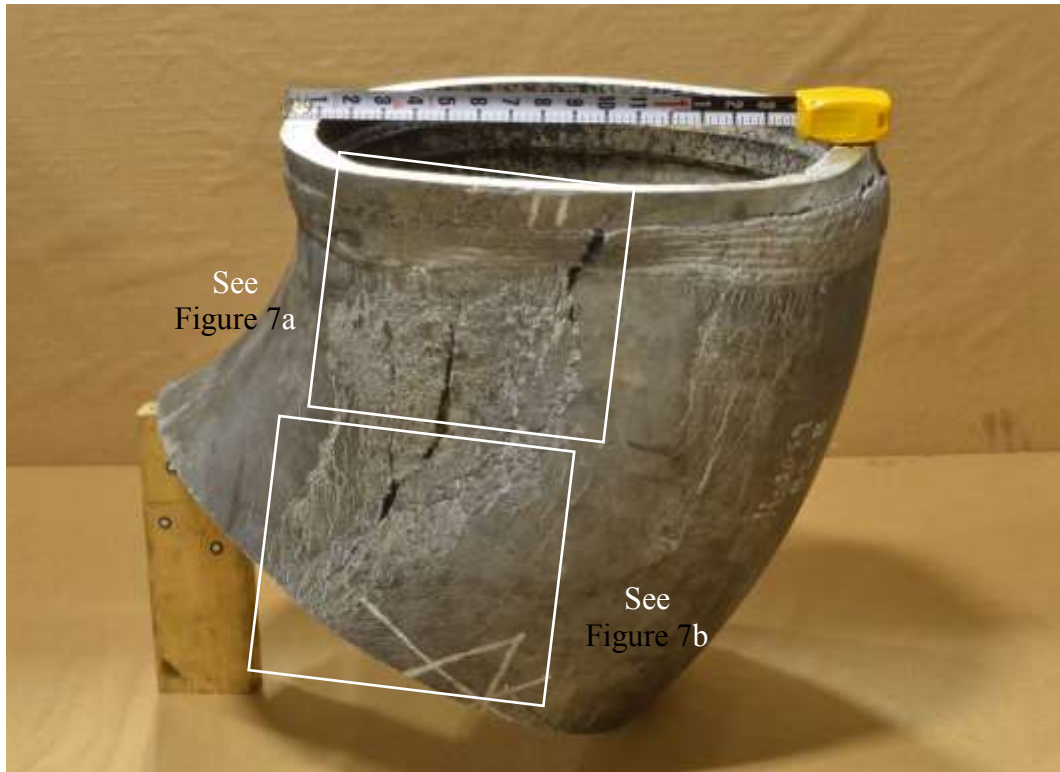


(a)



(b)

Figure 4 Simplified ACSR drawing with header samples indicated and photograph of the north side of the B stream inlet nozzle and header. Dashed lines indicate where were saw cuts made for samples BI-B and BI-C.

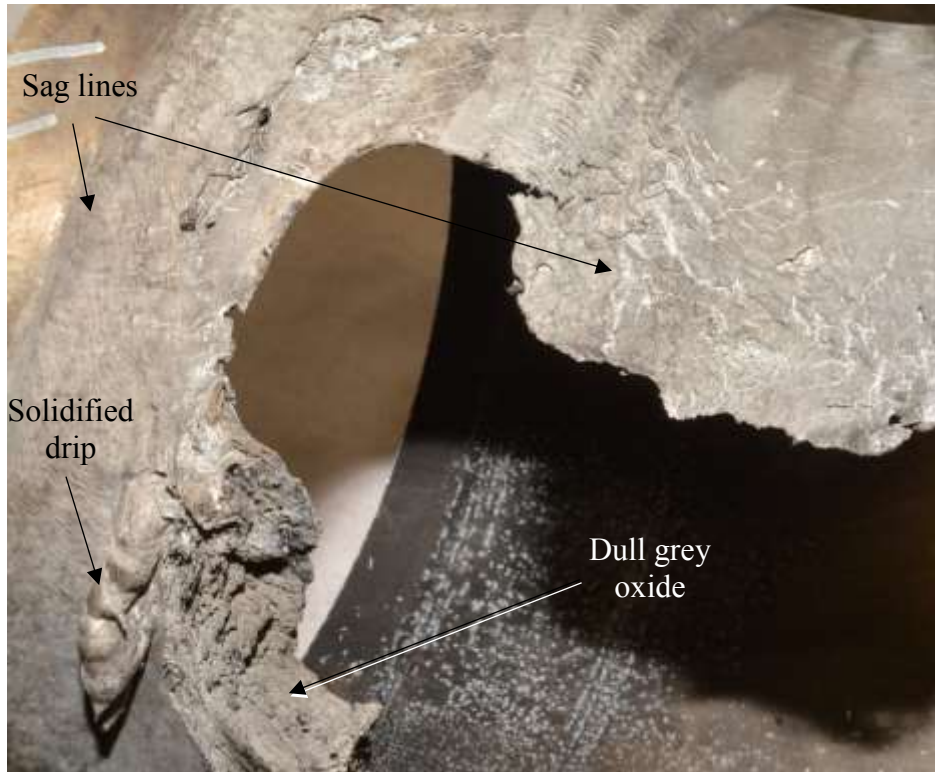


(a)

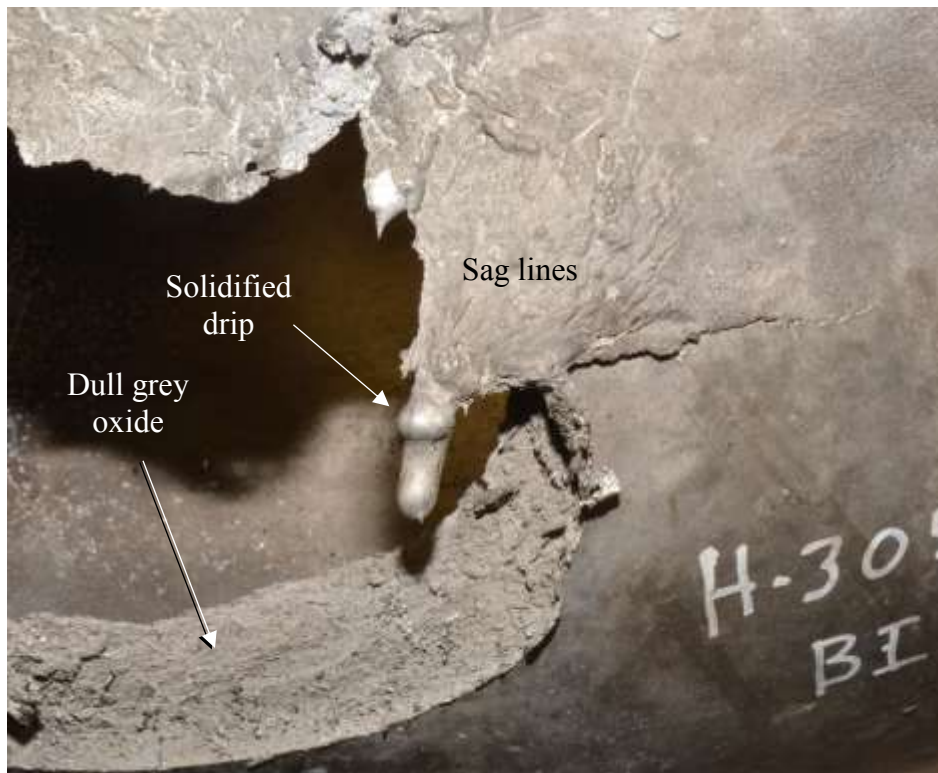


(b)

Figure 5 Photographs of the north side of nozzle samples BI-B and B-I-C.



(a)



(b)

Figure 6 Photographs of the outside surface of sample BI-C, boxed regions in Figure 5b.

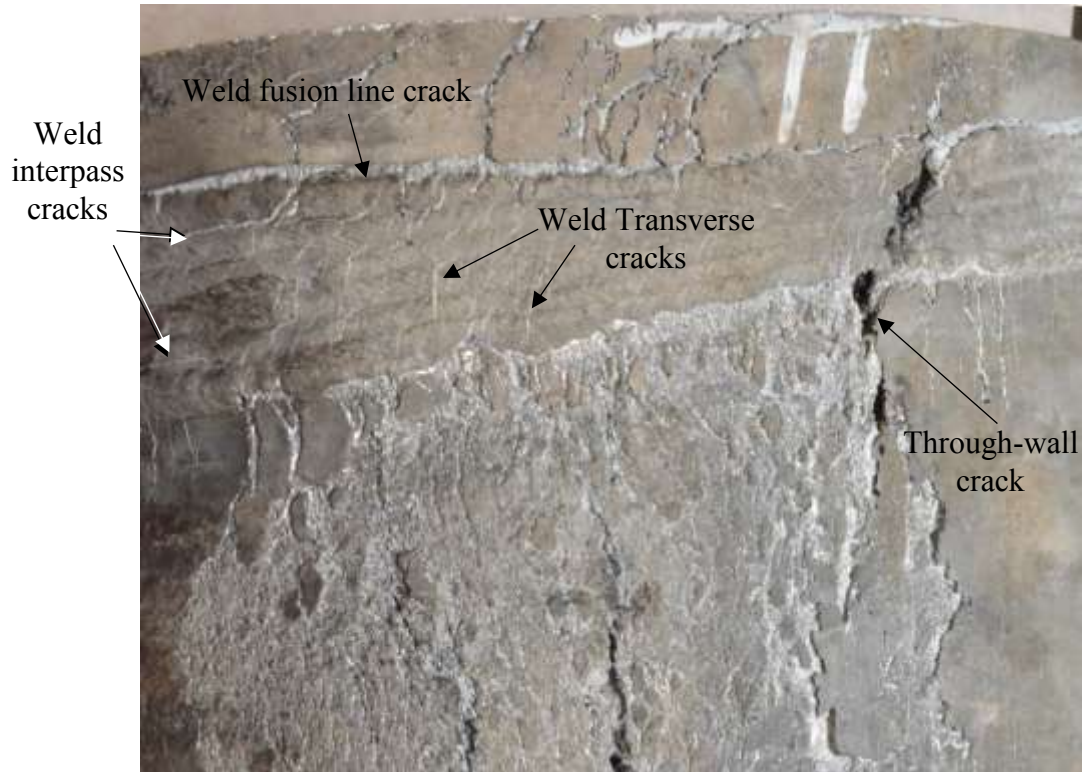


Figure 7 Photographs of the outside surface of sample BI-B, boxed regions in Figure 5a.



(a) BI-B



(b) BI-C

Figure 8 Photographs of the south side of nozzle samples BI-B and BI-C, indicated in Figure 4.



### **3.2. B Stream Inlet Header Visual Examination**

The location of the B pass inlet header sample BI-A on the ACSR is shown in a simplified drawing along with a photograph in Figure 9. The sample is shown as-received in Figure 10. The configuration of transverse header welds indicated the header had been cut open at some point after manufacture, and re-welded. Cutting open headers is typically done as part of a core leak testing or repair. Seams in the perforated plate located between the header and the core matched up with the header repair welds. The perforated plate had likely been cut after the header was opened to allow access to the end of the core. The plate had been re-welded to the header.

A large hole was present in the north end of the header, which extended from the repair weld to the weld that joined the end of the header to the core. At the north end, the header had been separated from the core by partial melting, evidenced by a rough oxidized surface. Had this section of weld been intact when the sample BI-A was cut from the core, a saw cut surface would have been present in this location. A hole in the perforated plate corresponded with the hole in the header. Edges of the hole in the plate were curved toward the inlet nozzle. Fragments of the plate had been found at the top of a pile of melted and re-solidified aluminum located at the base of the ACSR after the fire, prior to removal from the site. This indicated the hole in the perforated plate was caused by partial melting from the heat for the fire, after the hole in the header was created.

Key details of damage to the header are indicated in Figure 11 and Figure 12. A bulge in the header wall located along the edge of the hole parallel to the header repair weld indicated partial melting. Sag in the north end header to core weld coincided with the region of separation from the core caused by partial melting. Wide cracks in the header, header to nozzle weld, and small section of nozzle that was continuous with sample BI-B indicated partial melting.

### **3.3. B Stream Inlet Header Scanning Electron Microscopy (SEM)**

Although much of the hole in the B pass inlet header had evidence of partial melting, a few locations appeared more like fracture surfaces. Two of those regions are shown in Figure 13. Representative SEM micrographs from the boxed locations in the figure are shown in Figure 14 and Figure 15. Examination by SEM indicated a re-solidified morphology, evidenced by rounded inter connected features and thick, wrinkled surface oxide. The SEM results indicate that if a mechanism other than heat damage, such as fatigue or repair weld defect, caused the header hole prior to the fire, evidence of that mechanism was destroyed by the fire.

### **3.4. B Stream Inlet Header Metallography**

Metallography was performed on sections cut from the north end header to core weld. A representative section cut from the sample is shown in Figure 16. Specimens were embedded in clear epoxy, and polished through 0.05-micron colloidal silica using standard techniques for preparation of specimens for metallography. The specimens were examined as-polished and after etching with 5% HF. In the as-polished condition, numerous interpass weld cracks indicative of partial melting were visible. Photographs of specimen BI-A-1C-1 are shown in Figure 17.

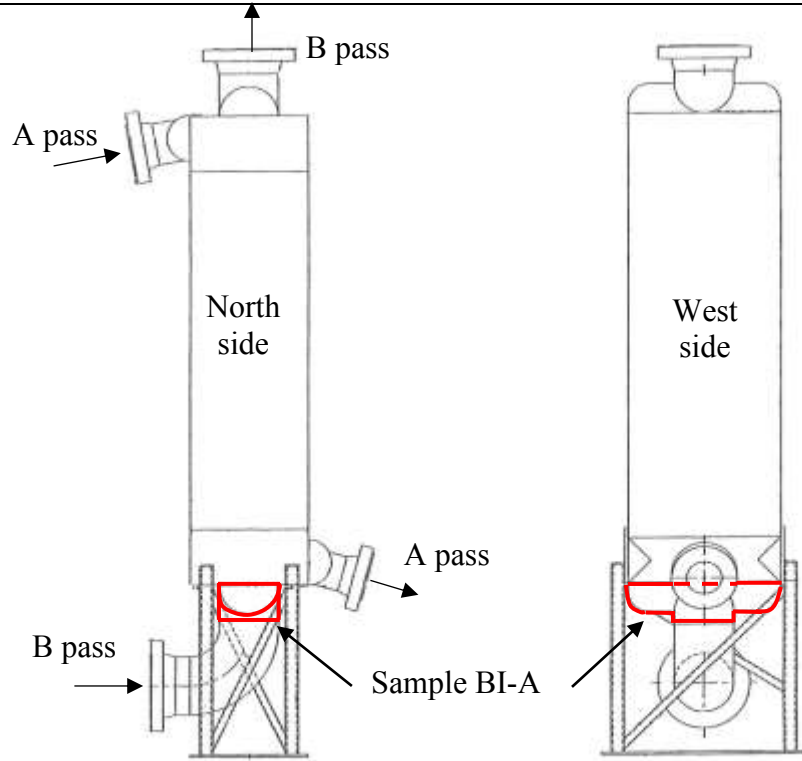
Representative optical micrographs of the section BI-A-1C-1 are shown in Figure 18. Rounded features indicative of localized melting corresponded to the rounded surface features revealed by SEM on the header hole edges. Elemental segregation that occurs during weld solidification



---

results in regions of lower melting point. During exposure to the heat of the fire, these regions melted or partially melted, resulting in interpass cracks in the weld.

Phased array ultrasonic testing (PAUT) was performed on the south side header repair weld by Team Qualspec. The purpose of the PAUT was to examine a header repair weld that had not been visibly affected by the fire. Indications of weld root discontinuities were detected in a number of locations in the repair weld. Representative locations are shown in Figure 19. Sections through locations F, G, and H were prepared for metallography. Representative optical micrographs of the section through indication G, labeled BI-A-10G, are shown in Figure 21 and Figure 22. Metallography revealed that the PAUT indication was caused by small regions of incomplete fusion in the weld root. Micro-shrinkage at the end of the larger portion of incomplete fusion indicated that no service related propagation of the discontinuity had occurred.



(a)

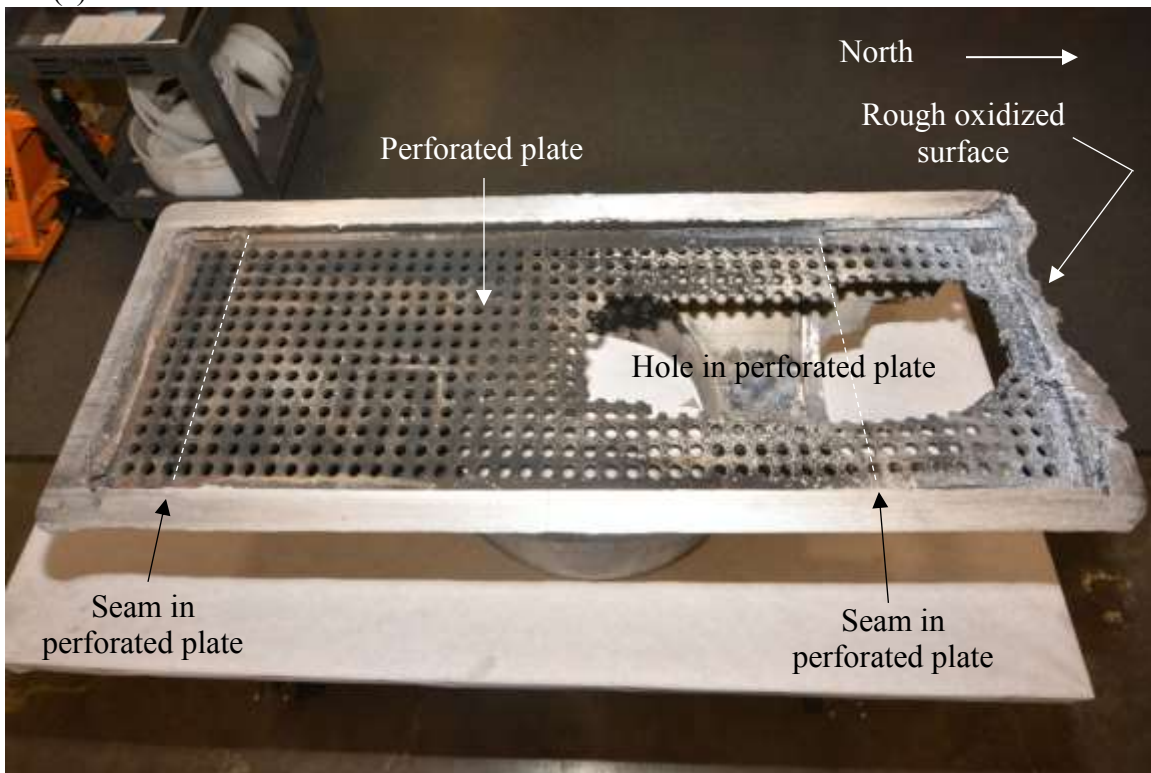


(b)

Figure 9 Simplified drawing of the ACSR with the location of the B pass inlet header sample indicated and a photograph of the header taken after the fire with the ACSR still in place. Dashed lines in (b) indicate where the header was cut from the core and nozzle.

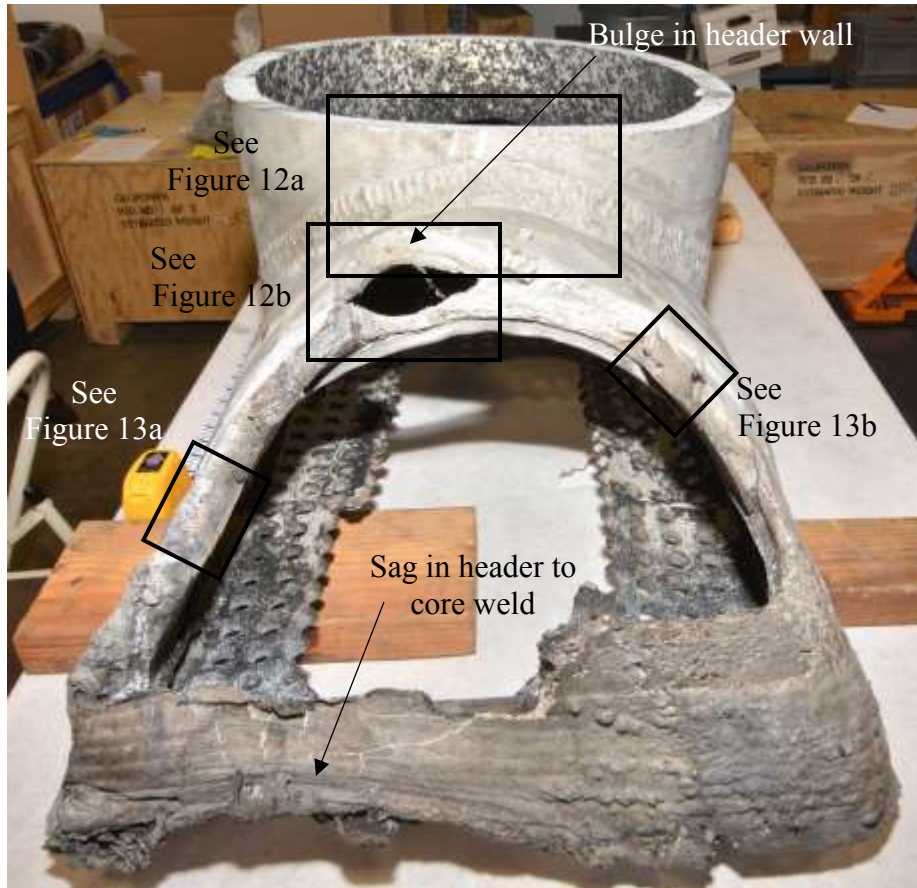


(a) Outside view

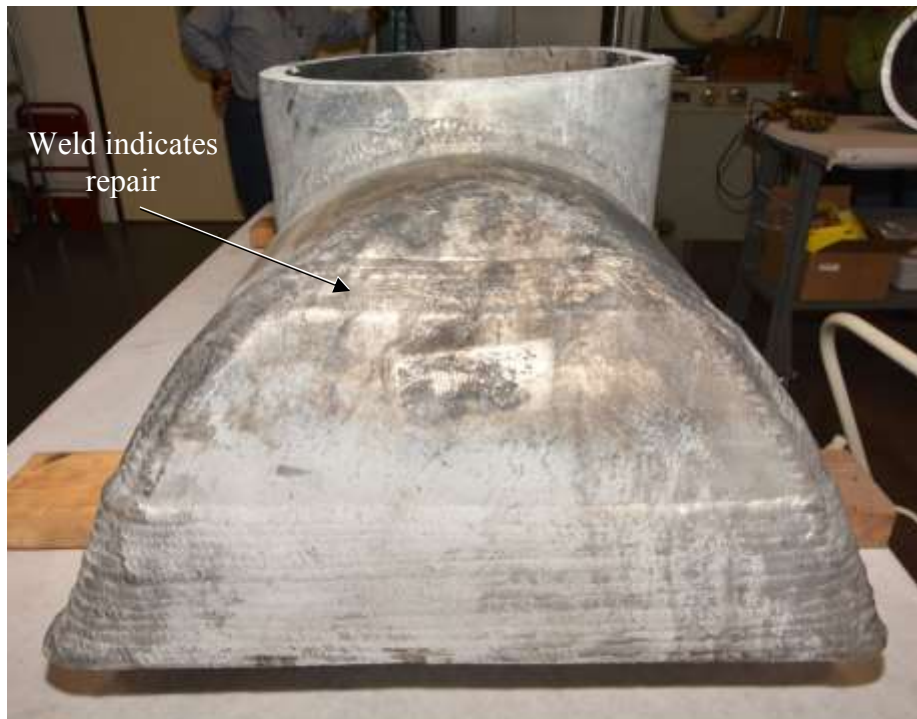


(b) Inside view

Figure 10 Photographs of the B stream inlet header BI-A cut from the ACSR.



(a) North end



(b) South end

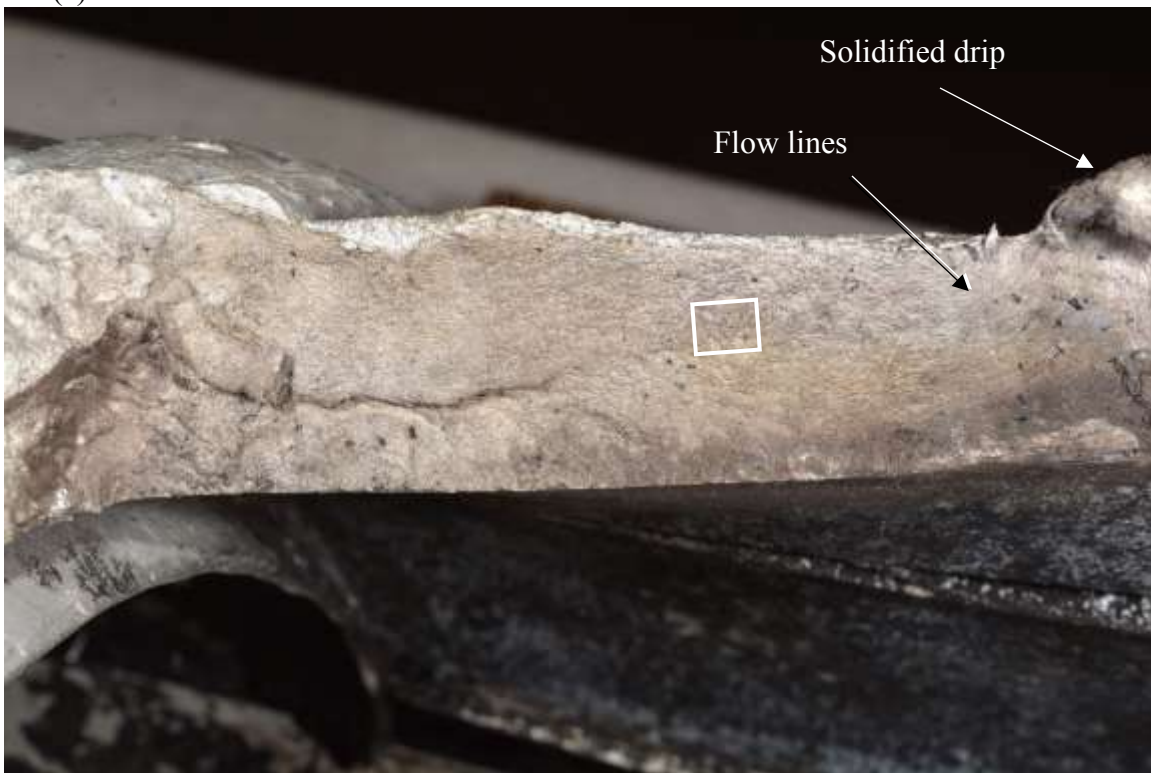
Figure 11 Photographs of the B stream inlet header BI-A cut from the ACSR.



Figure 12 Photographs of the header, boxed regions in Figure 11a.

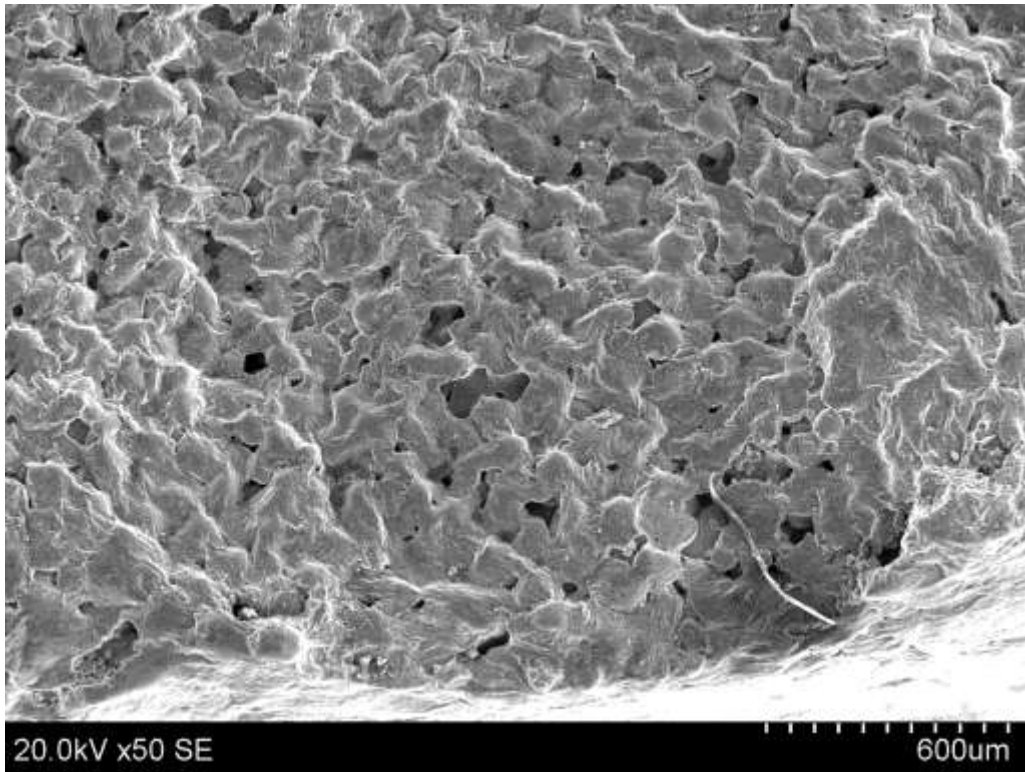


(a)

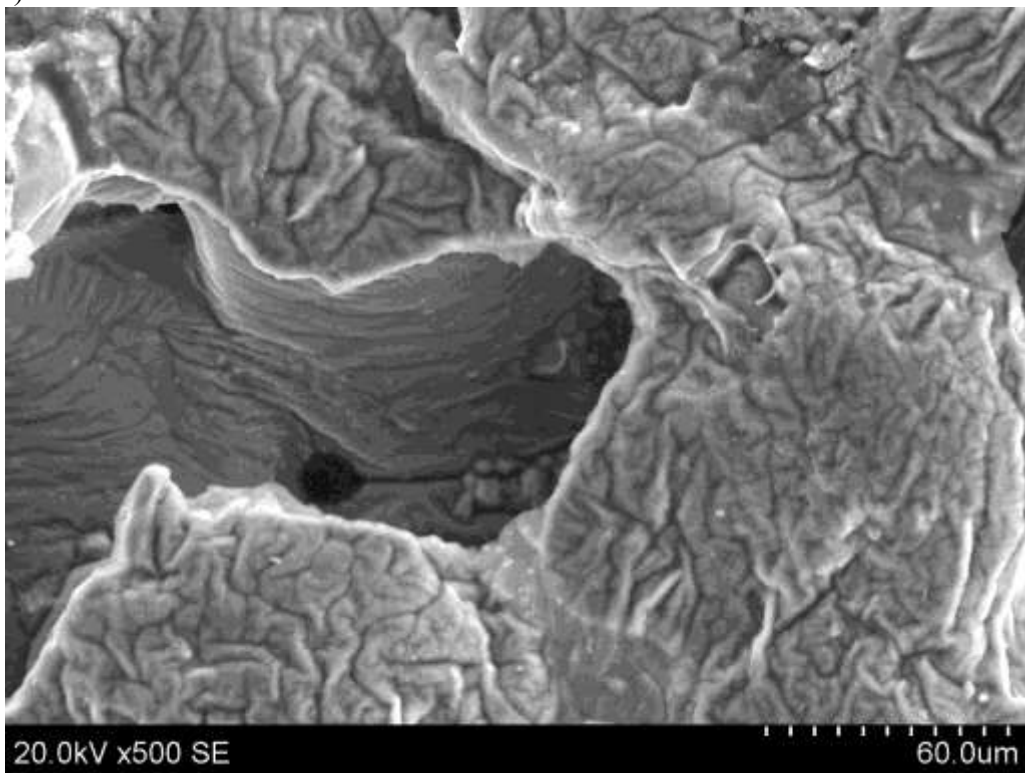


(b)

Figure 13 Photographs of the header sample, from the locations indicated in Figure 11a. The boxed region in (a) is shown in Figure 14, and the boxed region in (b) is shown in Figure 15.

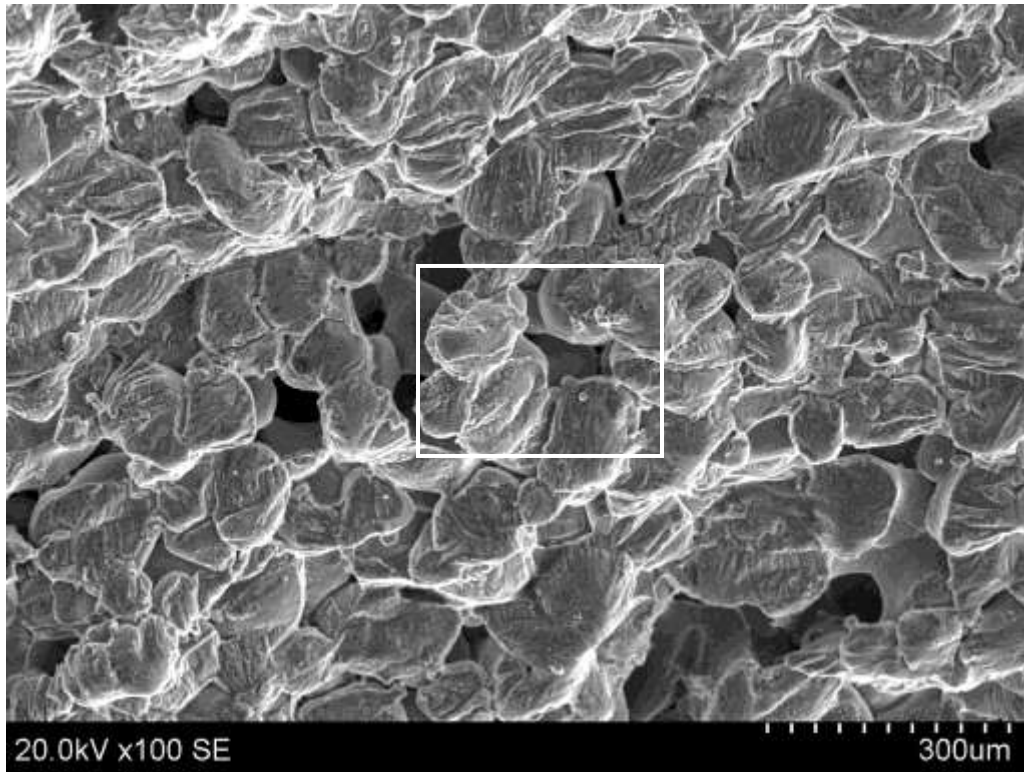


(a)

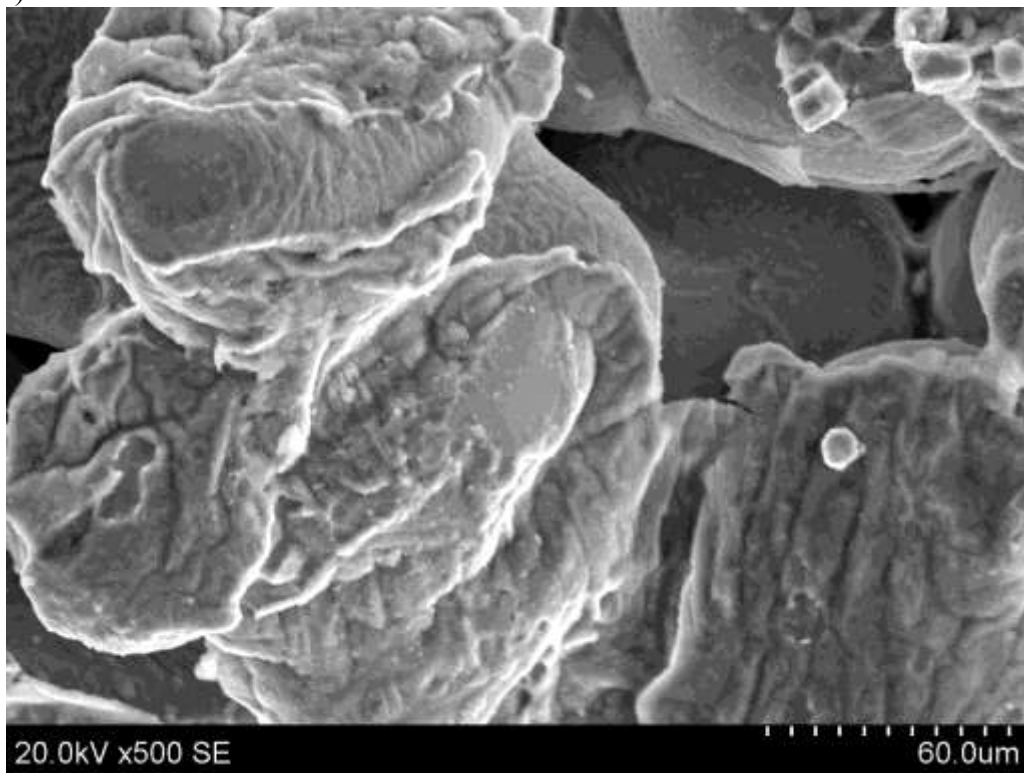


(b)

Figure 14 SEM micrographs of the boxed location indicated in Figure 13a.



(a)



(b) Boxed region in (a)

Figure 15 SEM micrographs of the boxed location indicated in Figure 13b.

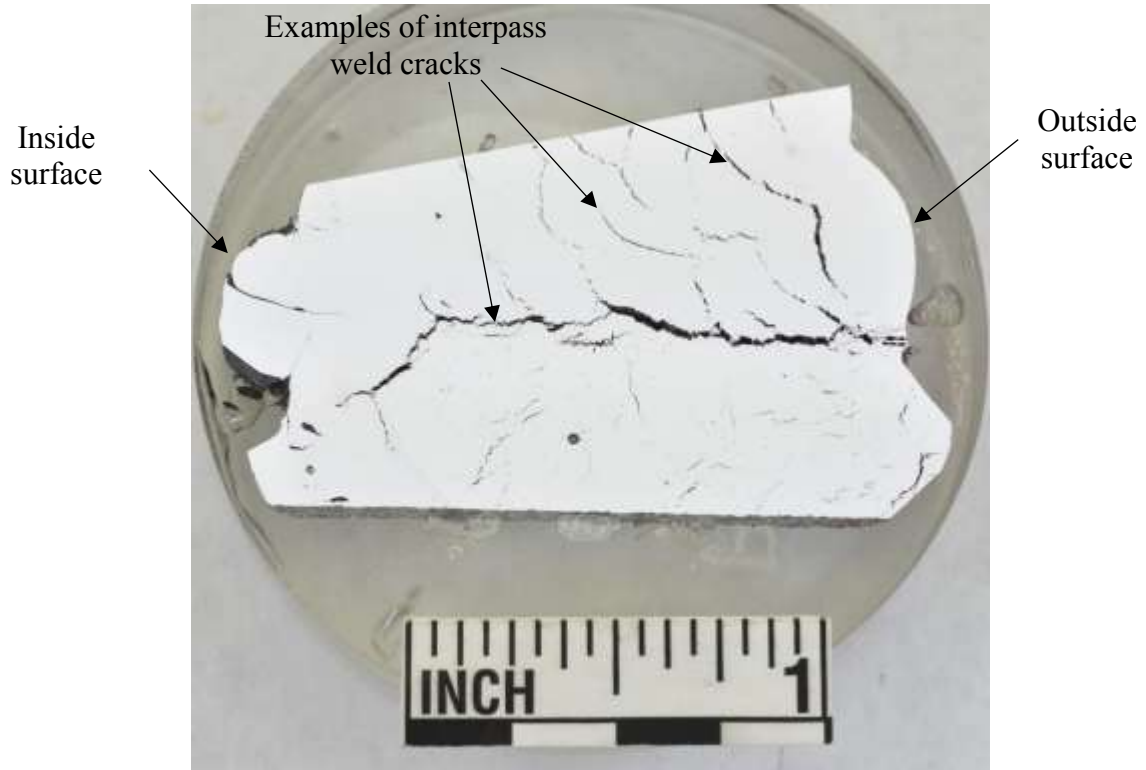


(a)



(b)

Figure 16 Photographs of the sample BI-A1, with cut lines indicated.

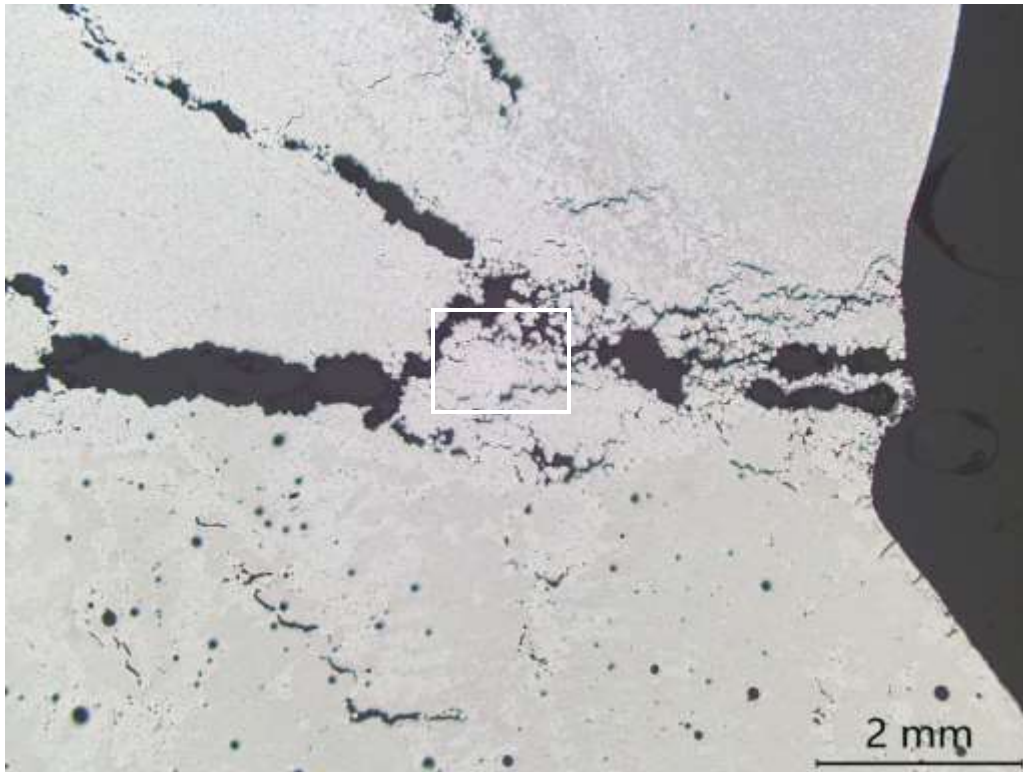


(a) As-polished



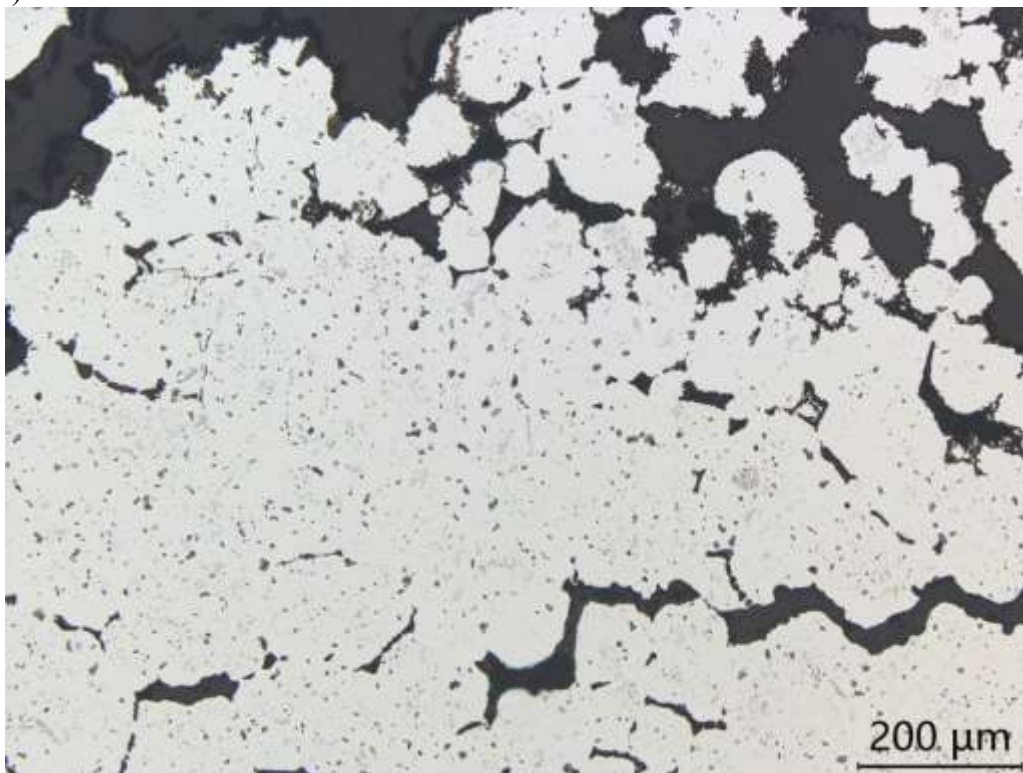
(b) Etched with 5% HF

Figure 17 Photographs of section BI-A-1C-1 indicated in Figure 16.



(a)

13X



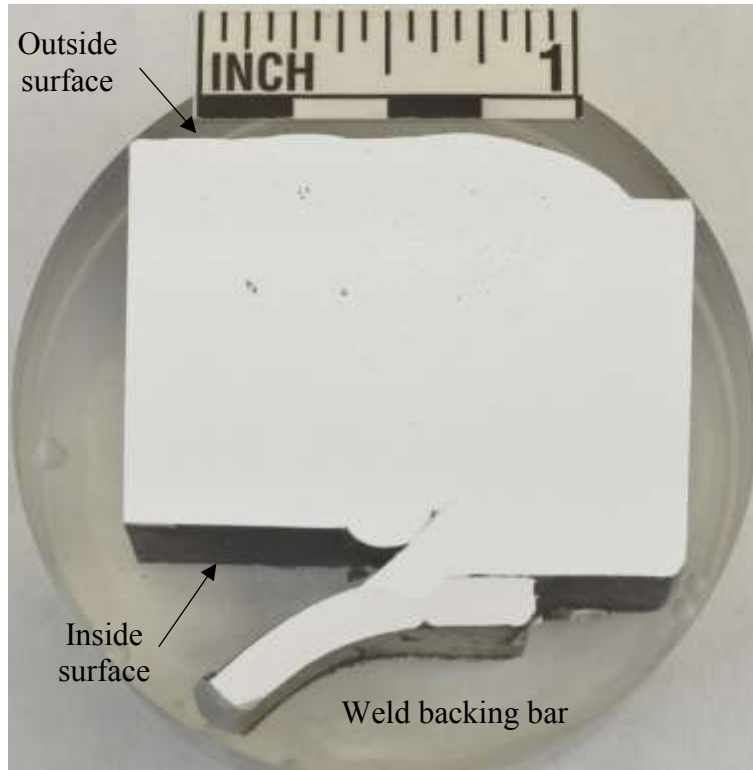
(a)

50X

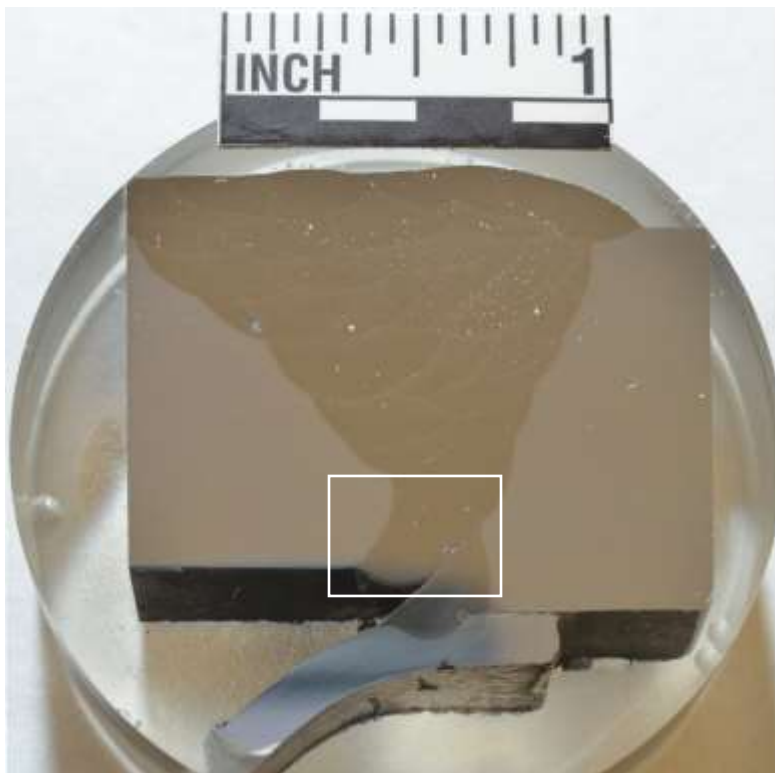
Figure 18 Micrographs of section BI-A-1C-1 from the boxed region in Figure 17b.



Figure 19 Photograph of the header sample BI-A, south west corner.

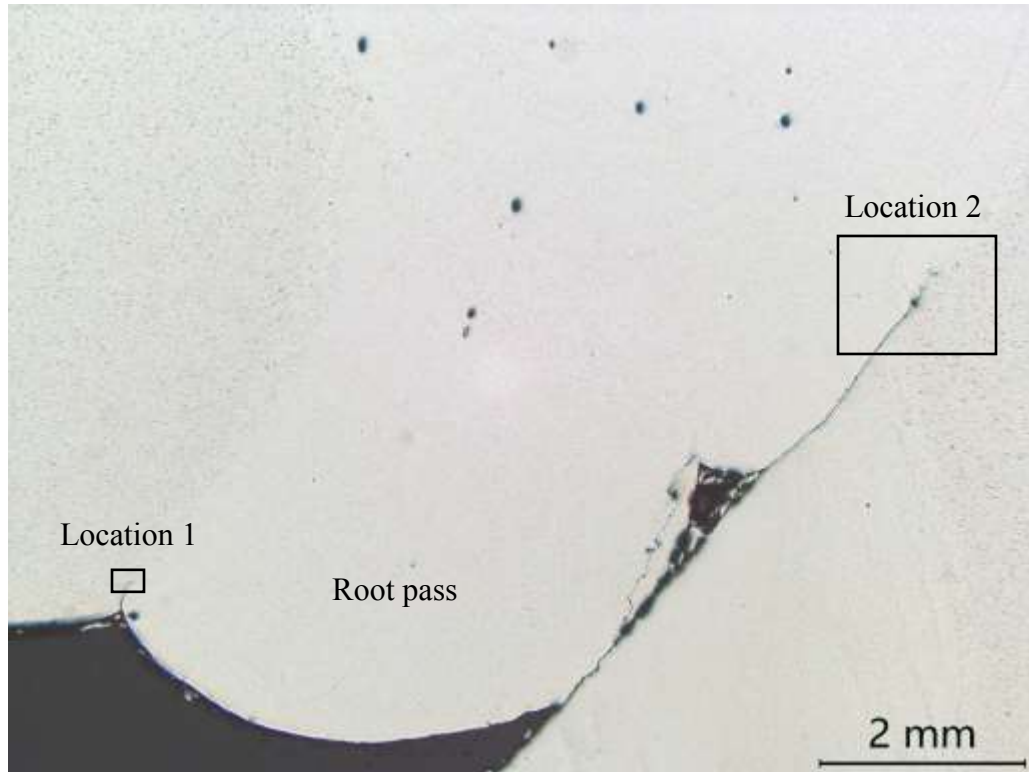


(a) As-polished

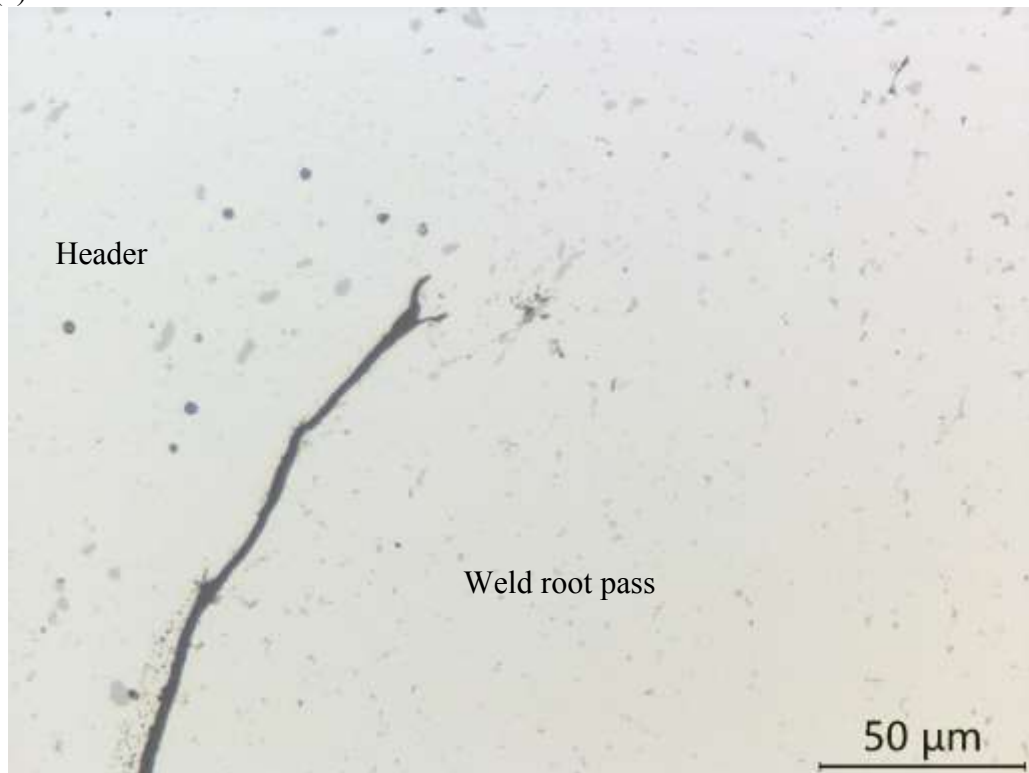


(b) Etched

Figure 20 Photographs of section BI-A-10G, indicated by dashed lines in Figure 19. Boxed region in (b) is shown in Figure 19a.



(a) 13X



(b) Boxed location 1 in (a) 500X

Figure 21 Micrographs of section BI-A-10G from the boxed region in Figure 20b.

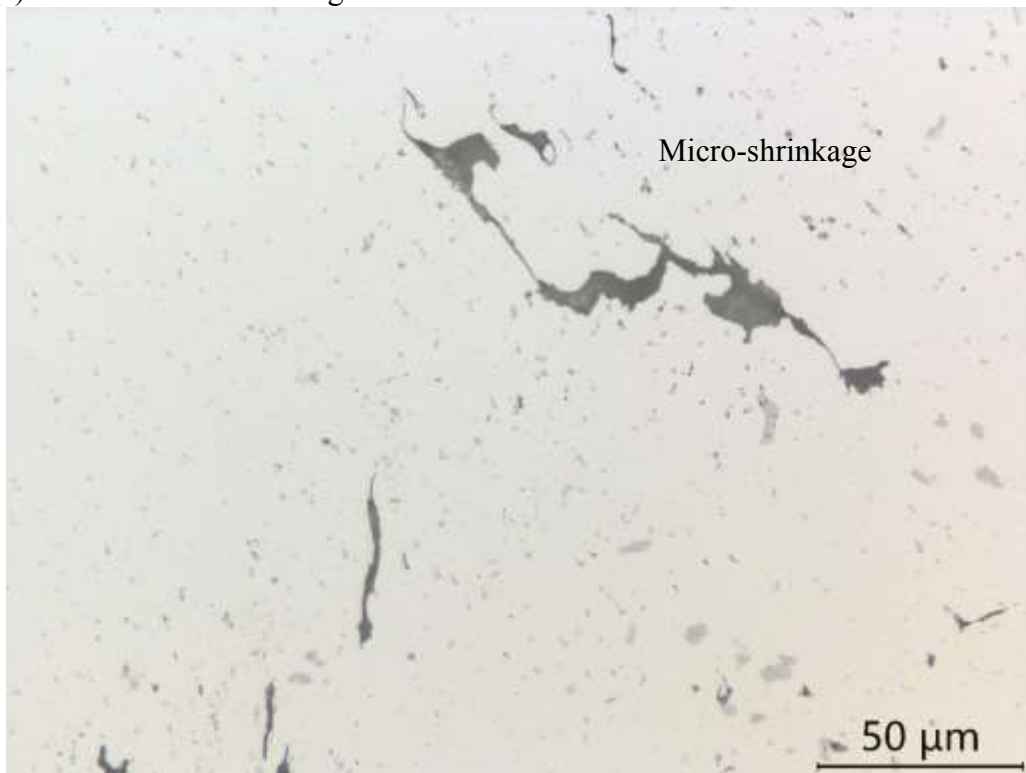
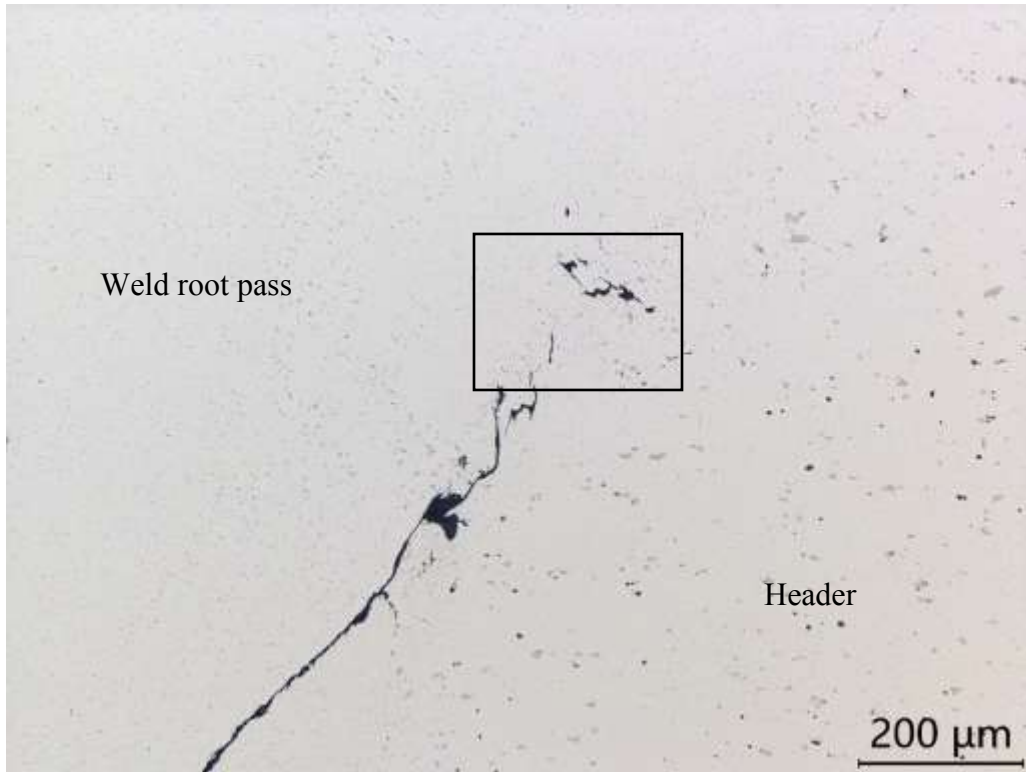


Figure 22 Micrographs of section BI-A-10G prepared for metallography.



### 3.5. ACSR Sample S042-C Visual Examination

Sample S042-C was cut from the north side of the ACSR just above the B pass inlet header. A simplified drawing of the reboiler and a photograph of sample S042-C are shown in Figure 23. The sample included the full width of the ACSR, extended slightly past the height of the attachment plate, and was eighteen layers thick. After the fire, the attachment plate and the cap sheet were missing in this region. As a result, the layer 99 fins, side bars, and end bars were exposed. The fin orientation revealed flow direction in the B pass, indicated in Figure 23b, along with the flow direction of the A pass in underlying layers. Inactive zones of the B pass layer are also noted in the figure. These zones are created by the angled side bars that channel flow from the inlet header into the full width of the B pass layers. Inactive zones were vented into square channels that are designed to be open to atmosphere through drains. A bulge and partially visible void were present in the lower east corner of the sample.

Solidified drips of aluminum and oxidized fins on the layer 99 surface indicated extensive heat damage. A fragment of the cap sheet and attachment plate, labeled S058, was found on the ground beside the ACSR, covered in aluminum that had melted during the fire. The outside surface of the attachment plate was toward the ground, and the molten aluminum was on the layer 99 side of the cap sheet. No metallurgical evidence of the mechanism by which the fragment separated from the reboiler was detected on the fragment, shown in Figure 24.

Sample S042-C was cut into smaller sections using a horizontal band saw. The resulting subsamples are shown in Figure 25a. The corner bulge, shown in Figure 25b, was caused by fin fracture in A pass layer 95. Fin compression was visible in layers 93, 94, 96, and 97. However, the remaining fins in layer 98 were not compressed. Furthermore, the bulge projected beyond the plane of the side and end bars. Therefore, the cap sheet and attachment plate had detached from the core before the bulge occurred.

To expose the inside of the void, the bulged layers were cut from the sample as indicated in Figure 26. Parting sheet fracture along the edges of the side and end bars had occurred from layer 95 through 99. Separation of layer 95 fins from the parting sheet was visible on the cut face of the sample approximately 3-feet from the B pass inlet, shown in Figure 25b. Partial separation of the parting sheet to side bar braze was also visible in this location.

The side bars and end bars around the bulge were cut from the sample, shown in Figure 27. Thick oxide was present on the fractured parting sheet edges. The image in Figure 27b was taken after cleaning with acetone, followed by scrubbing with a soft bristle brush and soapy water.

### 3.6. ACSR Sample S042-C Metallography

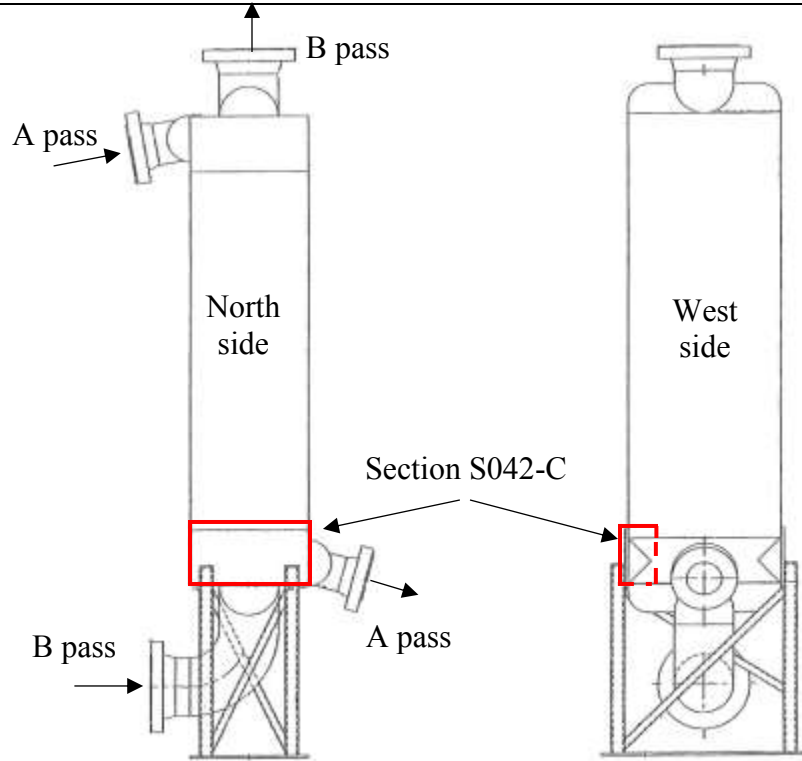
Sections of S042-C were embedded in clear epoxy, ground, and polished through 0.05-micron colloidal silica using standard metallographic techniques. The specimens were examined as-polished and after etching with Graff-Sargent Reagent. A photograph and representative micrograph of a section through the end bars, is shown in Figure 28. Ductile overload fracture of parting sheets bordering the corner bulge was evidenced by the tapered edges. A photograph and micrographs of a section through layers 95, 94, and 93, are shown in Figure 29 and Figure 30. The tapered ends of fractured fins indicate the fracture occurred in tension by ductile overload. Parting sheet deformation and compression buckling of fins in layers 93 and 94 was clearly visible in the section.



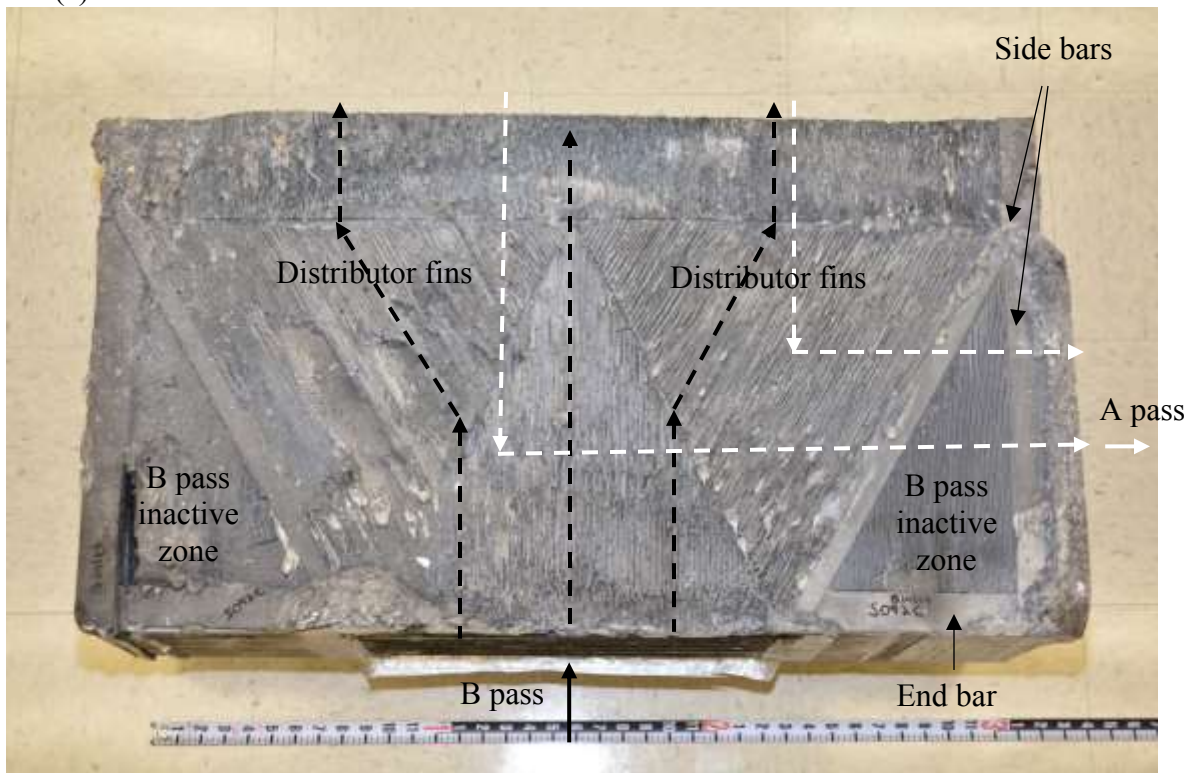
A section through the bulged layers, indicated in Figure 26a, was prepared for metallography. Although significant fire damage had occurred to the outer layers, lack of buckling in the layer 98 fins was clearly visible, indicating the bulge happened after the cap sheet and attachment plate had detached from the core. Ductile fracture and incipient melting of layer 95 fins was detected. Loss of fin root at the parting sheet likely occurred by erosion of molten 4004 braze that mixed with the 3003 fins during the fire. A photograph of the section and representative micrographs are shown in Figure 31 and Figure 32.

A section on the opposite side of the sample from the bulge was prepared for metallography. In this section, approximately 3-feet from the bulge, separation occurred in the layer 95 fin braze and parting sheet between layer 96. Separation in this section occurred because the braze metal had melted. A photograph of the section and representative micrographs are shown in Figure 33 and Figure 34.

A section from the center of the B-pass inlet region of the sample was prepared for metallography. This section, indicated in Figure 25a, was inside the B pass header. Separation within B pass layer 97 occurred by ductile fracture of the fins. Evidence of melting and re-solidification of the parting sheet and end bar of layer 98 is indicated by the dendritic structure shown in Figure 36.

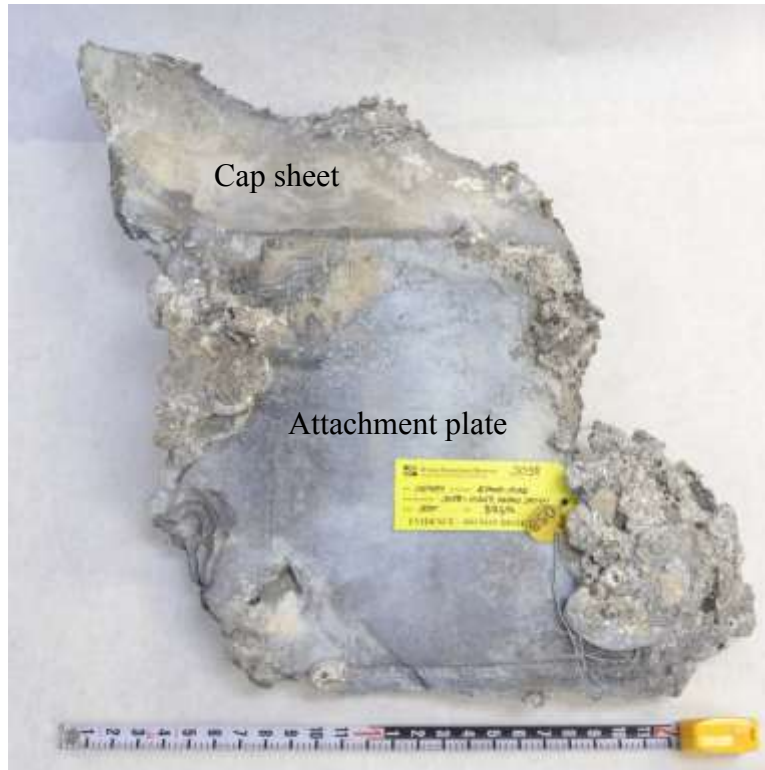


(a)



(b)

Figure 23 Simplified drawing of the ACSR and photograph of section S042-C. After the fire, the attachment plate and cap sheet were missing in this region, leaving the B stream layer 99 fins exposed. Black dashed arrows indicate flow in the B pass layers and white dashed arrows indicate flow in the A pass layers.



(a) Outside surface



(b) Inside surface covered with melted aluminum

Figure 24 Fragment of the ACSR attachment plate and cap sheet found on the ground beside the reboiler. The side shown in (b) was facing up and was mostly covered with aluminum that had melted in the fire.

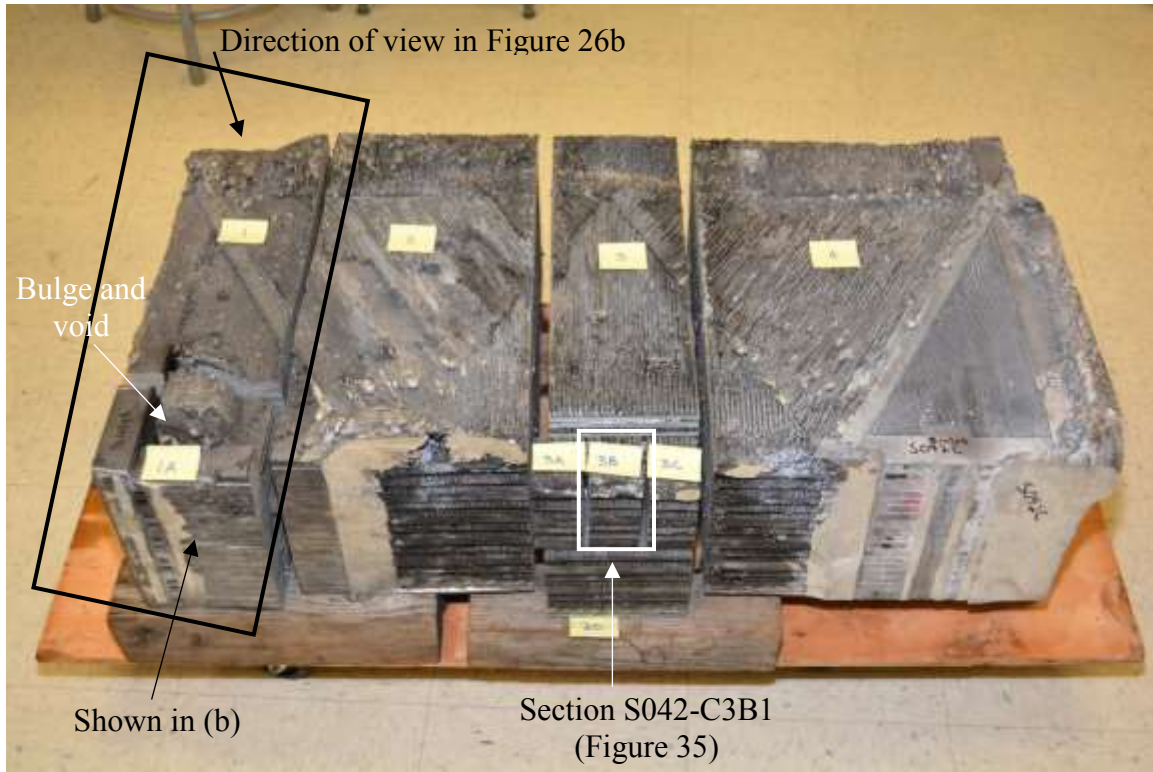
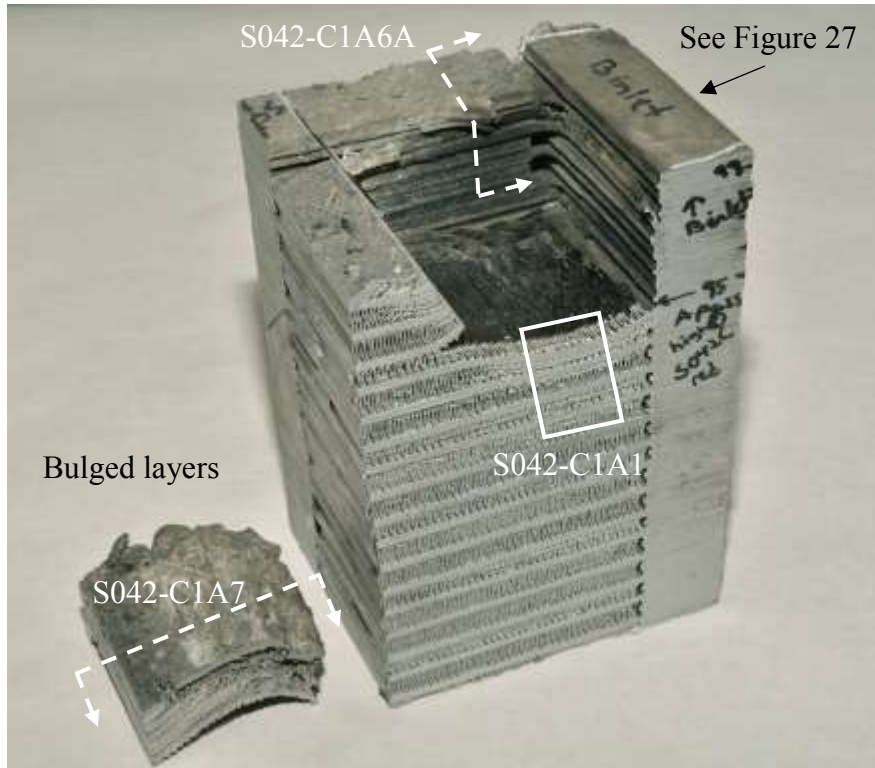
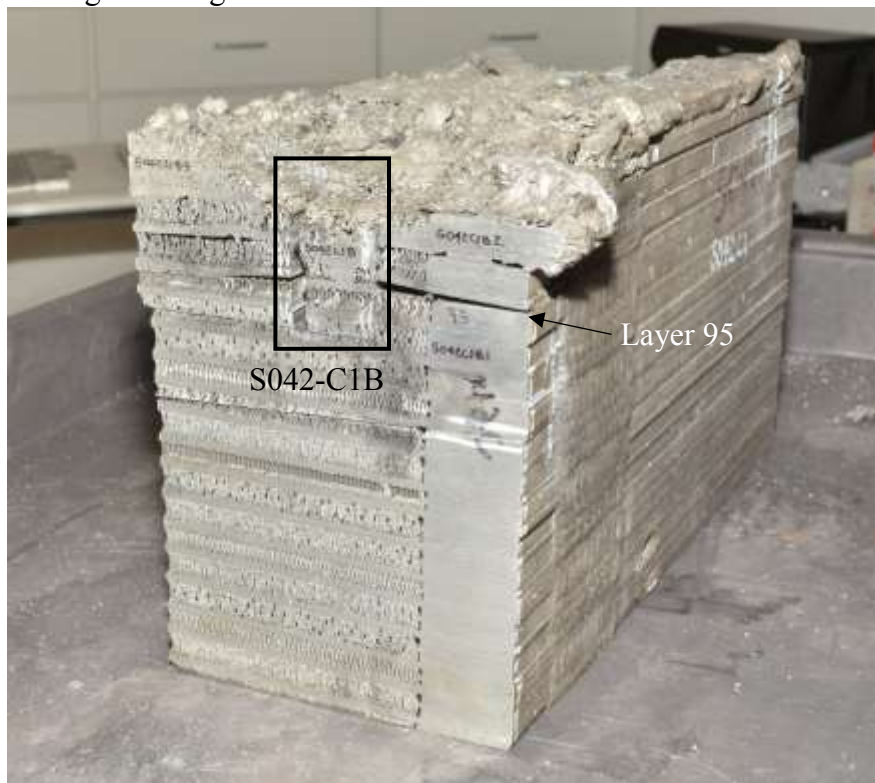


Figure 25 Photographs of section S042-C after cutting. Localized rupture in layer 95, A pass, was investigated.



(a) Boxed region in Figure 25b



(b) View indicated in Figure 25a

Figure 26 Boxed regions in Figure 25.

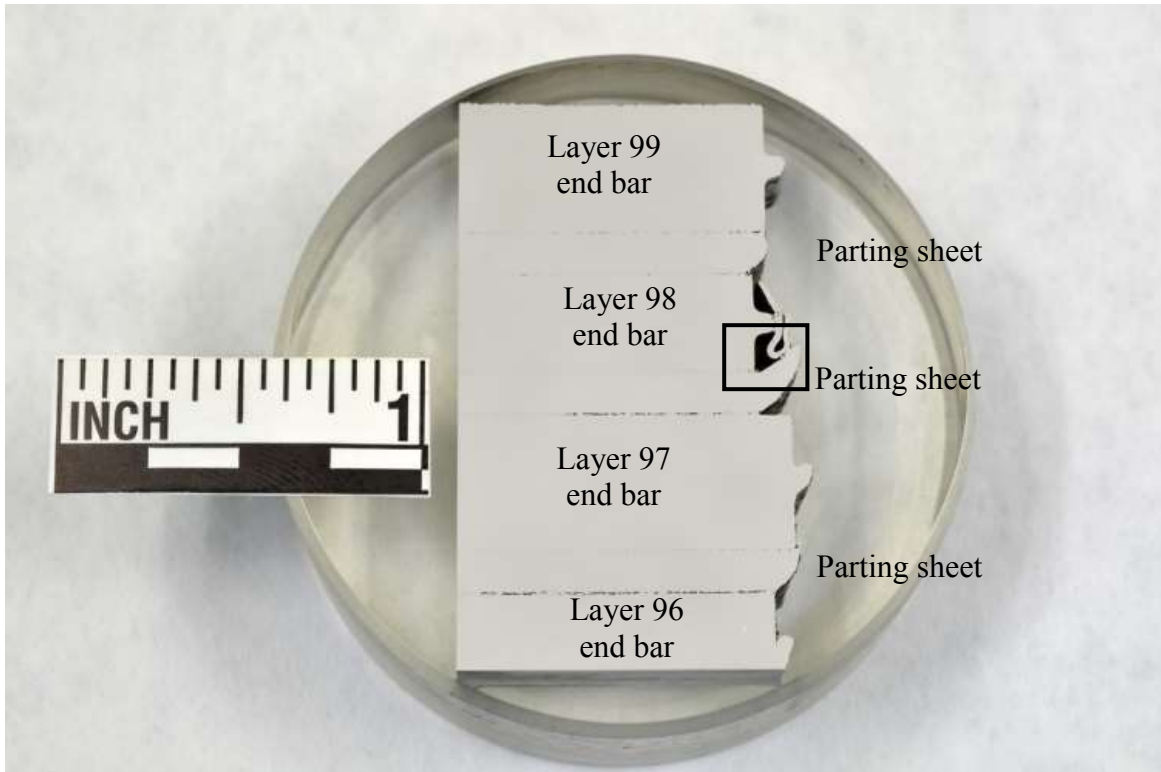


(a)

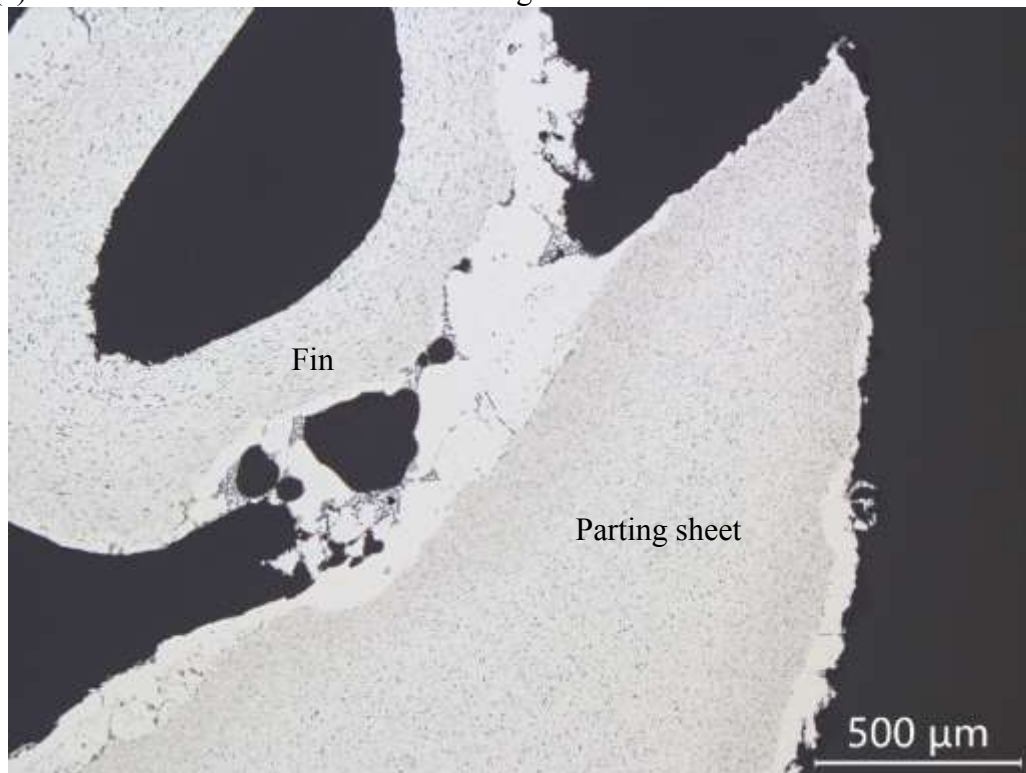


(b)

Figure 27 Images of side bar and side bar section from sample S042-C, indicated in Figure 26. Thick oxide covered fractured parting sheets and side bars.

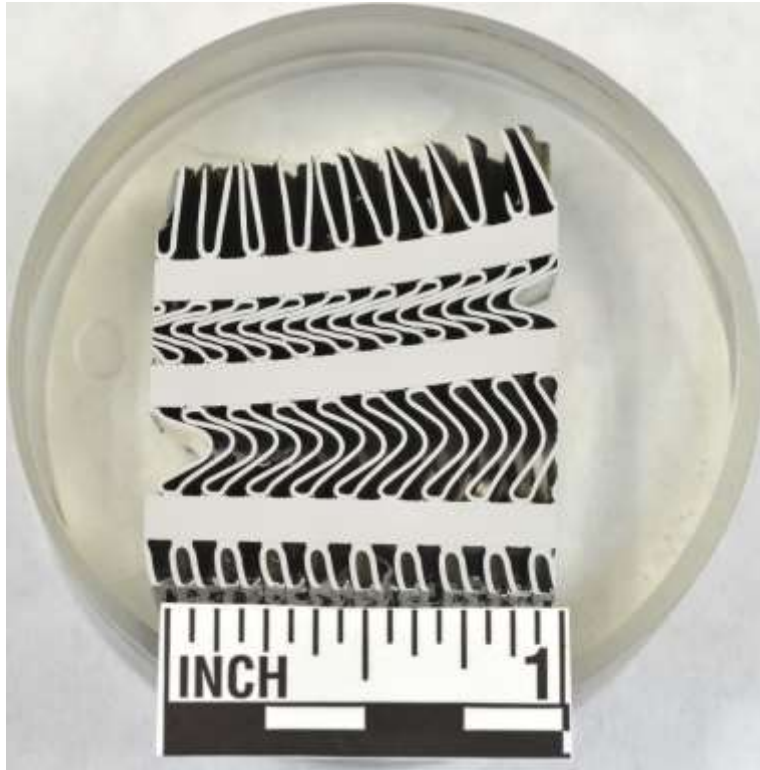


(a) Section S042-C1A6A indicated in Figure 26a

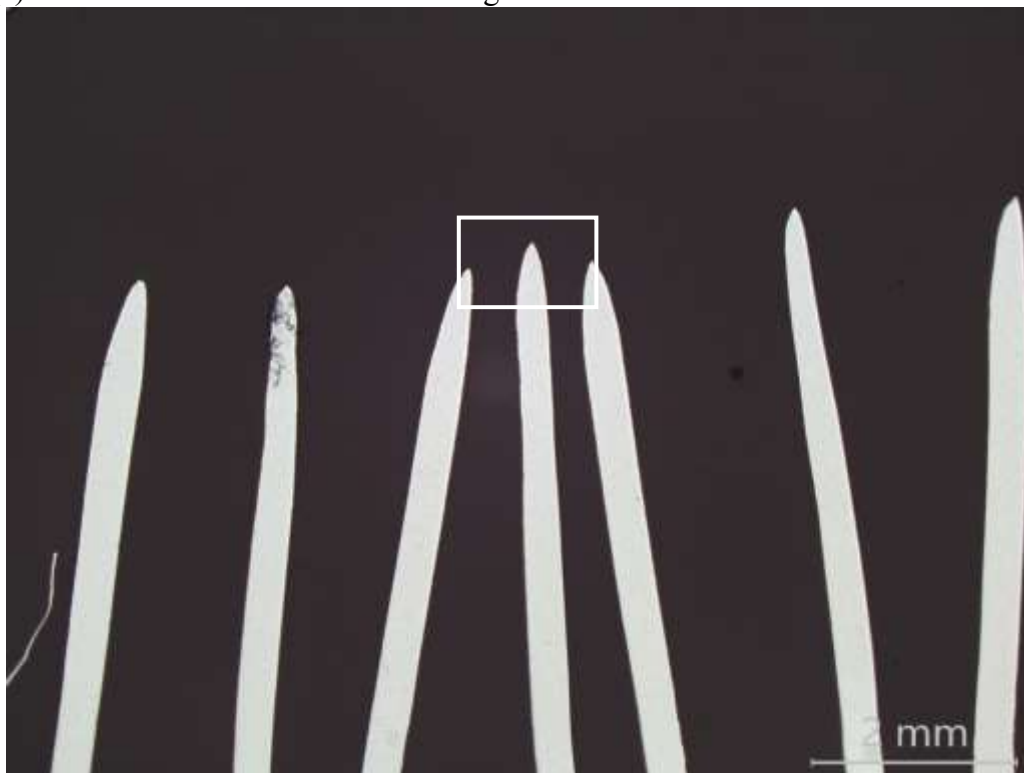


(b) Parting sheet between layers 97 and 98 50X

Figure 28 Photograph and micrograph of section S042-C1A6A, indicated in Figure 26a, prepared for metallography.

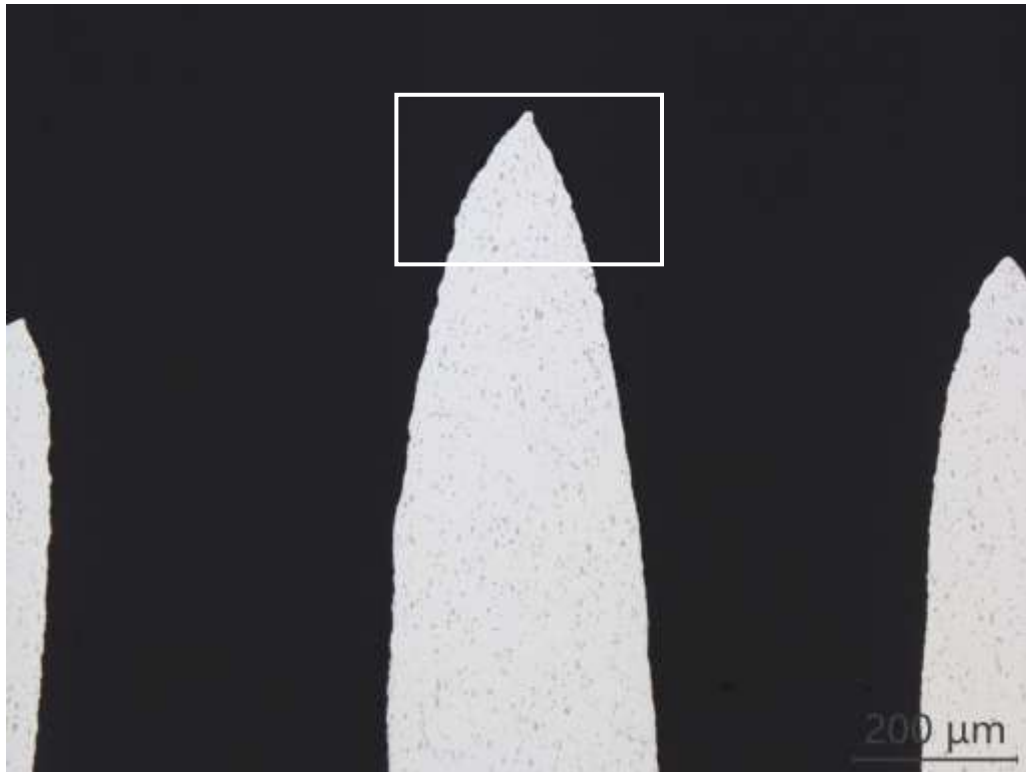


(a) Section S042-C1A1 indicated in Figure 26a



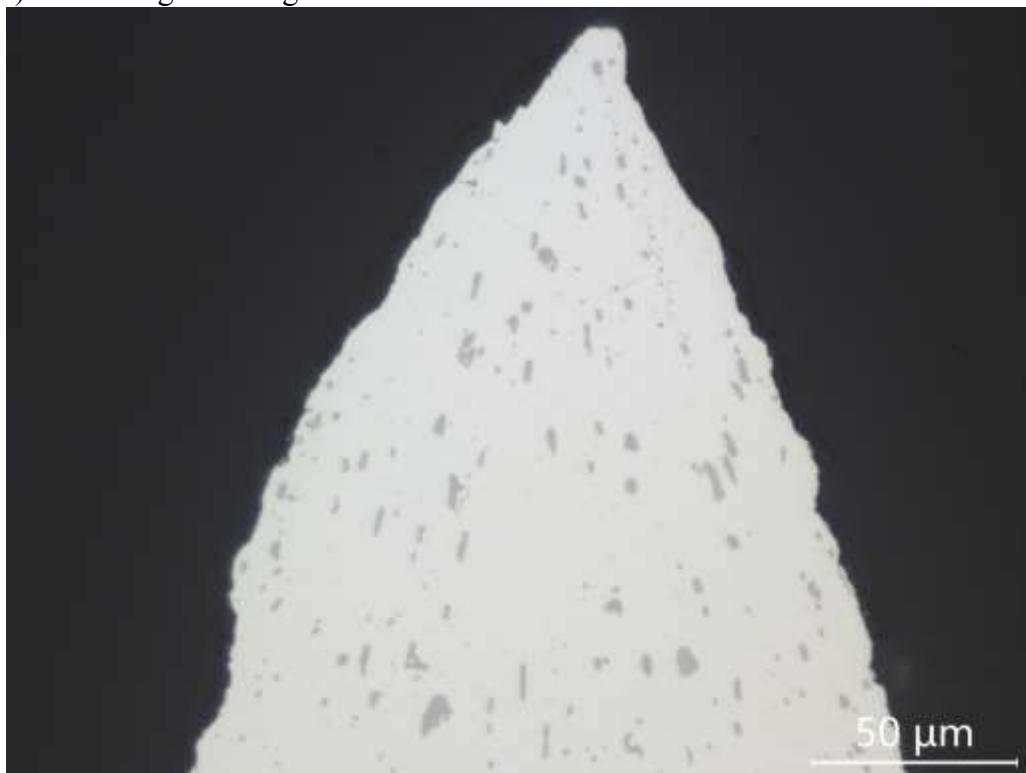
(b) 13X

Figure 29 Images of section S042-C1A1, indicated in Figure 26a, prepared for metallography.



(a) Boxed region in Figure 29b

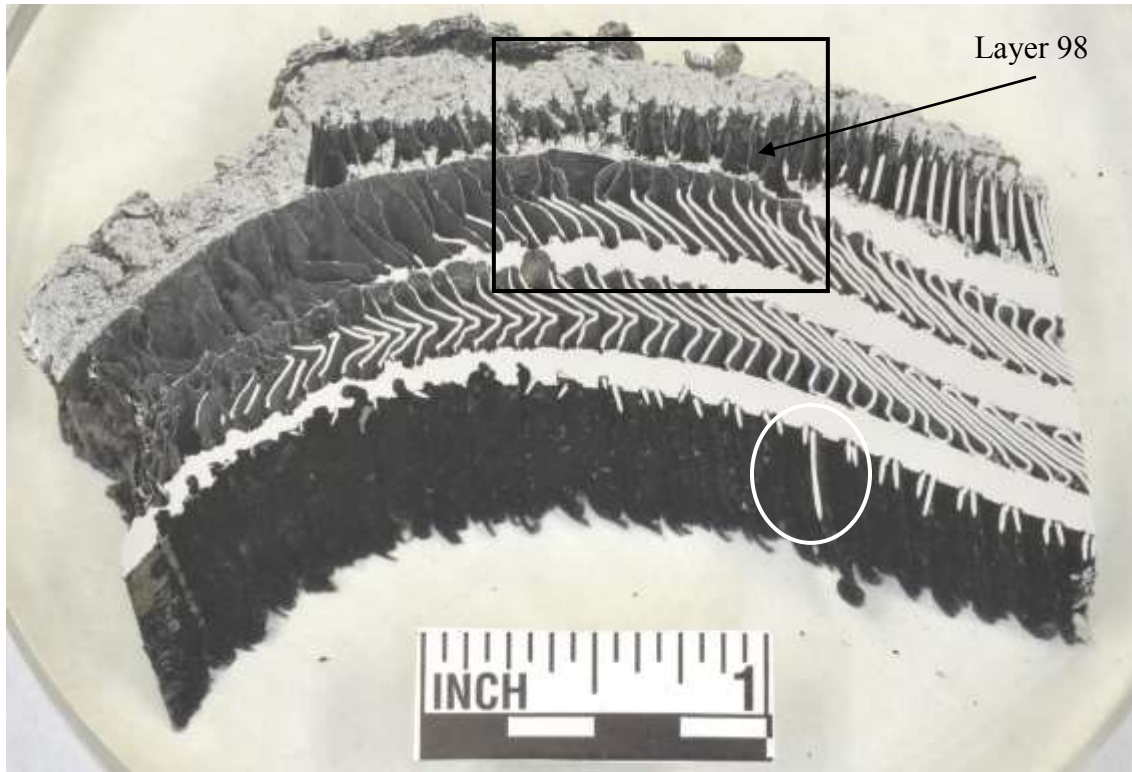
100X



(b) Boxed region in (a)

500X

Figure 30 Micrographs of the end of a fractured fin in section S042-C1A1. Tapered ends of fins indicates ductile fracture.

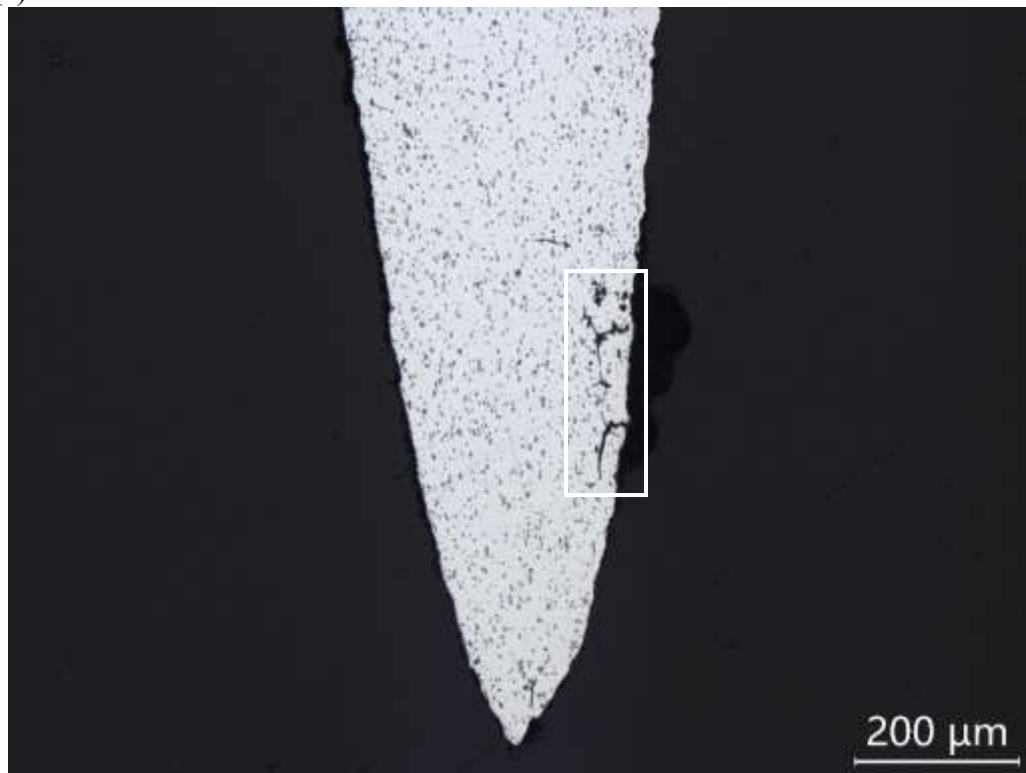
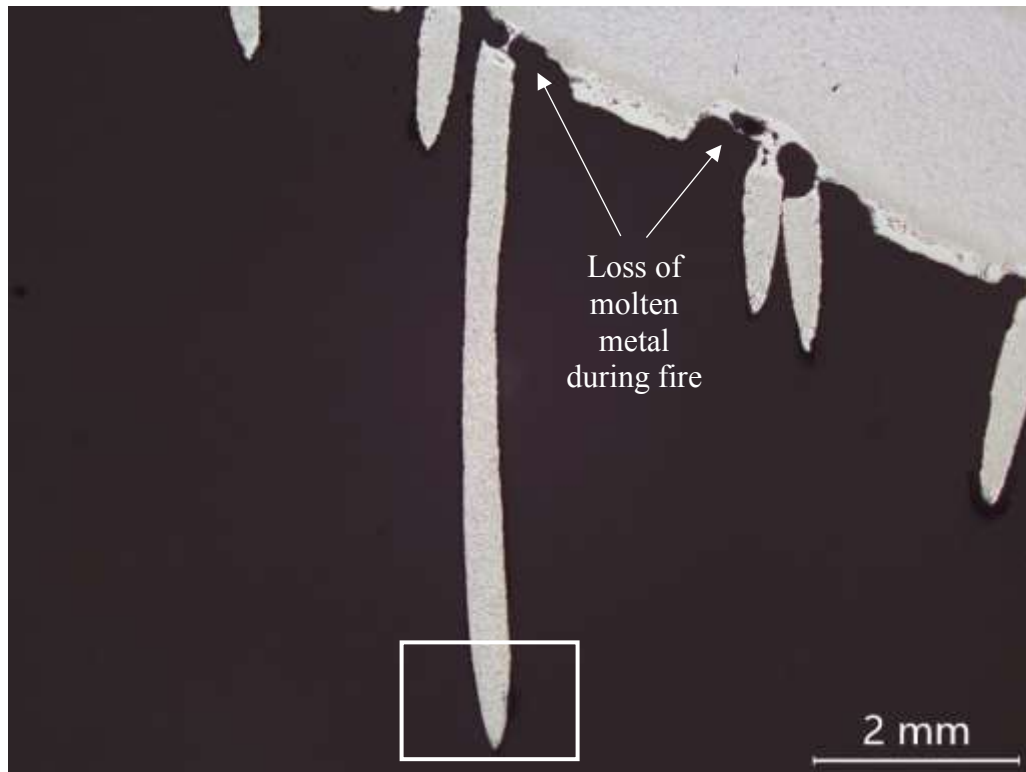


(a)



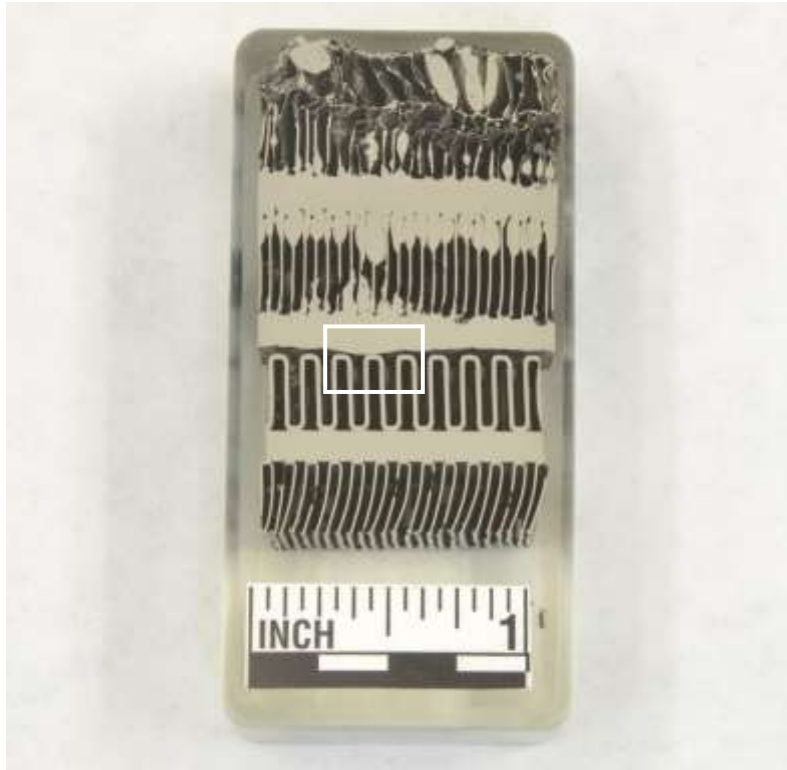
(b) Boxed region in (a)

Figure 31 Images of section S042-C1A7, indicated in Figure 26a. Circled region in (a) is shown in Figure 32. In (b), arrows point to examples of fins that were heat damaged but not buckled.

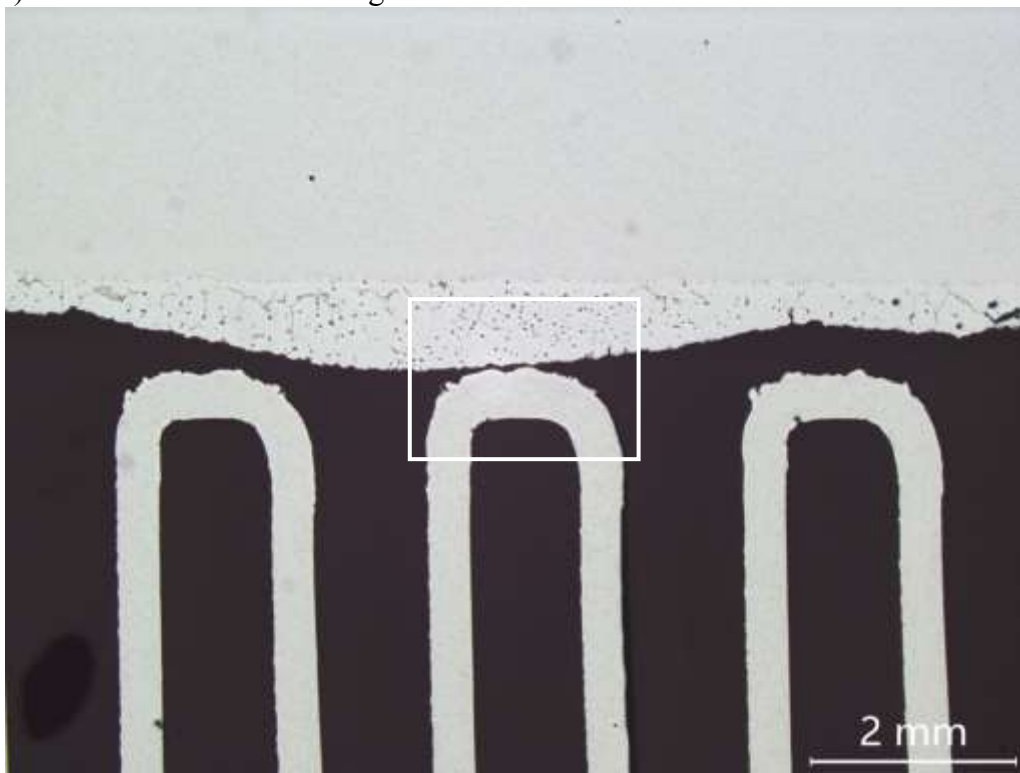


(b) Boxed region in (a)

Figure 32 Images of section S042-C1A7 from the circled region in Figure 31a. The boxed region in (b) indicates evidence of incipient melting.



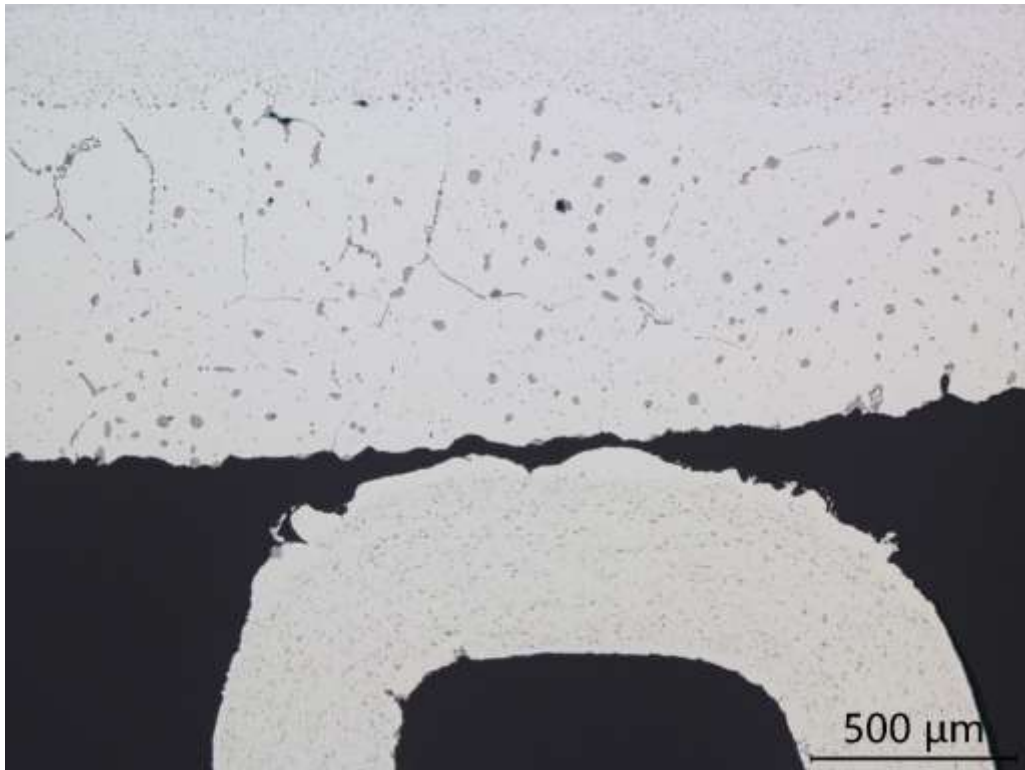
(a) S042-C1B indicated in Figure 26b.



(b) Boxed region in (a)

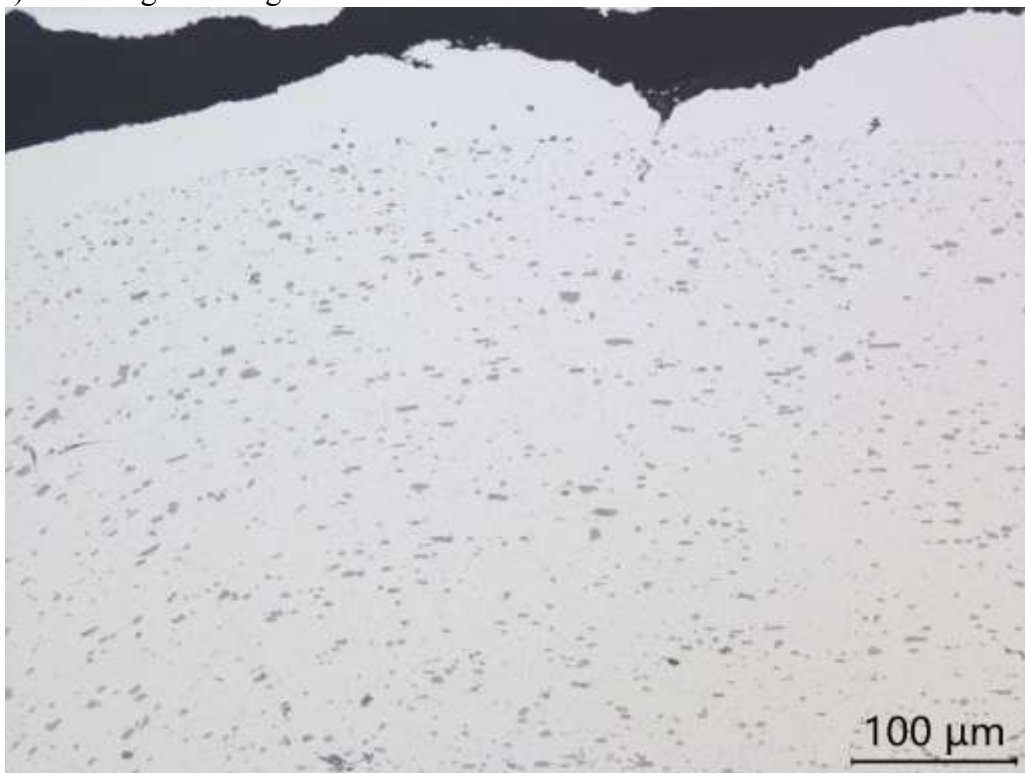
13X

Figure 33 Images of section S042-C1B indicated in Figure 26b.



(a) Boxed region in Figure 33b

50X



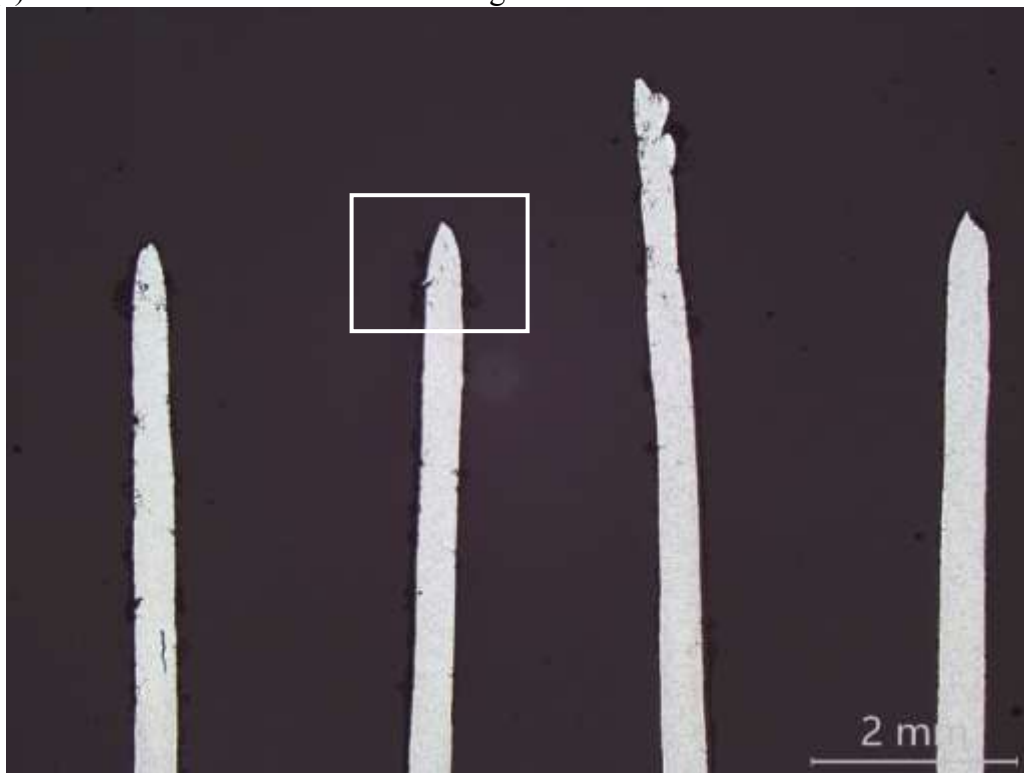
(b) Boxed region in (a)

200X

Figure 34 Micrographs of section S042-C1AB prepared for metallography. In this section of layer 95, the fins had detached from the parting sheet between layer 95 and 96.



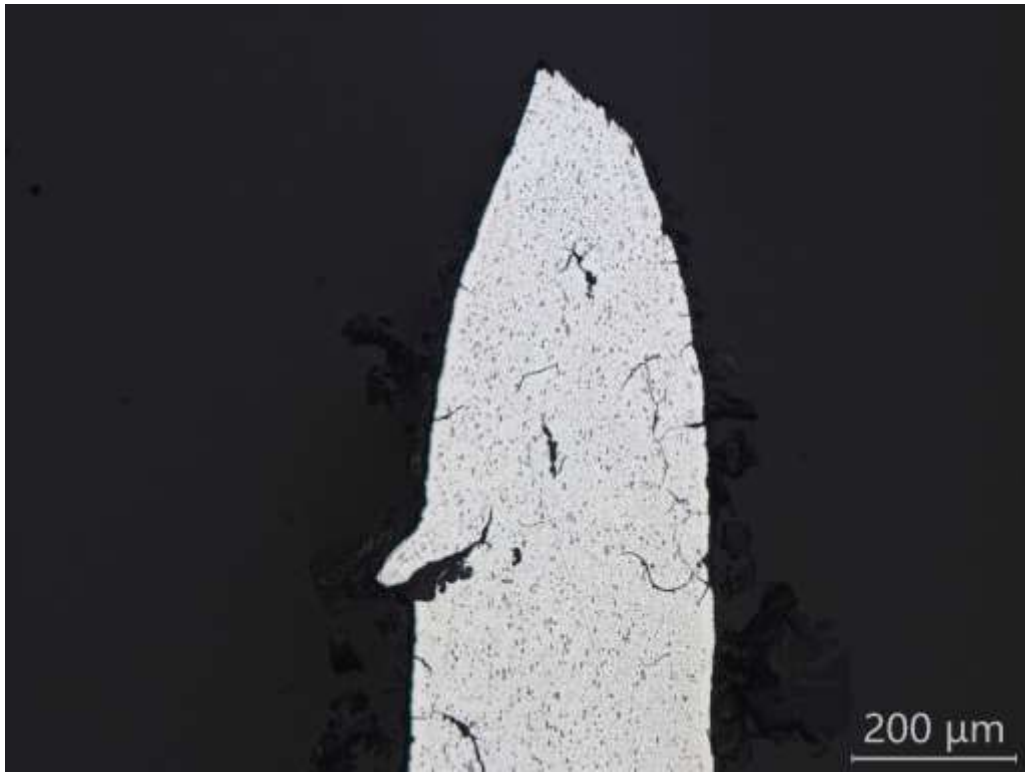
(a) Section S042-C3B1 indicated in Figure 25a



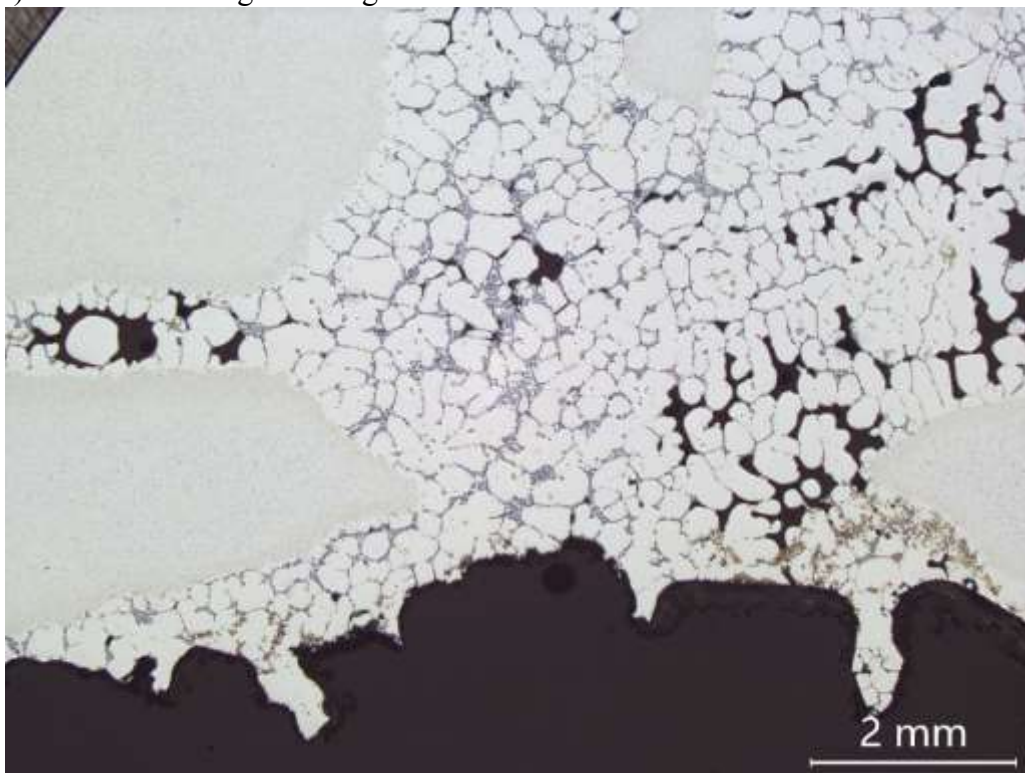
(b) White boxed region in (a)

13X

Figure 35 Images of section S042-C3B1 prepared for metallography.



(a) White boxed region in Figure 35b 100X



(b) Black boxed region in Figure 35a 13X

Figure 36 Micrographs of section S042-C3B1 prepared for metallography.



### 3.7. ACSR S042-B Visual Examination

Sample S042-B was sectioned from the upper north side of the ACSR. A drawing with the sample location indicated, and a photograph of the sample are shown in Figure 37. The majority of the attachment plate had melted off the section during the fire. Remnants of the attachment plate were removed from the sample by cutting approximately 0.5-inch inside the attachment plate edge with a carbide tipped circular saw, and the entire sample was cut with a large horizontal band saw along the dashed lines indicated in Figure 37b. A wide through-cap sheet crack parallel to the inner edge of the side bar was present under the remnants of attachment plate. At the ends of the crack, depressions in the cap sheet were present, consistent with large scale plastic deformation. The crack and depressions are shown in Figure 38.

The cracked section of cap sheet was cut from the sample through layer 99 and the crack was isolated by additional cuts near the crack tips. A remaining cap sheet ligament was broken by hand to reveal the crack surfaces. The crack morphology was macroscopically brittle with the exception of a narrow lip along the outside edge that had fractured by ductile overload. One end of the crack was located under the attachment plate fillet weld. A photograph of the mating crack surfaces is shown in Figure 39. The crack was examined with a stereomicroscope, which revealed a brittle, stepped morphology with progression marks indicative of fatigue crack growth. The crack had initiated on the inside surface of the cap sheet at numerous sites, evidenced by ratchet marks and the local curvature of progression marks, and grown toward the outside surface. Representative low-magnification images are shown in Figure 40. Cap sheet depressions at the ends of the crack and the lip of ductile overload at the outside surface indicated a large plastic strain event, likely the fire, widened the crack. It is possible the crack was not open to the surface beneath the attachment plate until the heat of the fire caused sufficient thermal strain to open the crack.

Parting sheets between layers 96-97, 97-98, and 98-99 were sectioned from below the through-cap sheet crack. Low-power optical examination of the parting sheets indicated a crack in the layers 98/99 parting sheet. While attempting to isolate part of the indicated crack, the crack opened by bending about the crack tip, leaving the two mating surfaces joined by a ductile hinge. The crack had initiated on the layer 99 side of the parting sheet, in the corner formed by the side bar and had propagated approximately half-way through the sheet. Low-power optical microscopy revealed the fatigue crack characteristics of macroscopically brittle crack growth, ratchet marks, and progression marks. Images of the section and part of the crack are shown in Figure 41.

### 3.8. ACSR S042-B Scanning Electron Microscopy (SEM)

Sections of the through-cap sheet crack and the layer 98/99 parting sheet crack were examined by SEM. Both cracks were covered with oxide, likely as a result of the fire, that reduced the image quality. However, progression marks and remnants of striations caused by fatigue were present on both crack faces. Fine detail of the fatigue striations was predominantly obscured or destroyed by the oxide. Progression marks are features that indicate the position of the crack front at different points in time.

Fatigue progression marks indicate changes in the stress/strain amplitude that is driving the fatigue crack propagation. For example, a change from low stress/strain amplitudes with a steady crack growth rate to a higher stress/strain amplitude can be indicated on the crack surface by a progression mark. Fatigue striations indicate individual crack growth increments. In many regimes of



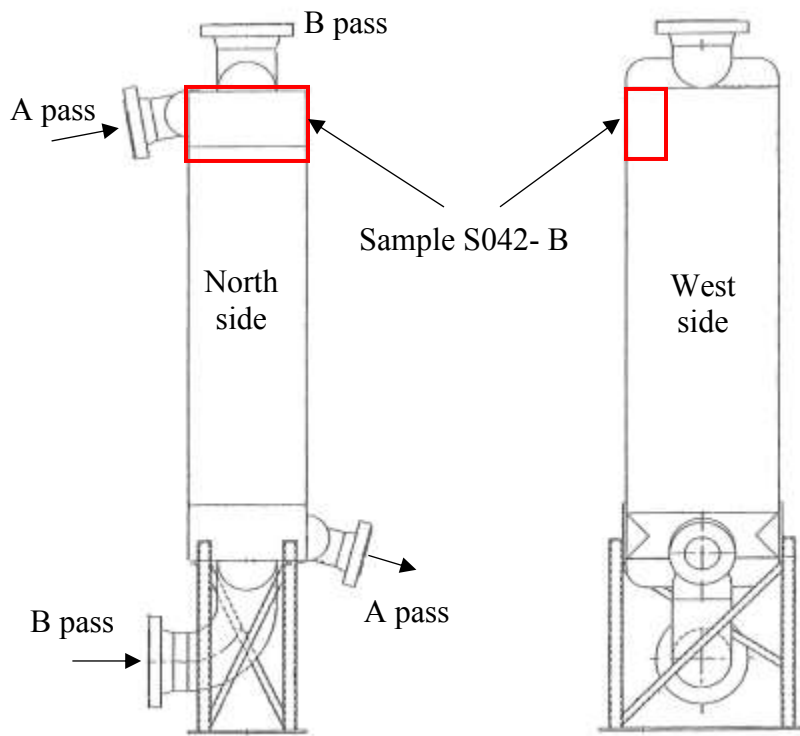
stress/strain amplitude and frequency, each striation correlates to a stress/strain cycle. Example micrographs of the cracks are shown in Figure 42 and Figure 43.

### **3.9. ACSR Sample S042-B Metallography**

Sections of sample S042-B were prepared for metallography by embedding in clear epoxy, grinding wet with SiC metallurgical papers, and polishing with 9-micron diamond through 0.05-micron colloidal silica. The specimens were examined as-polished and after etching with Graff-Sargent reagent. All of the micrographs shown here are of the etched condition.

Low-power optical microscopy of the layers 97/98 parting sheet indicated a crack in the layer 97 side, located in the corner formed by the side bar. To investigate the indication, a section through the region was prepared for metallography and a small crack was found. Similarities in location between the small crack and larger cracks examined by SEM, indicated the crack was caused by fatigue. The crack was wide, indicating large plastic strains were applied after the crack had grown to the length shown. Narrow crack branches indicate the likely width of the main crack before it was widened (blunted) by plastic strains. Photographs and micrographs of the section are shown in Figure 44.

Two spot welds were present on the west side of sample S042-B. The spot welds were cut from the larger sample, shown in Figure 46. Sections through the spot welds demonstrated that holes had been drilled in sidebars to layers 98 and 99, and the holes had been spot welded closed. These types of holes can be made for a number of reasons, one of which is leak testing whereby the hole is monitored for gas introduced into an adjacent layer. A photograph and micrographs of a specimen through the layer 98 spot weld prepared for metallography are shown in Figure 48 and Figure 49. The spot weld had a dendritic structure typical of weld metal and semi-quantitative energy dispersive x-ray spectroscopy indicated the composition of the weld metal was consistent with alloys used to weld 3003 aluminum.



(a)



(b)

Figure 37 Simplified drawing of the ACSR with the location of sample S042-B indicated, and a photograph of the sample. Most of the attachment plate had been melted. Dashed lines indicate cuts made with a horizontal band saw. Boxed region is shown in Figure 38.

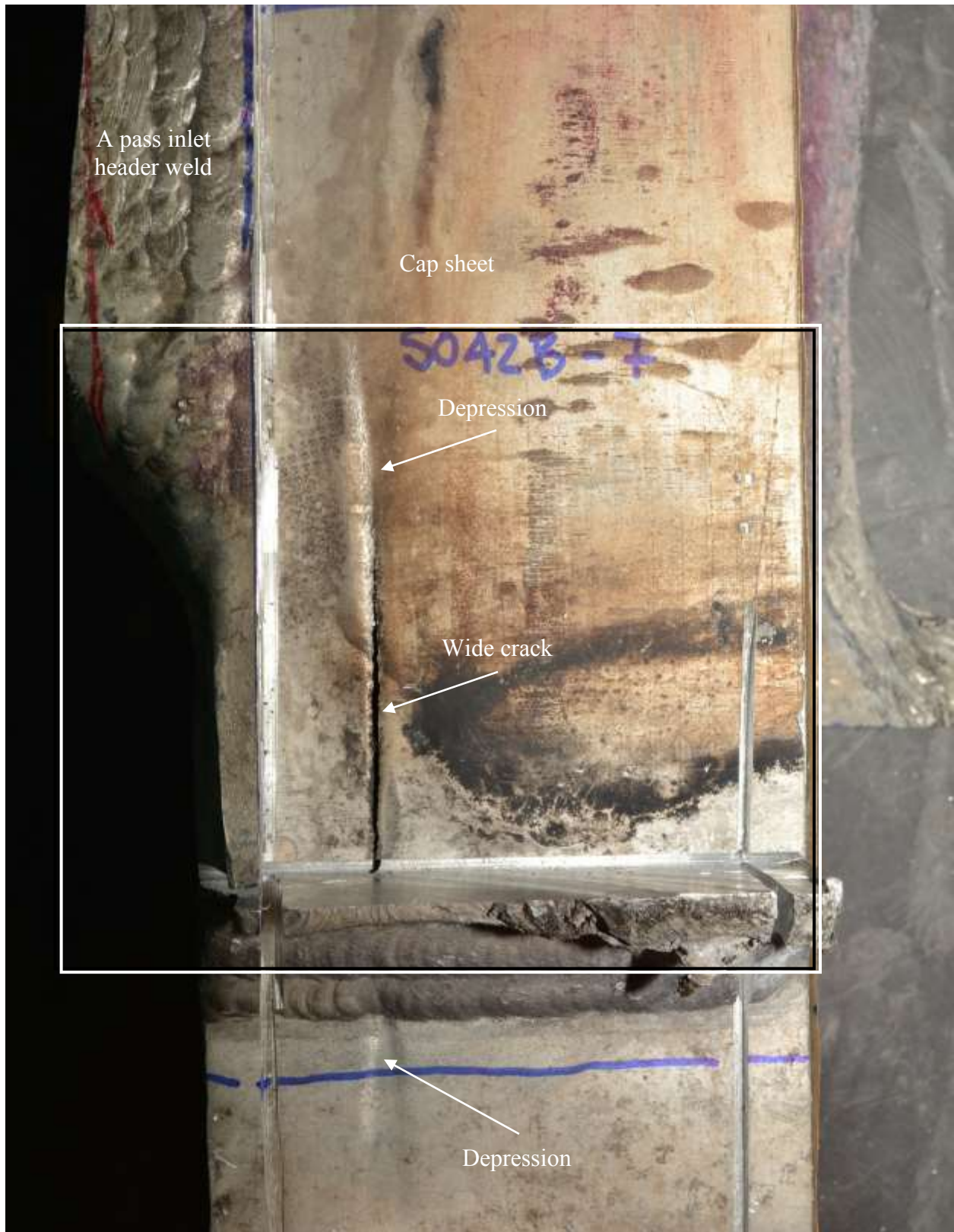


Figure 38 Photograph of S042-B after remnants of the attachment plate had been removed and the sample was cut into three pieces. Area shown is boxed region in Figure 37. A wide through-cap sheet crack and depressions at the ends of the crack are indicated.

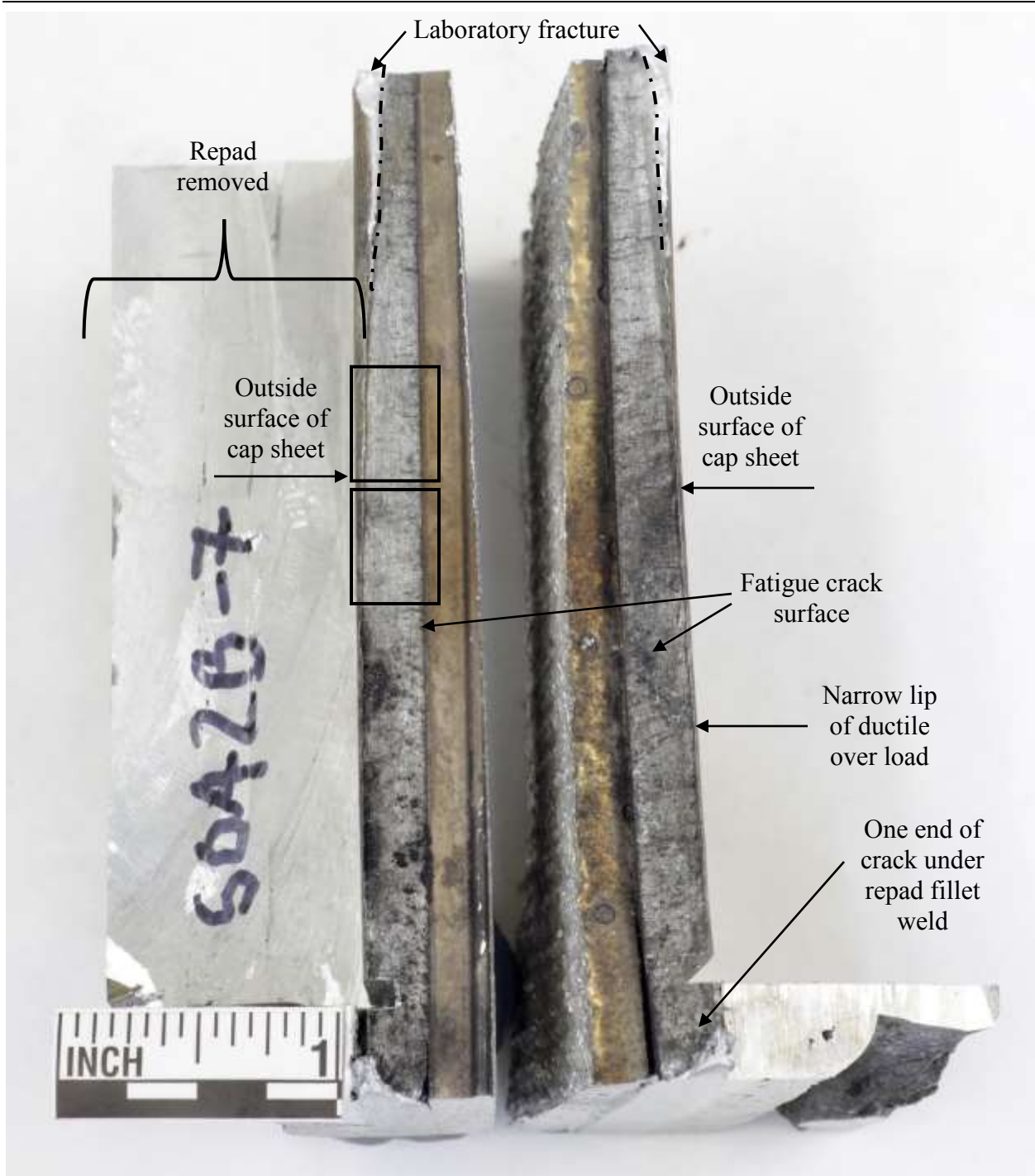


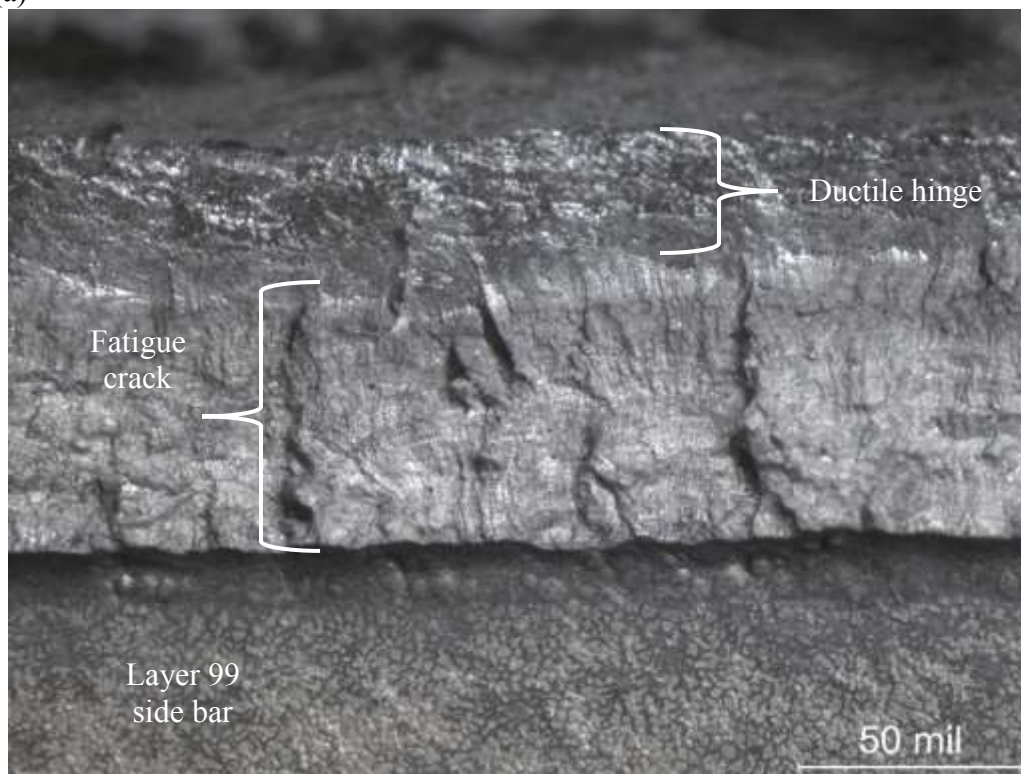
Figure 39 Photograph of the sample S042-B-7 cap sheet mating crack surfaces. Cut from the boxed region in Figure 38.



Figure 40 Images of the sample S042-B-7 cap sheet crack taken from the boxed locations in Figure 39. The specimen was rotated 90° from the orientation in Figure 39.

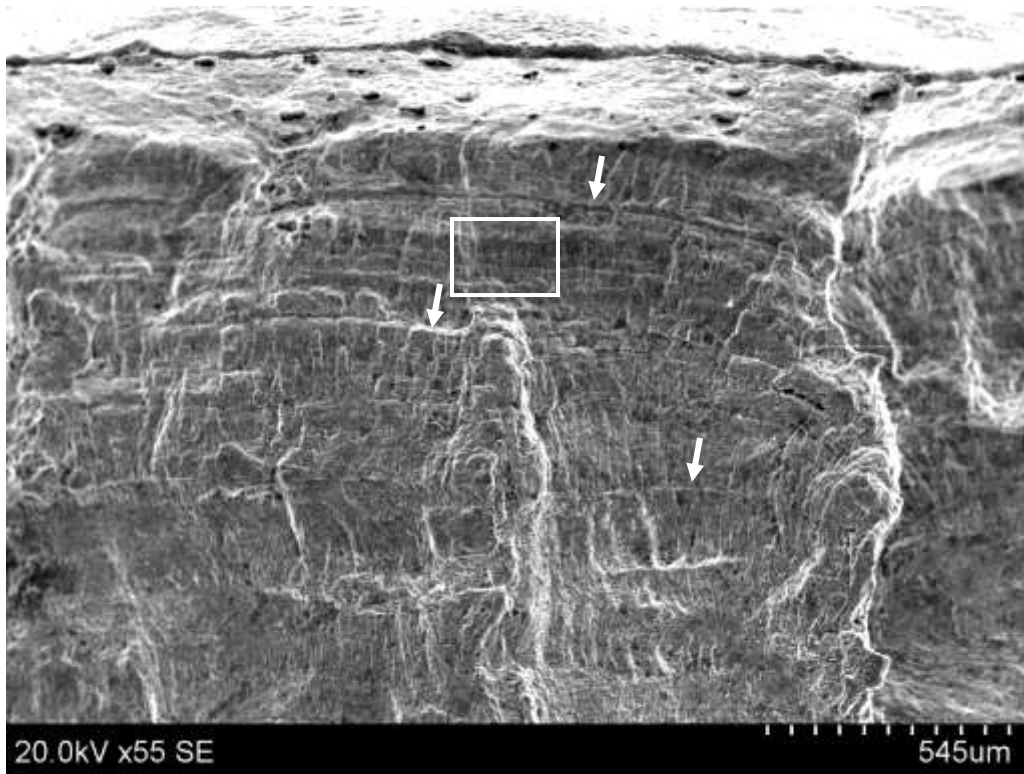


(a)

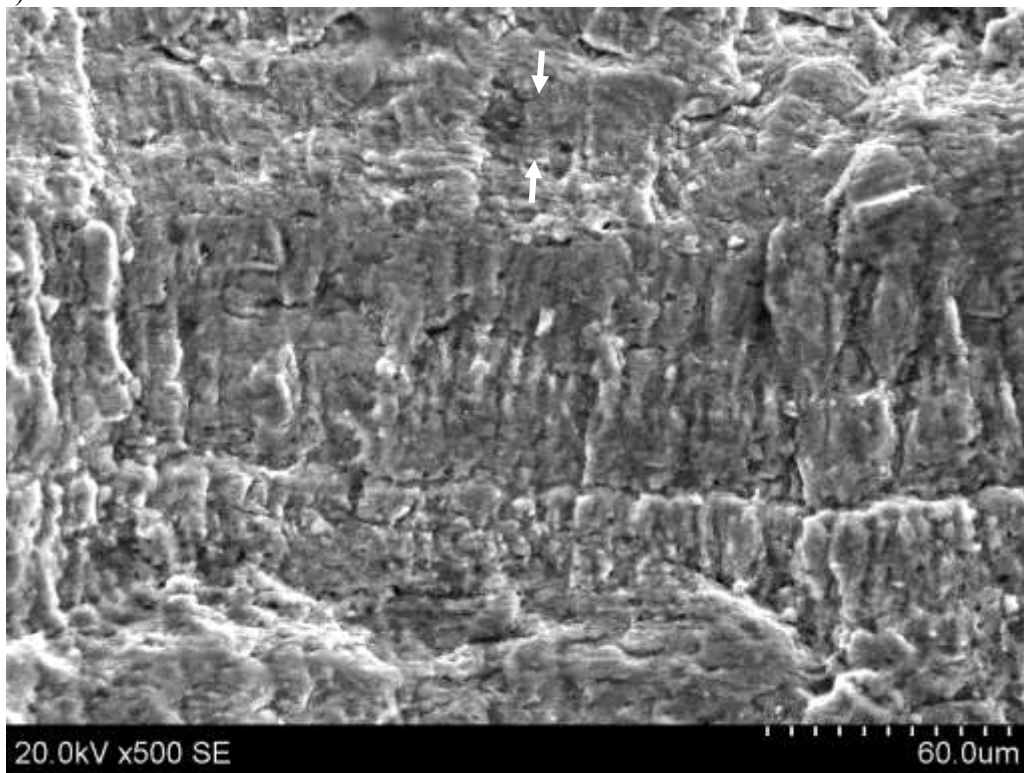


(b) Boxed region in (b), rotated 90°

Figure 41 Images of the sample S042-B-7 parting sheet between layer 98 and 99.

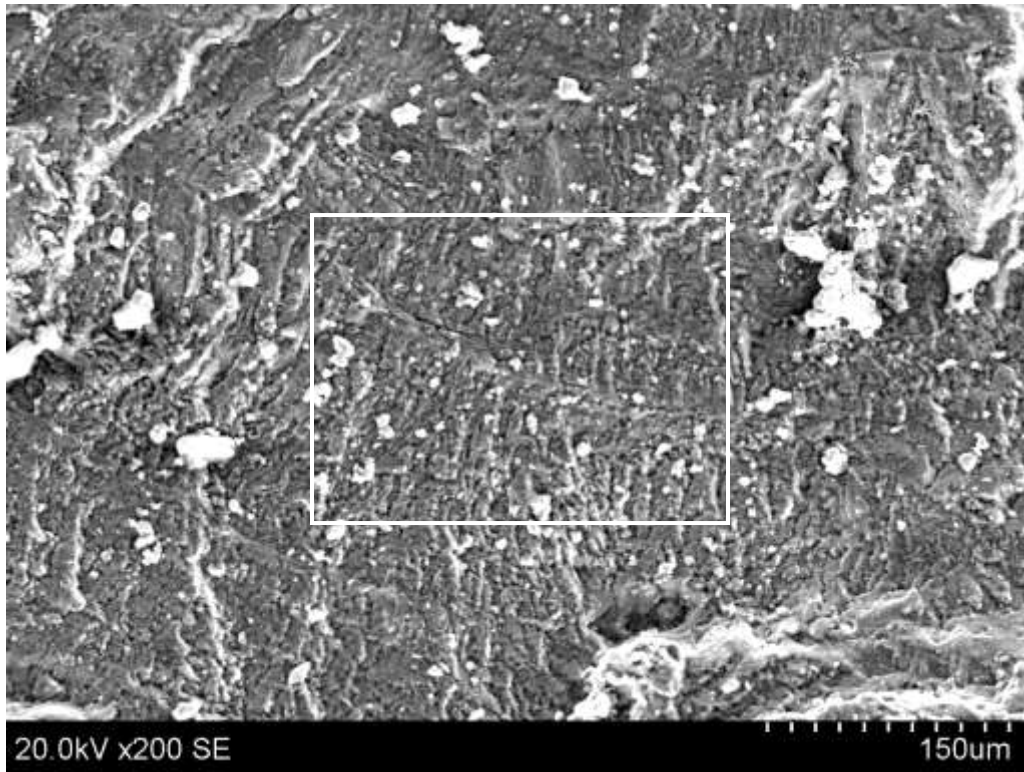


(a)

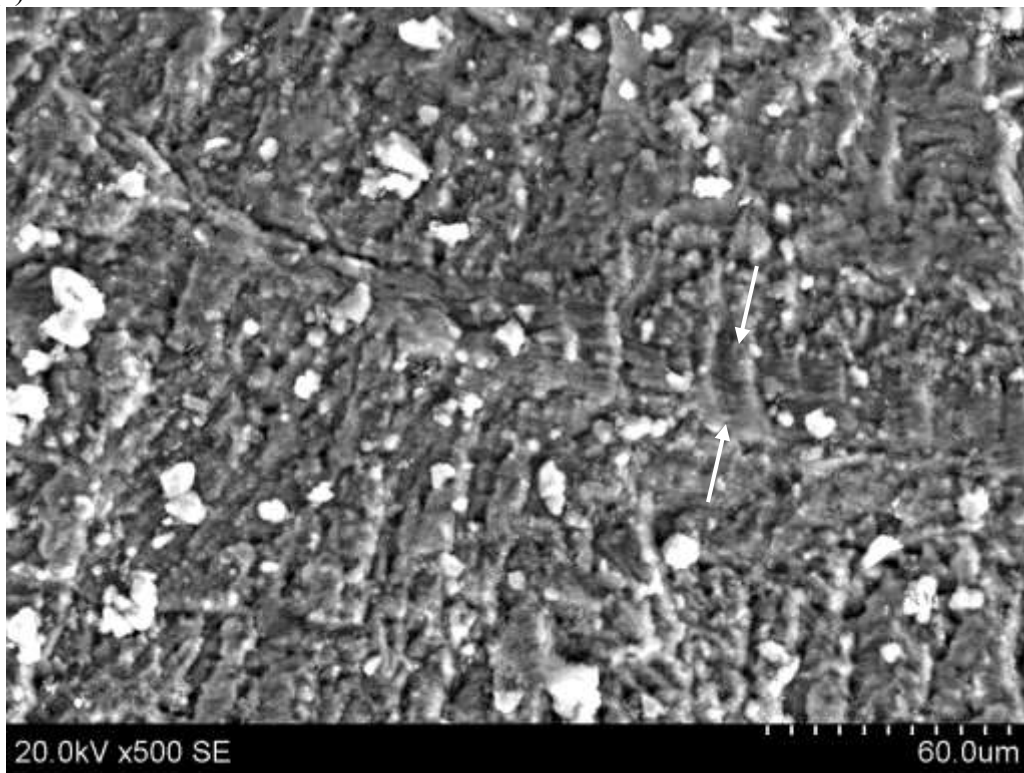


(b) Boxed region in (a)

Figure 42 SEM micrographs of the fatigue crack surface in the sample S042-B-7 cap sheet. In (a), arrows point to examples of progression marks. In (b) arrows bracket striations degraded by oxide layer.

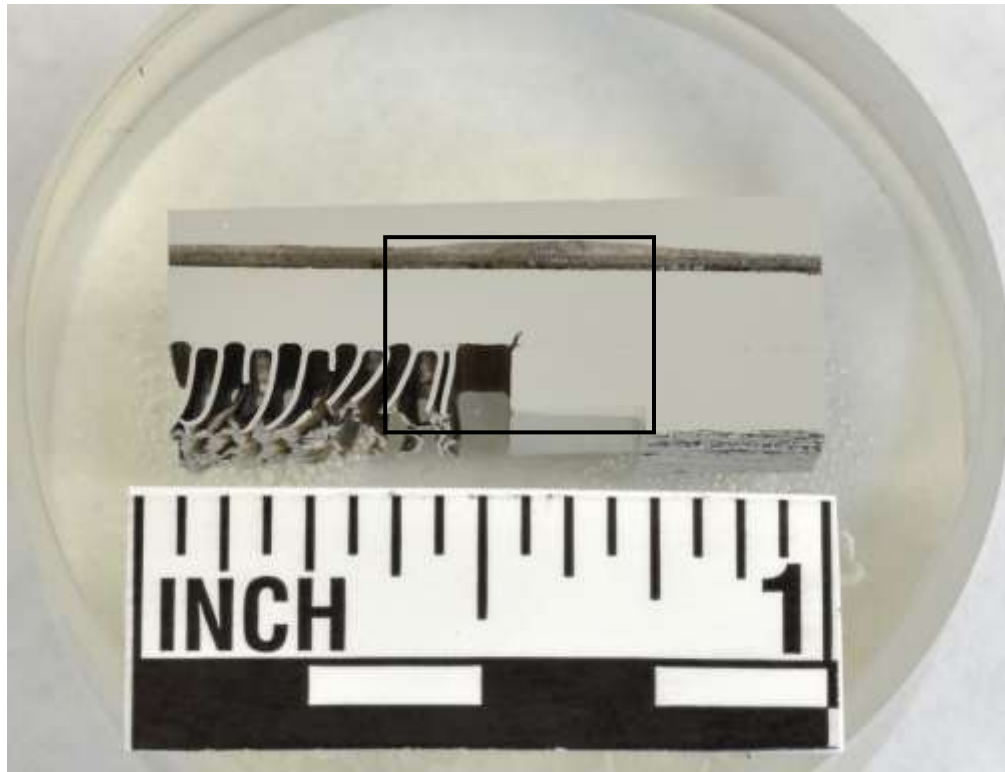


(a)

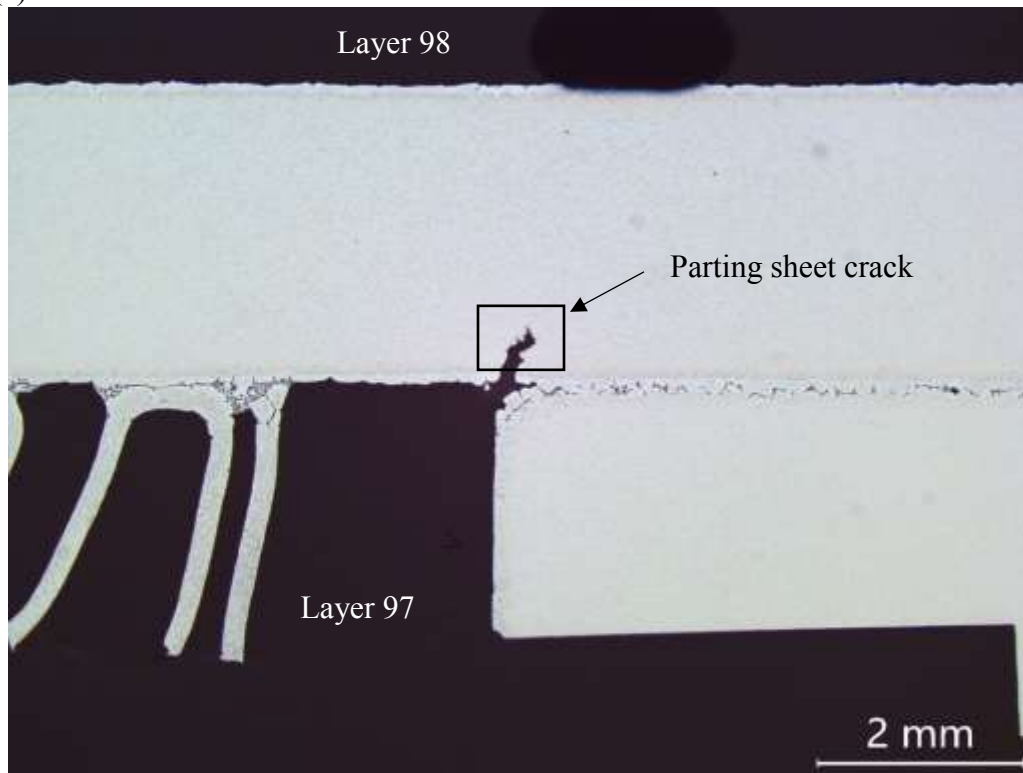


(b) Boxed region in (a)

Figure 43 SEM micrograph of the S042-B-7 parting sheet crack that initiated on the layer 99 side. Arrows in (b) bracket approximately ten fatigue striations.



(a)



(b) Boxed region in (a)

13X

Figure 44 Images of section S407-B-7 parting sheet between layers 97 and 98 prepared for metallography.



Figure 45 Optical micrographs of crack in sample S042-B-7 parting sheet between layer 97 and 98, boxed region in Figure 44b. Arrows indicate small crack branches that were not opened when the main crack was blunted by plastic strains.

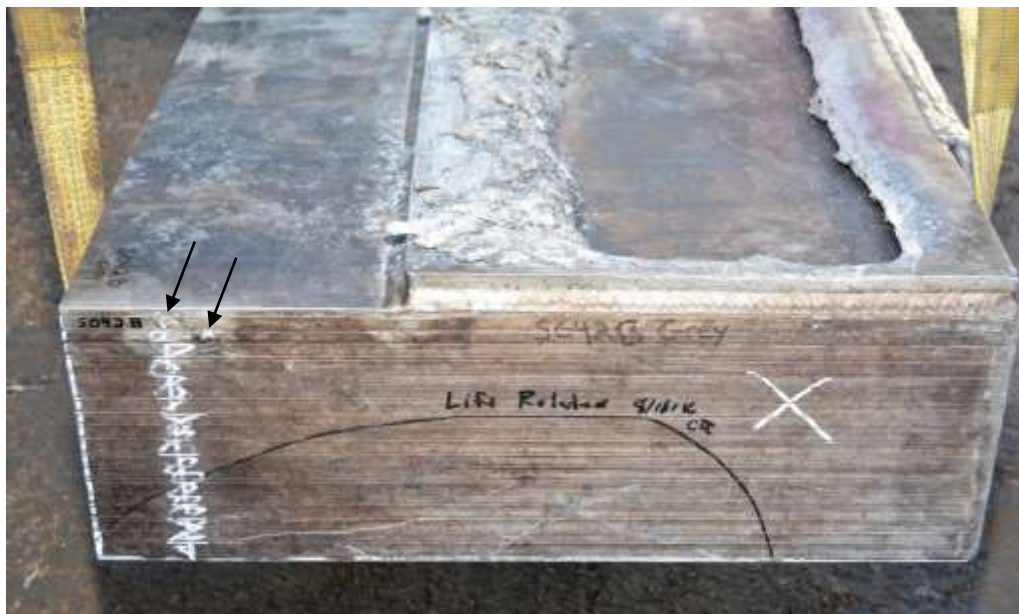
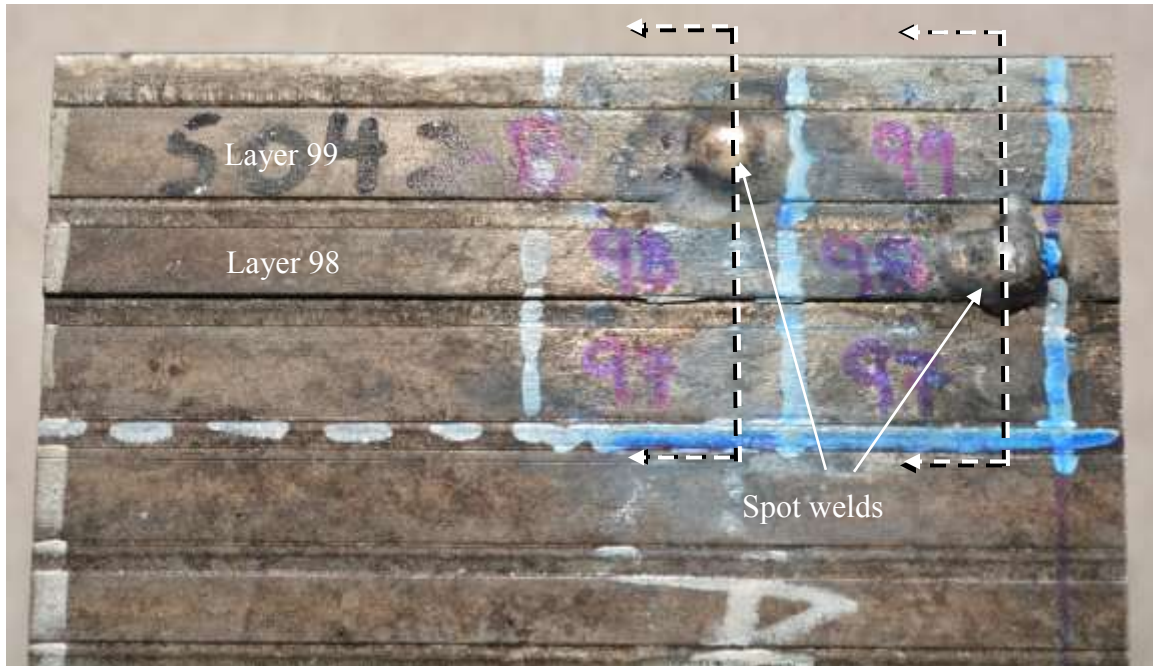
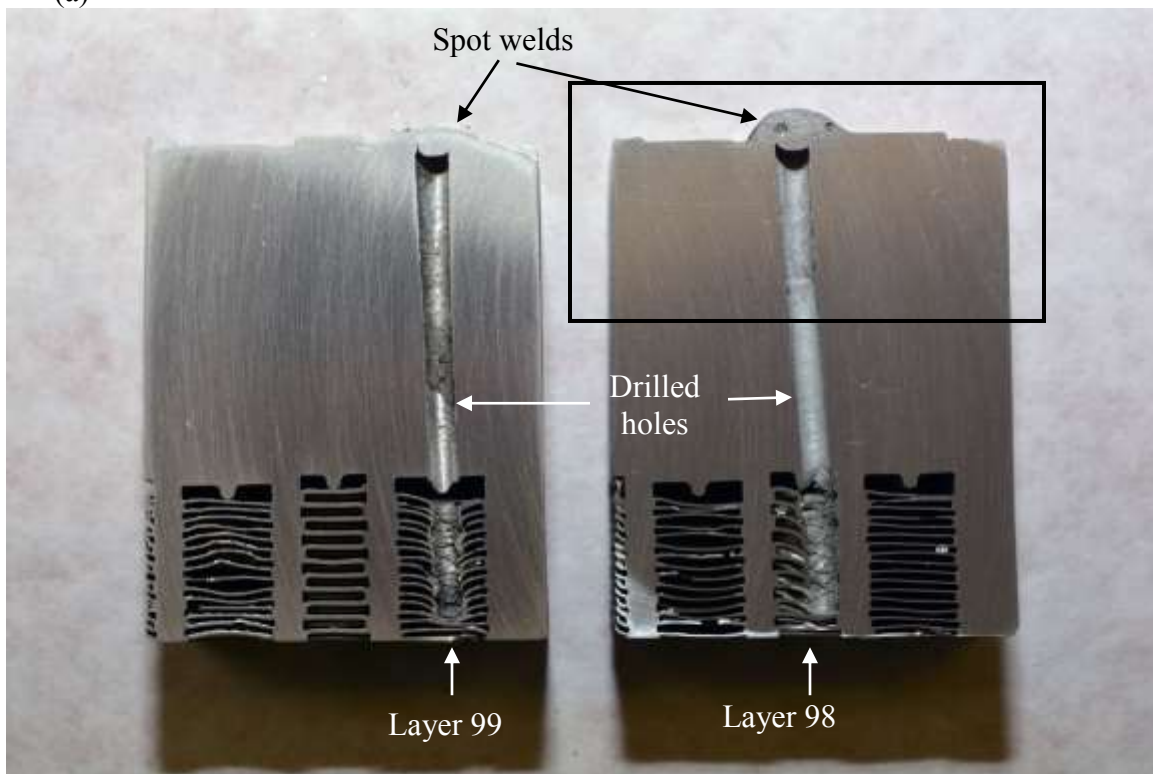


Figure 46 Photograph of the west side of sample S042-B. Arrows point to two spot welds located on side bars of layers 98 and 97.

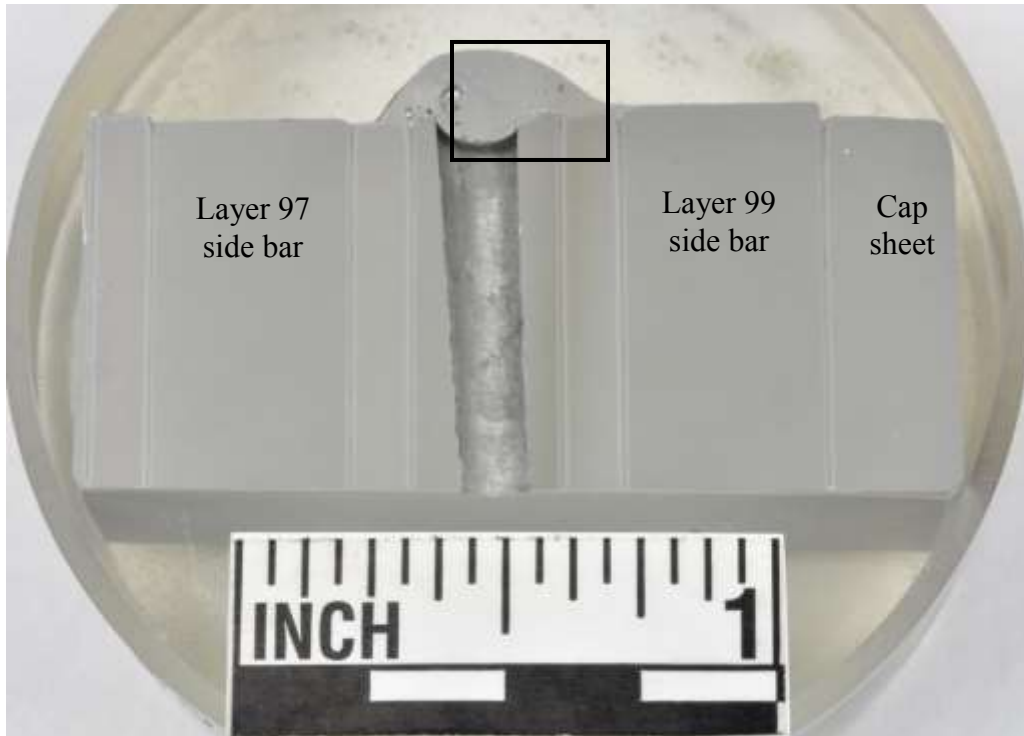


(a)

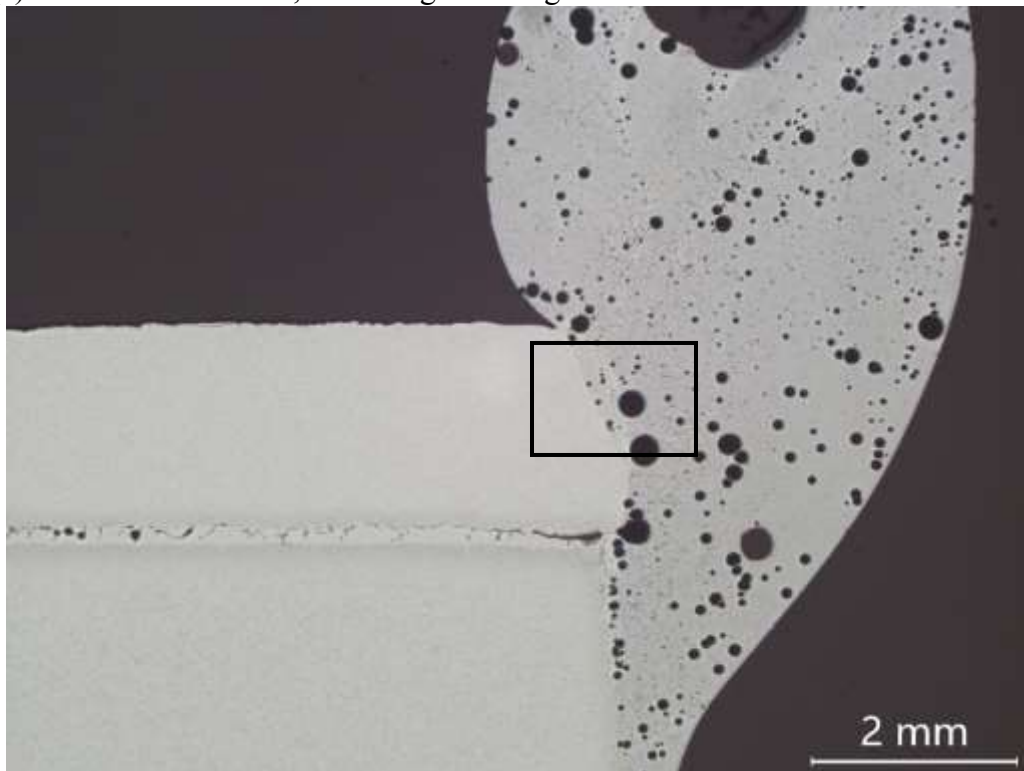


(b) Sections indicated in (a)

Figure 47 Photographs of the S042-B spot welds and sections through the spot welds. Boxed region in (b) was prepared for metallography.



(a) Section S042-B-1A, boxed region in Figure 47b



(b) Boxed region in (a), specimen rotated 90° from the orientation in (a) 13X

Figure 48 Photograph and micrograph of spot weld section S042-B-1A prepared for metallography. Boxed region in (b) shown in Figure 49.



Figure 49 Micrograph of the boxed region in Figure 50b.



### 3.10. ACSR S042-D1 Visual Examination

Sample S042-D1 was cut from the top, south side of the ACSR. The sample included the full width of the reboiler, extended from the B pass outlet header weld to approximately 6-inches below the attachment plate, and contained the layer 1/2 parting sheet, cap sheet, and attachment plate. A simplified drawing with the location of sample S042-D1 indicated, and a photograph of the sample are shown in Figure 50. The sample was in good condition visually. The CSB reported that during leak testing before the reboiler was cut into samples, an interpass leak had been detected between layers 1 and 2. The leak location was marked on the outside of the sample, shown in Figure 51, although the leak itself was internal.

The attachment plate was removed from sample S042-D1 by milling a continuous slot approximately 0.5-inch inside of the edge of the attachment plate. With the attachment plate removed, visual examination and visible dye penetrant testing (PT) was performed on the cap sheet. No crack indications were detected. Both sides of the sample were cut approximately 4-inches inboard of the outer edges with a band saw. Visual examination of the layer 2 side of the parting sheet was performed where gaps in the fin sheets exposed the parting sheet. A crack in the corner formed by the west side was found that corresponded to the interpass leak location, indicated in Figure 52. The visible crack path tended to follow interdendritic regions of the parting sheet braze alloy. Low-power optical images of the crack are shown in Figure 53.

A transverse section through the visible crack was ground wet through 600-grit silicon carbide metallurgical paper. A through-parting sheet crack was visible in the section, and a small cap sheet crack was also present. The through-parting sheet crack face was exposed by cutting the layer 1 fins just below the cap sheet and easily breaking a small remaining ligament of the parting sheet by hand. Images of the section and exposed parting sheet crack surface are shown in Figure 54. The crack face was examined with low-power optical microscopy and found to have a brittle morphology with progression marks indicative of fatigue cracking and multiple crack initiation sites on the layer 1 side of the parting sheet. Oxide coated the crack surface, and was resistant to scrubbing with a soft bristle brush and soapy water. Images of the crack face are shown in Figure 55.

A shallow depression on the outside surface of the cap sheet, aligned with the inside edge of the west side bar was investigated by cutting a transverse section. A near through-cap sheet crack that had initiated on the inside surface was found in the section. The crack surface was exposed by cutting through the layer 1 fins and breaking the remaining ligament by hand. The crack morphology was brittle, with progression marks and ratchet marks that indicated fatigue cracking had initiated at numerous locations on the inside surface of the cap sheet. Oxide was present on the crack surface, and was resistant to scrubbing with a soft bristle brush and soapy water. Images of the section and crack surface are shown in Figure 56 and Figure 57.

A crack was visible in the west corner of the attachment plate lower edge fillet weld. A leak test performed during this evaluation indicated the crack extended through the fillet weld. As shown in Figure 58, the crack path closely followed the plane of the cap sheet and extended from the toe of the fillet weld through the root of the weld. Examination of the fillet weld crack indicated that it intersected an extension of the cap sheet crack in section S042-D1-1D-1.



### **3.11. ACSR Sample S042-D1 Scanning Electron Microscopy (SEM)**

Scanning electron microscopy was performed on the through-parting sheet crack, cap sheet crack, and attachment plate fillet weld crack described in Section 2.10. Both the parting sheet crack and cap sheet crack surfaces had fatigue morphologies that included crack progression marks and remnants of fatigue striations covered with oxide. Fine detail of fatigue striations was obscured or destroyed by the oxide. As described in Section 2.8, fatigue progression marks indicate changes in the stress/strain amplitude that is driving the fatigue crack propagation. For example, a change from low stress/strain amplitudes with a steady crack growth rate to a higher stress/strain amplitude can be indicted on the crack surface by a progression mark. Fatigue striations indicate individual crack growth increments. In many regimes of stress/strain amplitude and frequency, each striation correlates to a stress/strain cycle. Micrographs of the parting sheet and cap sheet crack surfaces are shown in Figure 59 and Figure 60.

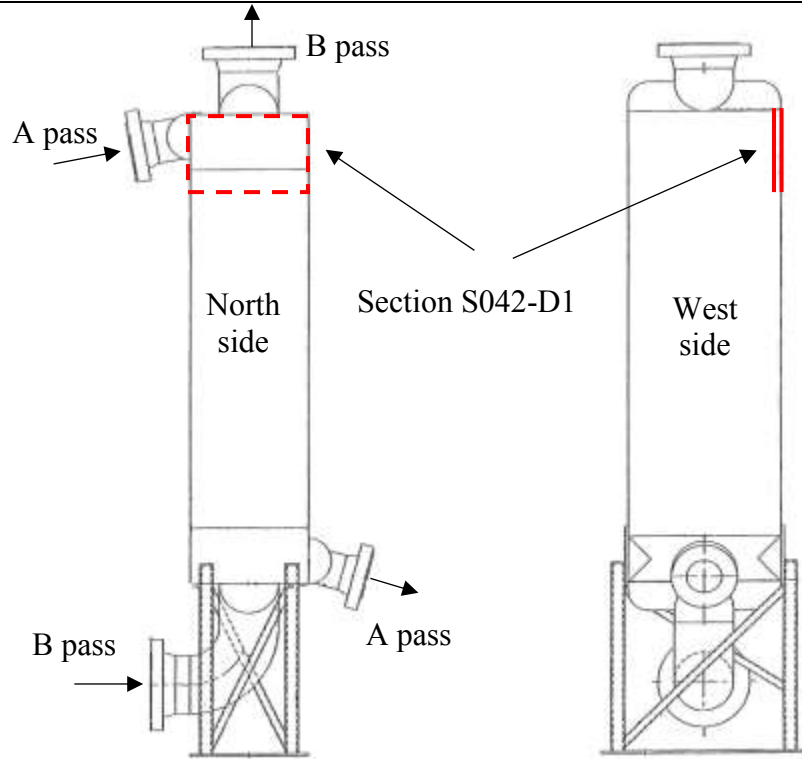
Ductile overload morphology with a strong shear component evidenced by elongated dimples was present on the attachment plate fillet weld crack surface. Based on the general orientation of the dimples, overload was generated by thermal stresses that developed between the attachment plate and the core of the ACSR. Representative SEM micrographs of the fillet weld crack surface are shown in Figure 61. These micrographs were taken directly through the wide crack opening.

### **3.12. ACSR Sample S042-D1 Metallography**

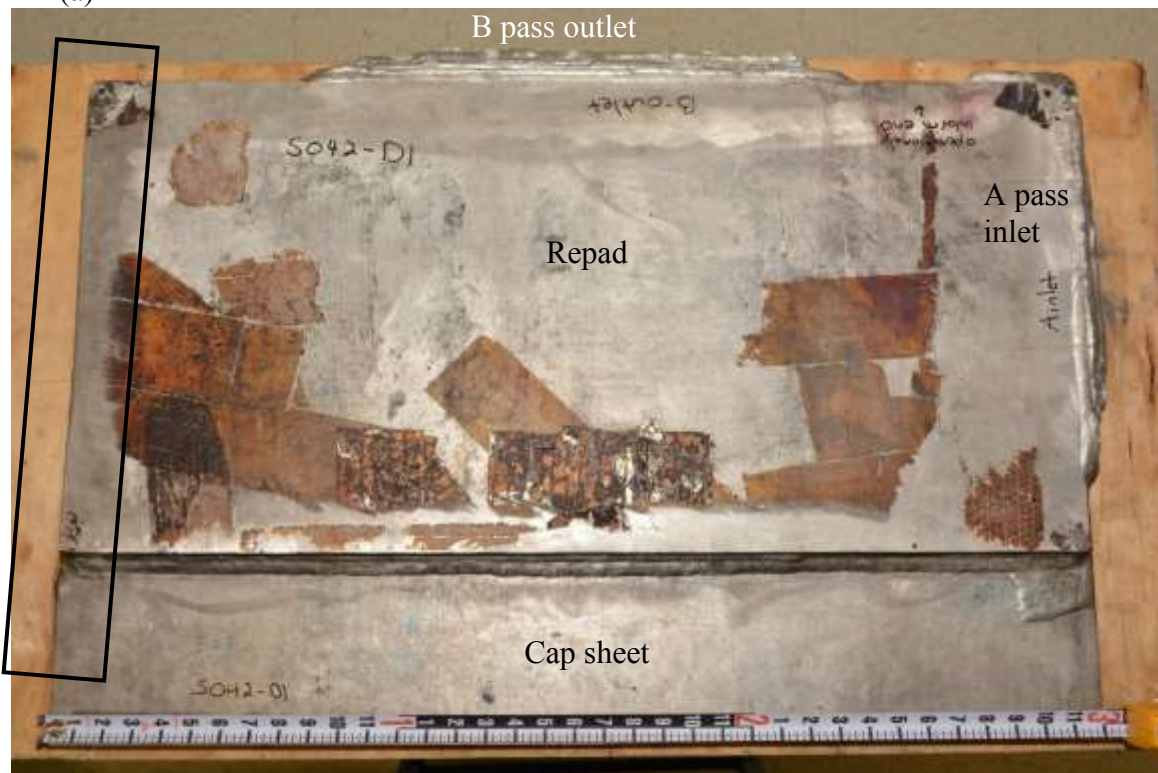
Sections through sample S042-D1 were prepared for metallography by embedding in clear epoxy, grinding, and polishing from 9-micron diamond through 0.05-micron colloidal silica using common metallographic techniques. The specimens were examined as-polished and after etching with Graff-Sargent reagent. All of the micrographs shown here are of the etched condition.

Photographs and micrographs of the sections are shown in Figure 62 through Figure 65. All of the main cracks in these sections had been widened (blunted) by plastic strain. The predominantly uniform width of the individual cracks, indicated that a single strain event was responsible for the widening. Crack branches and cracks that were outgrown by neighboring cracks were narrow, consistent with high cycle fatigue cracks. These narrow cracks represent the character of the wide cracks before the plastic strain event, most likely the fire, caused larger than normal stresses and strains in the ACSR.

Micrographs of a section through the attachment plate fillet weld revealed elongated dimples consistent with the SEM micrographs of the same crack. The overload crack intersected the cap sheet crack, which created a leak path from the B pass layer 1 to atmosphere. However, it is possible that this leak path only existed after the large strain event that created the weld crack. A photograph and micrographs of the weld crack specimen are shown in Figure 66.

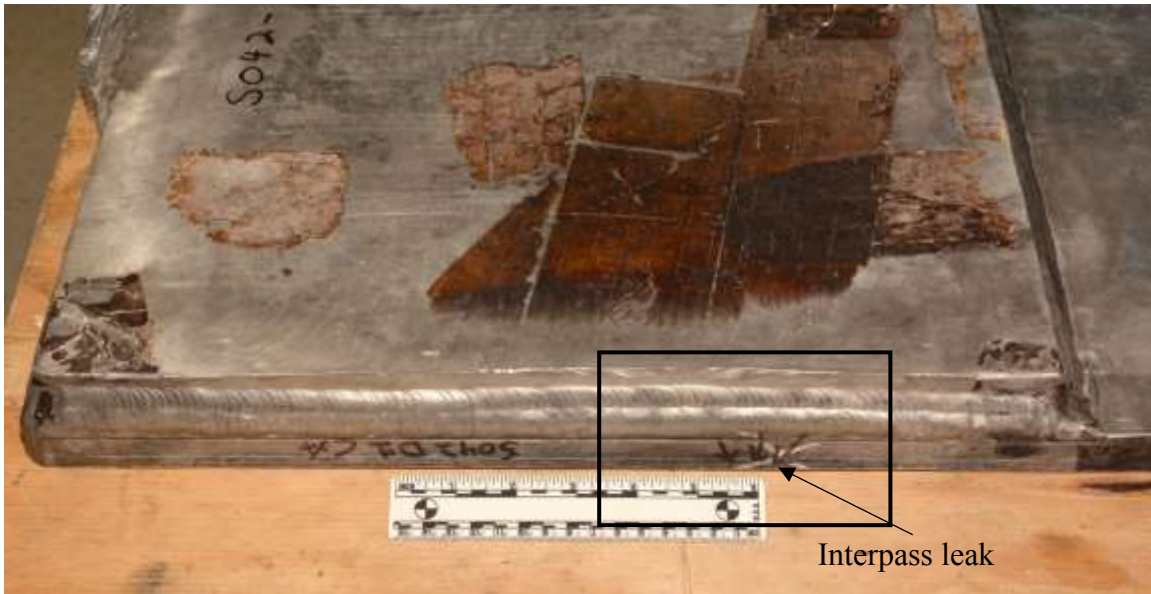


(a)



(b)

Figure 50 Simplified drawing of the ACSR and photograph of sample S042-D1-1D. The boxed region in (b) is shown in Figure 51.

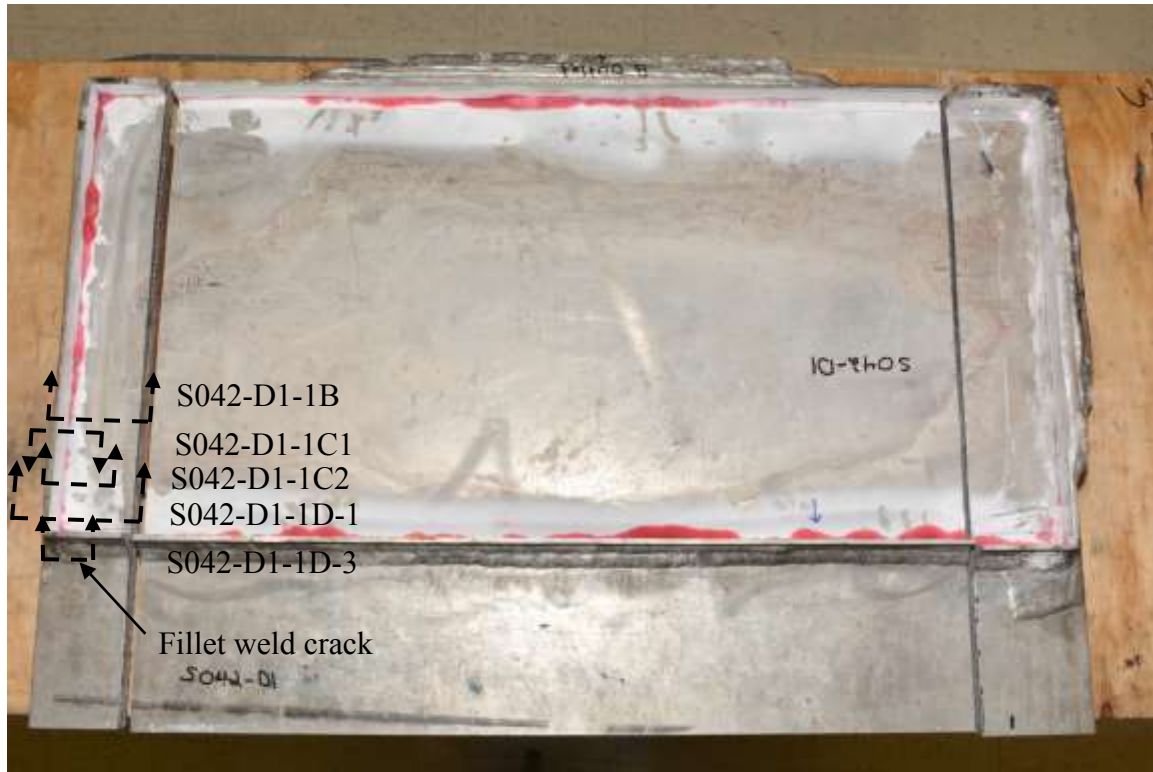


(a)

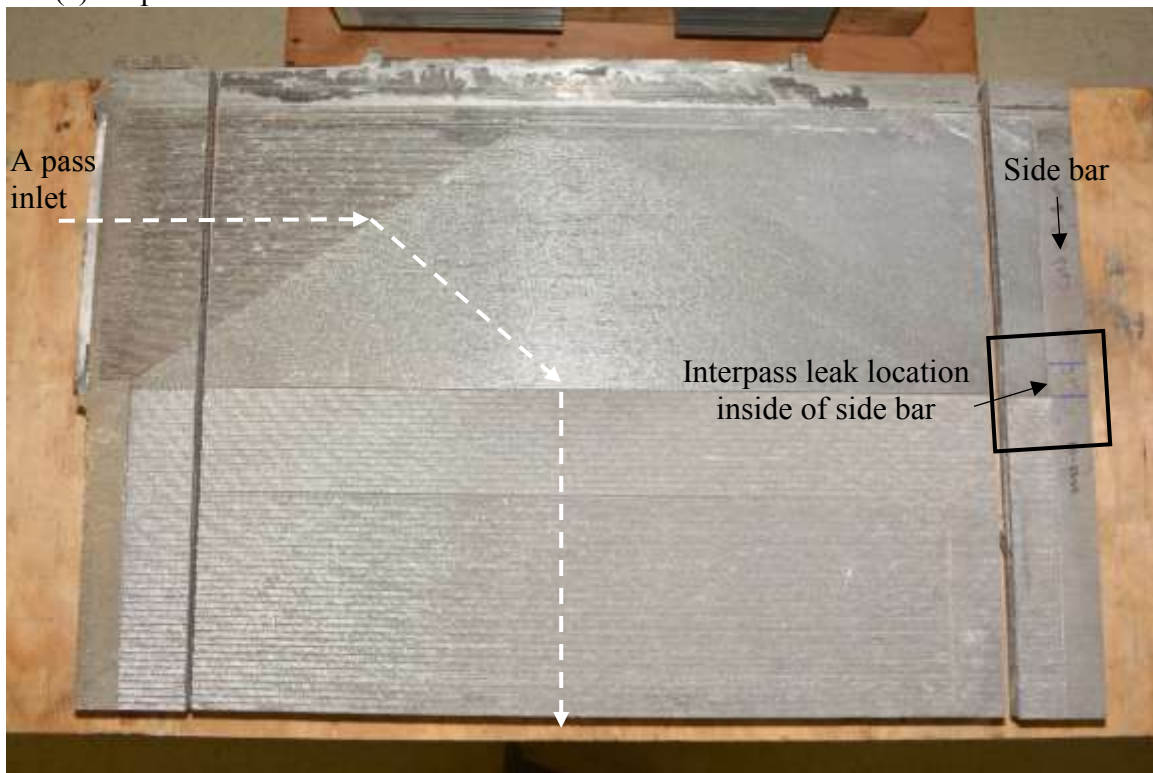


(b) Boxed region in (a)

Figure 51 Photograph of Boxed region in Figure 50a. Layer 1 to 2 internal leak location, indicated by arrows, was reported by the CSB to have been detected during leak testing prior to cutting the ACSR. Dashed lines in (b) indicate where the section shown in Figure 54 was cut.



(a) Cap sheet side



(b) Fin side

Figure 52 Photographs of sample S042-D1. In (a), the sample is shown after the attachment plate had been removed and a visible dye penetrant test had been performed on the cap sheet. In (b) the sample is viewed from the layer 2, A pass, fin side, and the A pass flow direction is indicated.

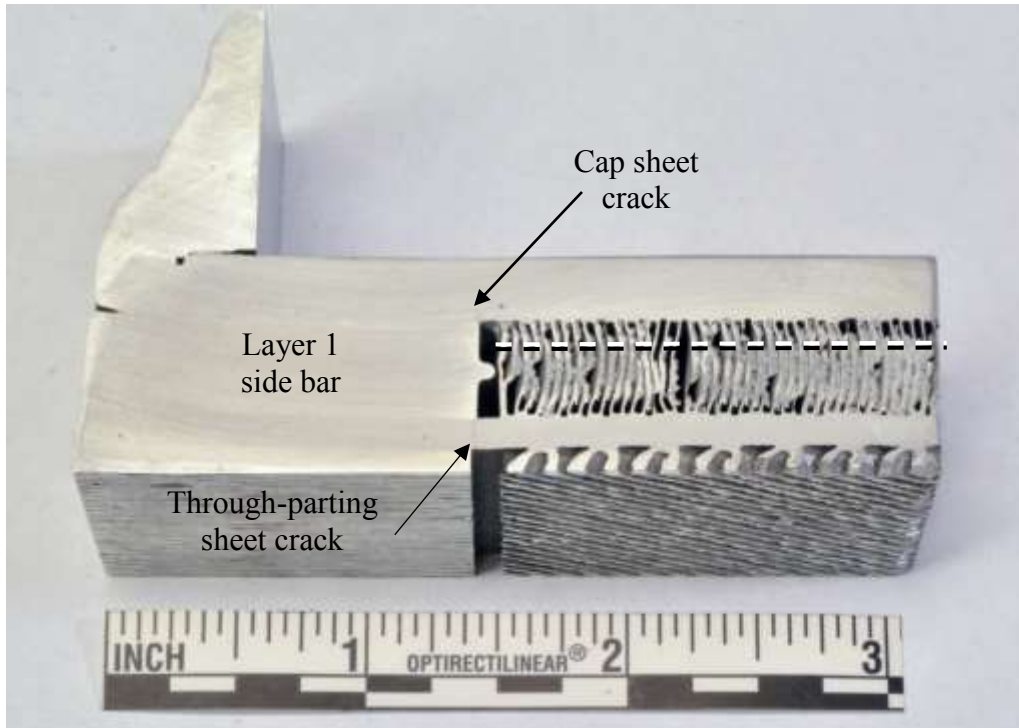


(a)

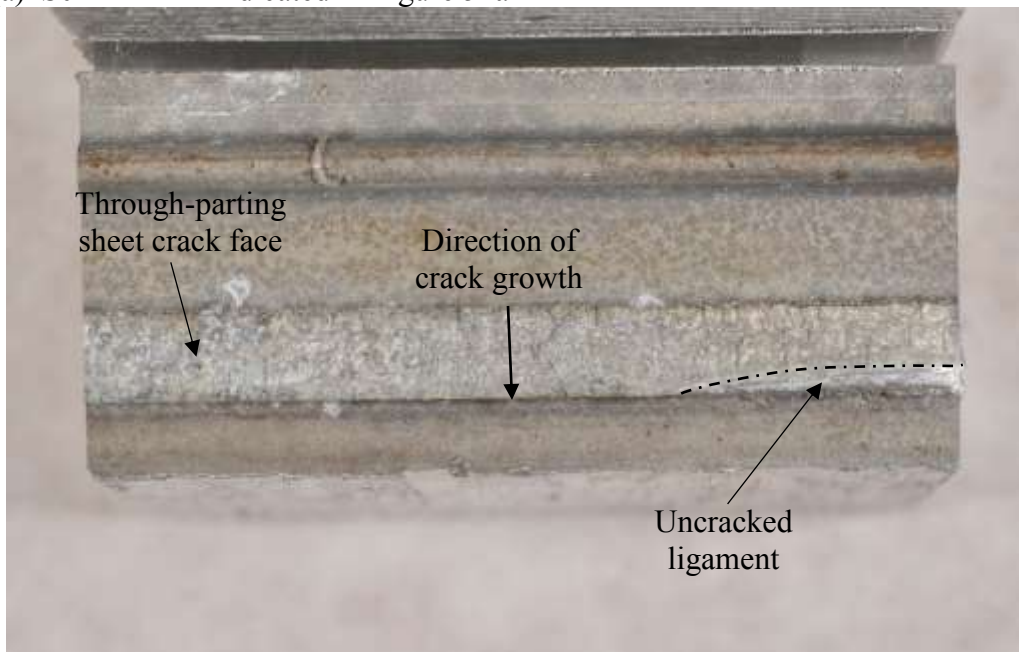


(b)

Figure 53 Images of the interpass crack between layers 1 and 2, viewed from the layer 2 side. Arrows point to the crack.

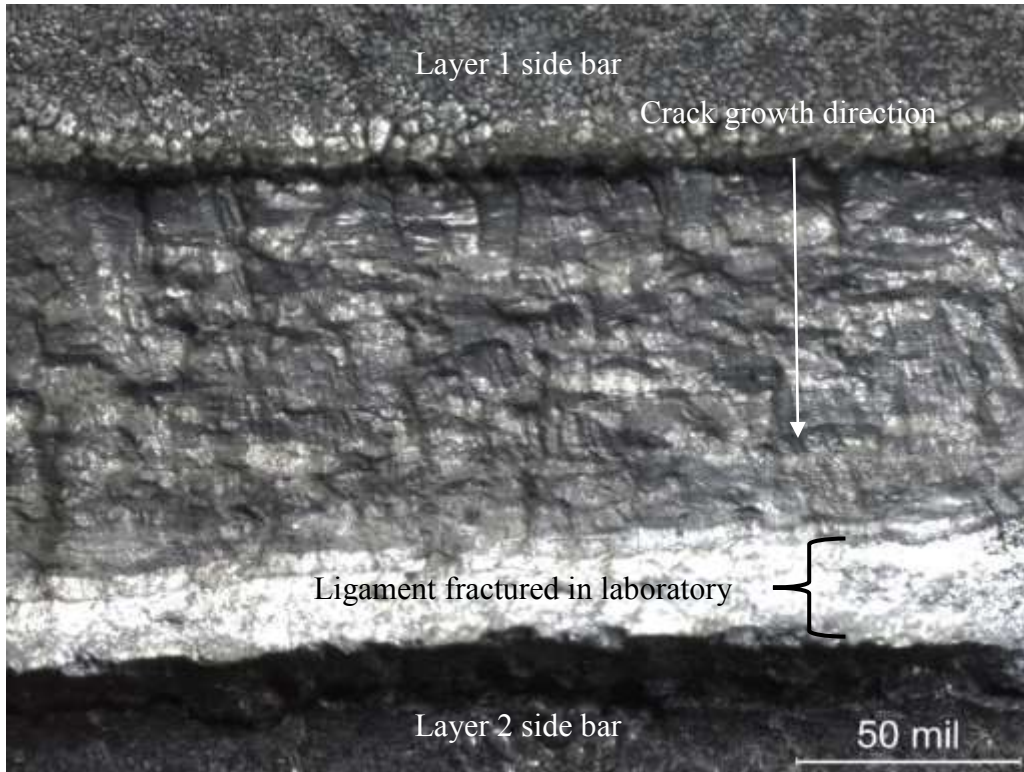


(a) S042-D1-1B indicated in Figure 52a

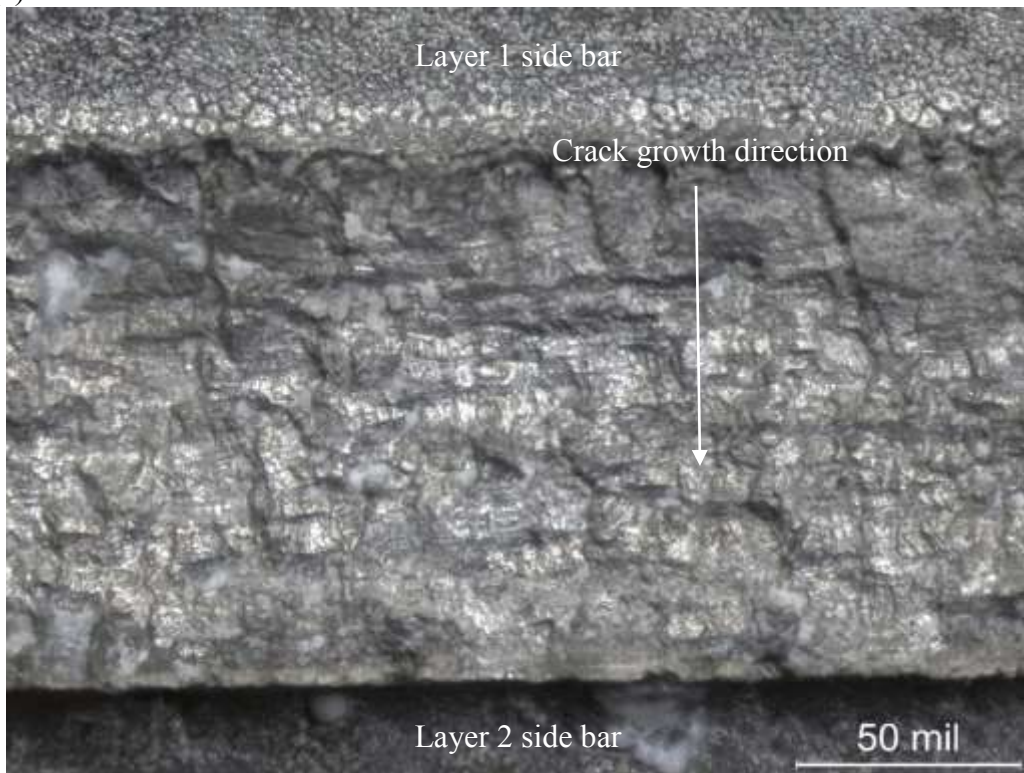


(b)

Figure 54 Photographs section S042-D1-1B, indicated in Figure 52a, through the interpass crack, and of the crack face. To expose the crack face, the layer 1 fins were cut along the dashed line in (a) and a small ligament of uncracked parting sheet was easily broken by hand. The cut location for this section is indicated in Figure 51b and Figure 52a.

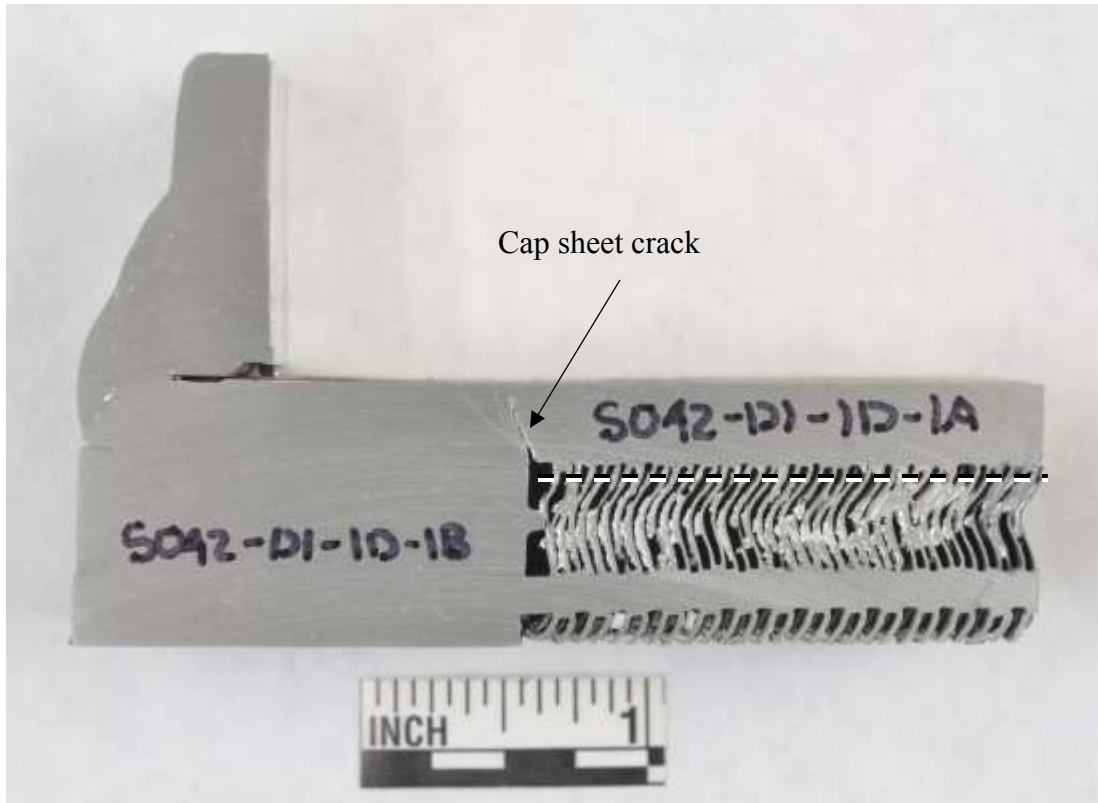


(a)

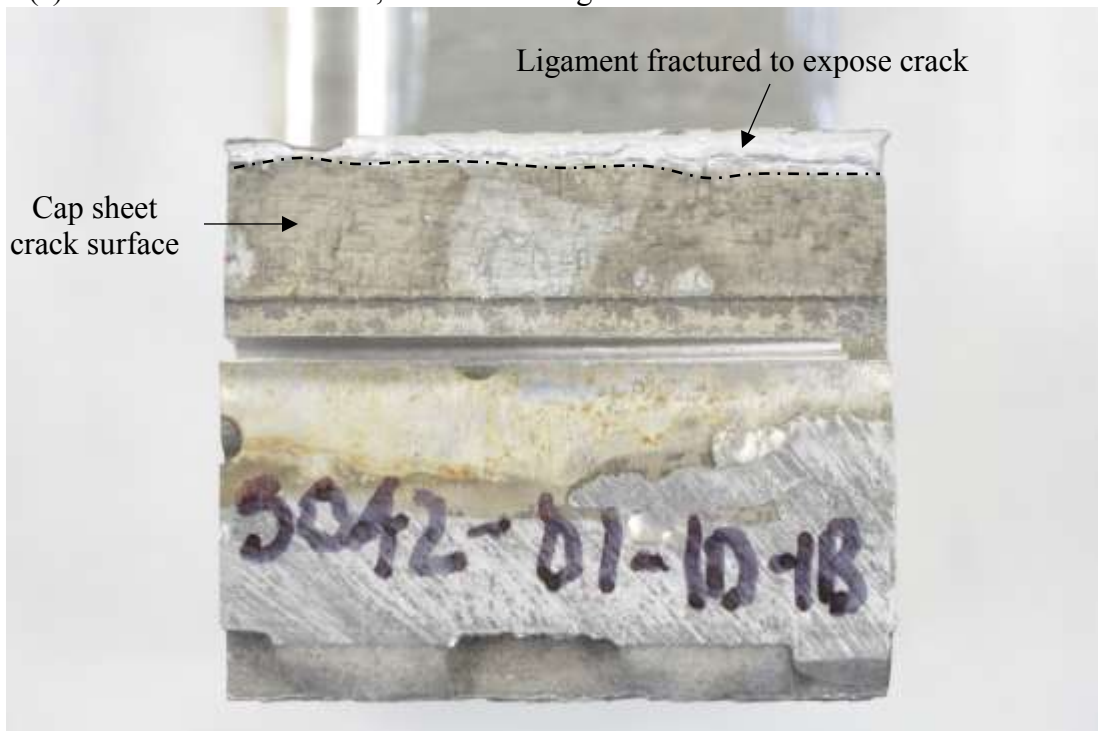


(b)

Figure 55 Images of the S042-D1-1B through-parting sheet crack face.

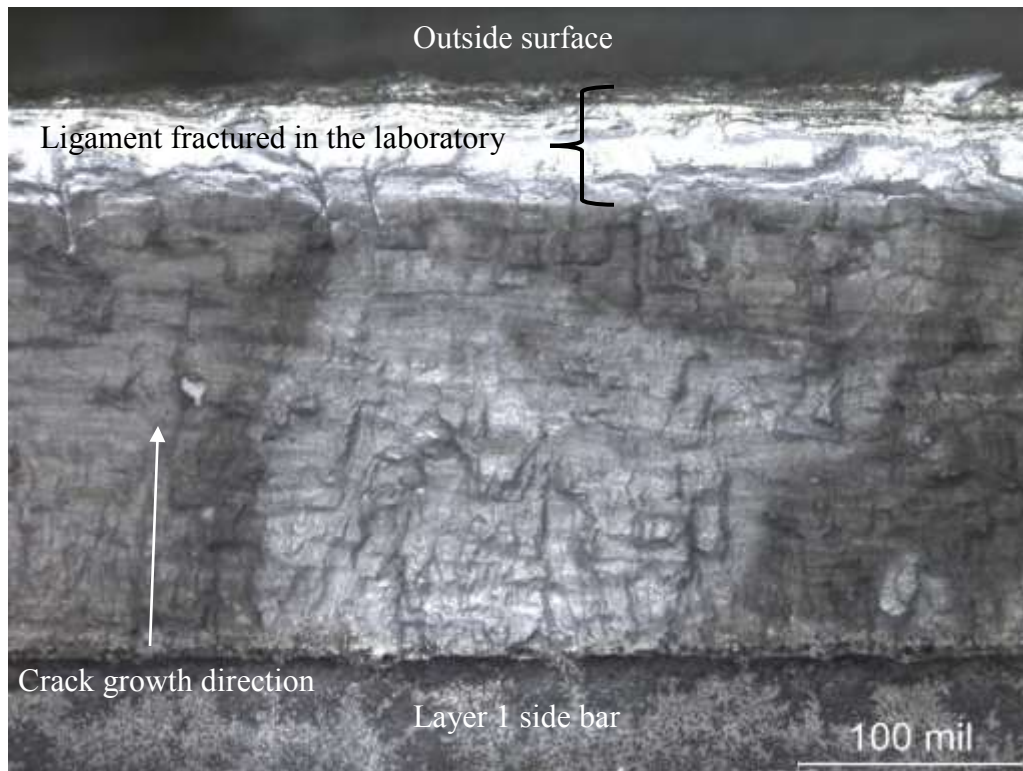


(a) Section S042-D1-1D-1, indicated in Figure 52a

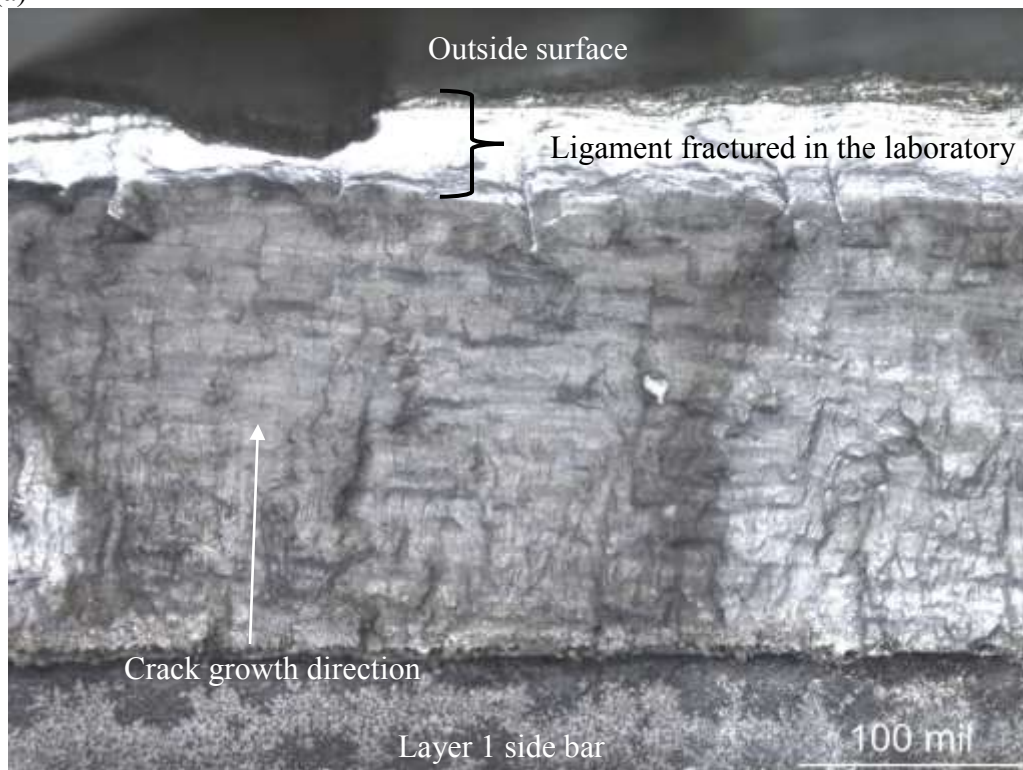


(b)

Figure 56 Photographs of Section S042-D1-1D-1, indicated in Figure 52a, and of the cap sheet crack surface in that section. Dashed line in (a) indicates where fins were cut to expose crack surface. Dashed line in (b) indicates the remaining cap sheet ligament broken by hand to expose the crack surfaces.

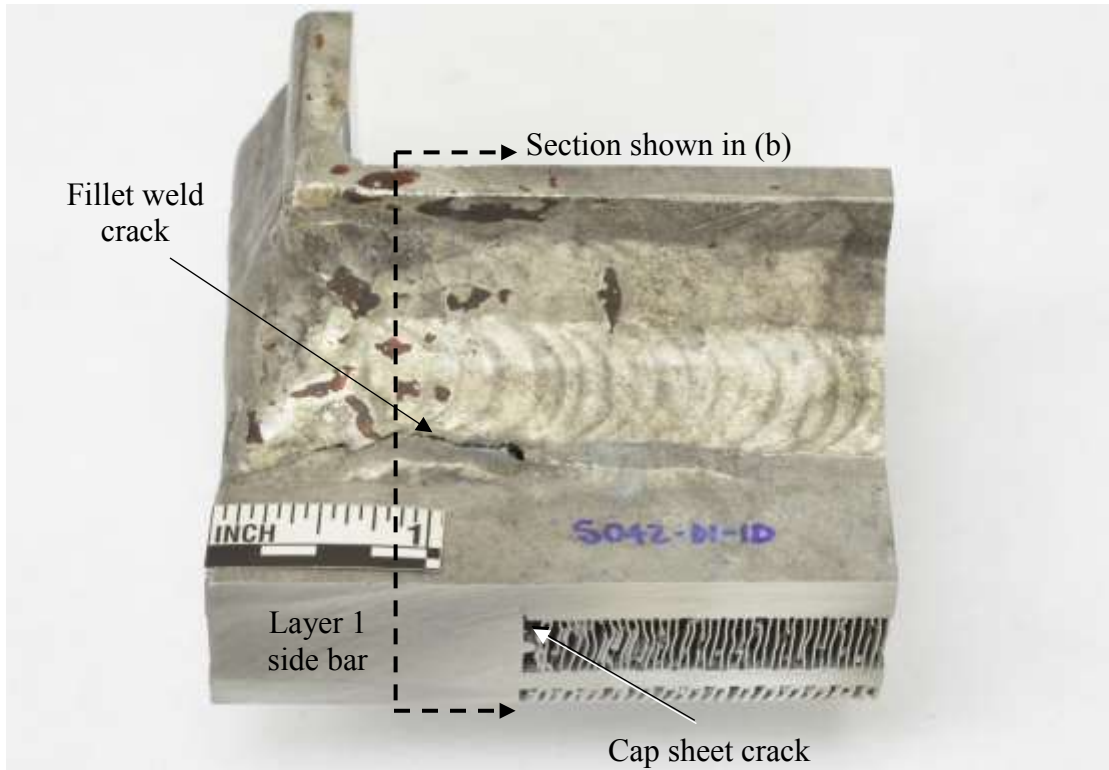


(a)

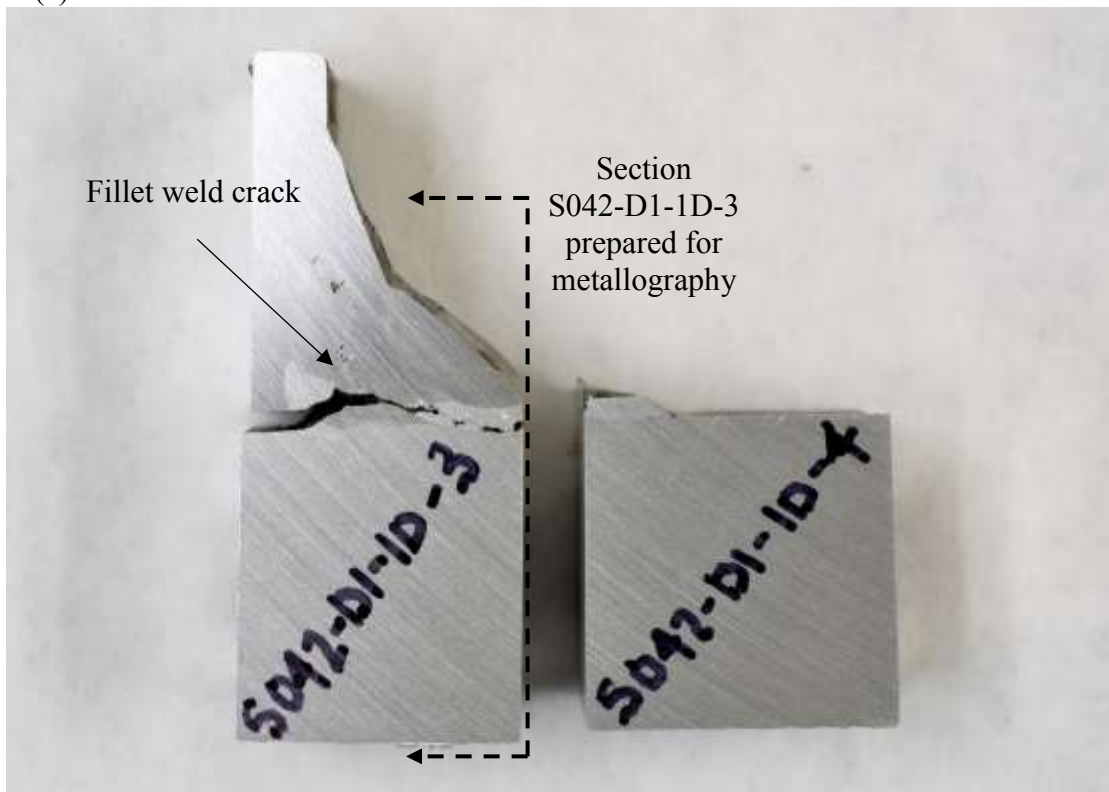


(b)

Figure 57 Images of the section S042-D1-D1-1 cap sheet crack surface.

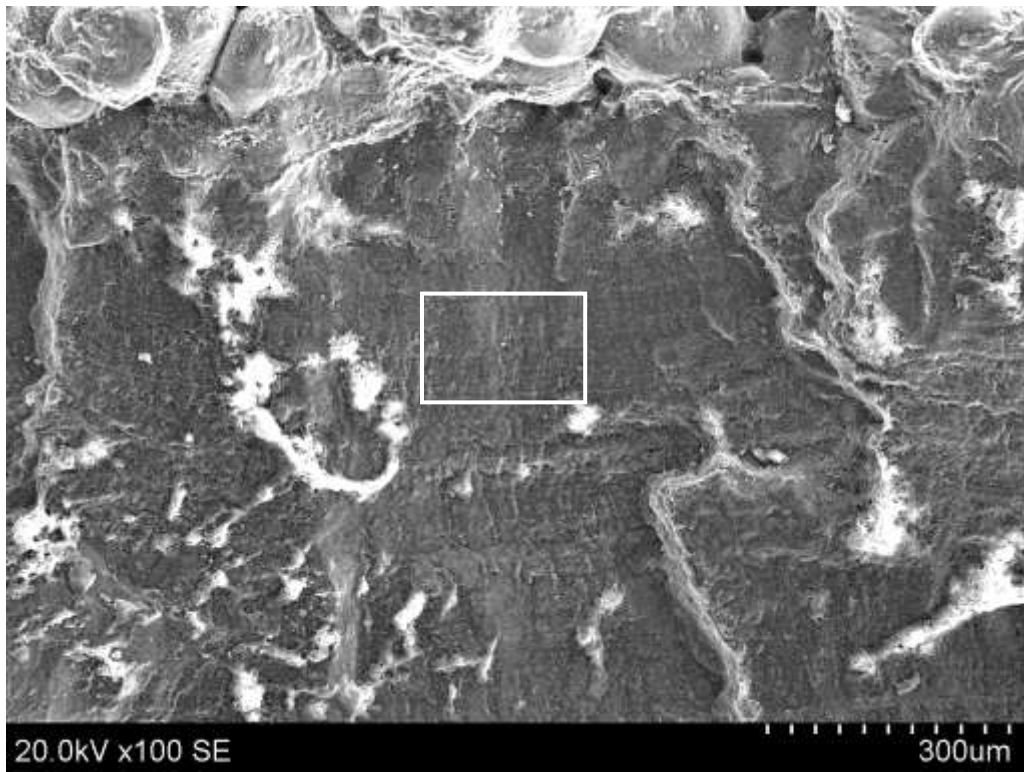


(a)

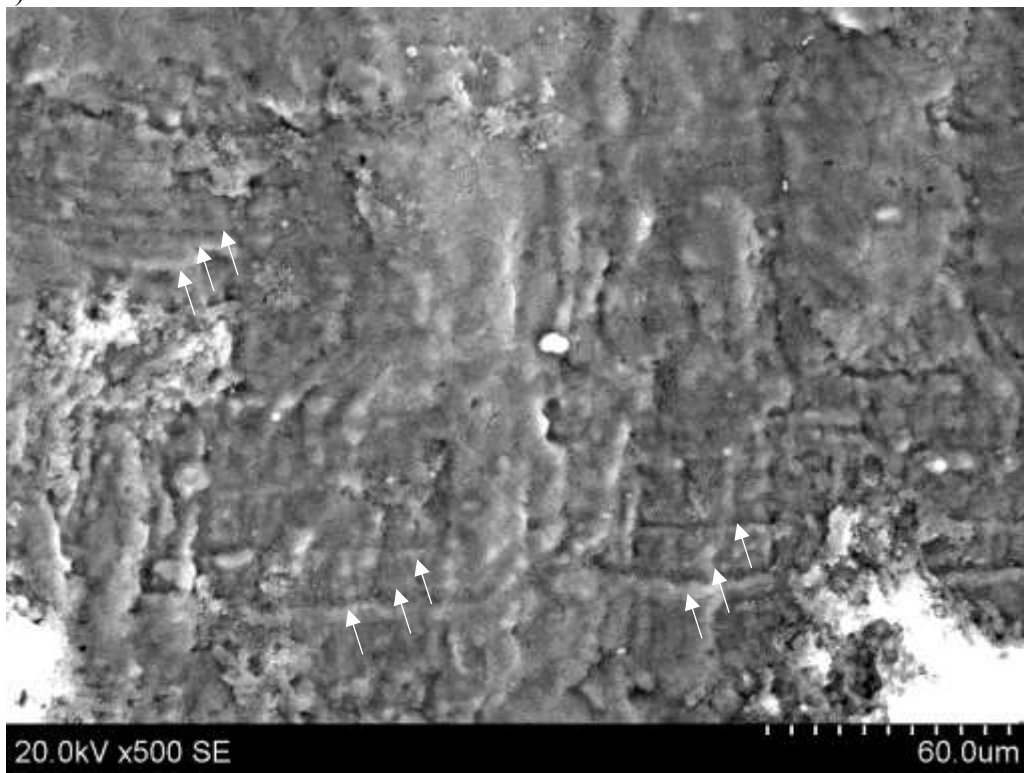


(b) Section indicated by dashed lines in (a)

Figure 58 Photographs of sections through the sample S042-D1 attachment plate corner. The location of section S042-D1-1D-3 is indicated in Figure 52a.

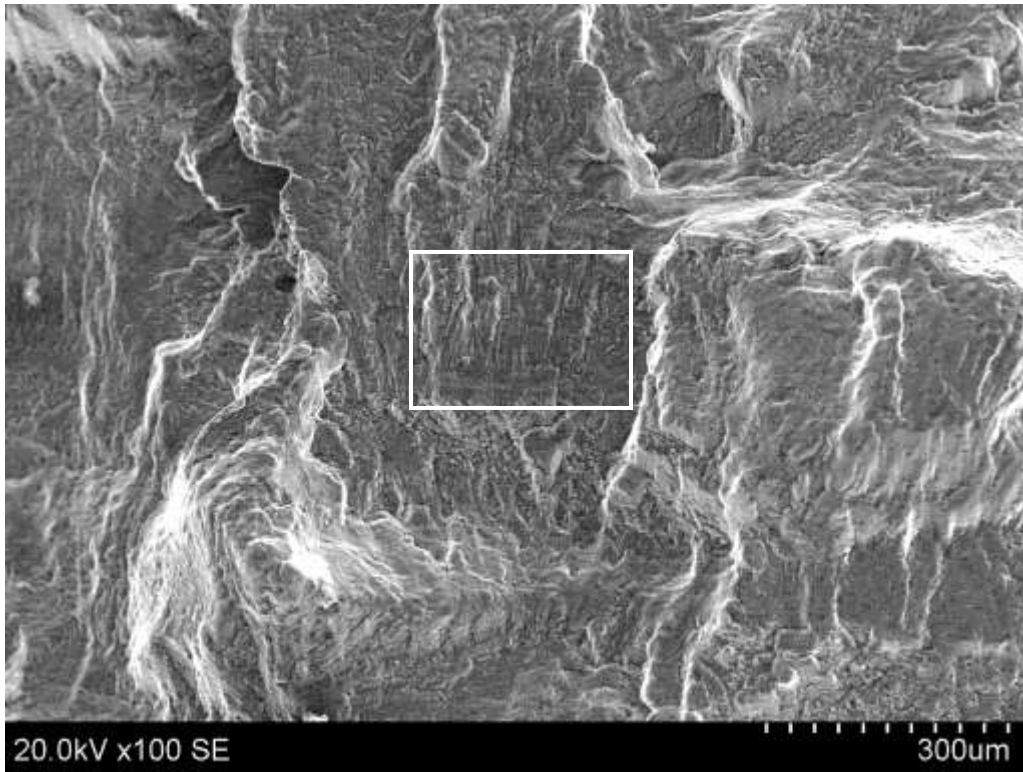


(a)

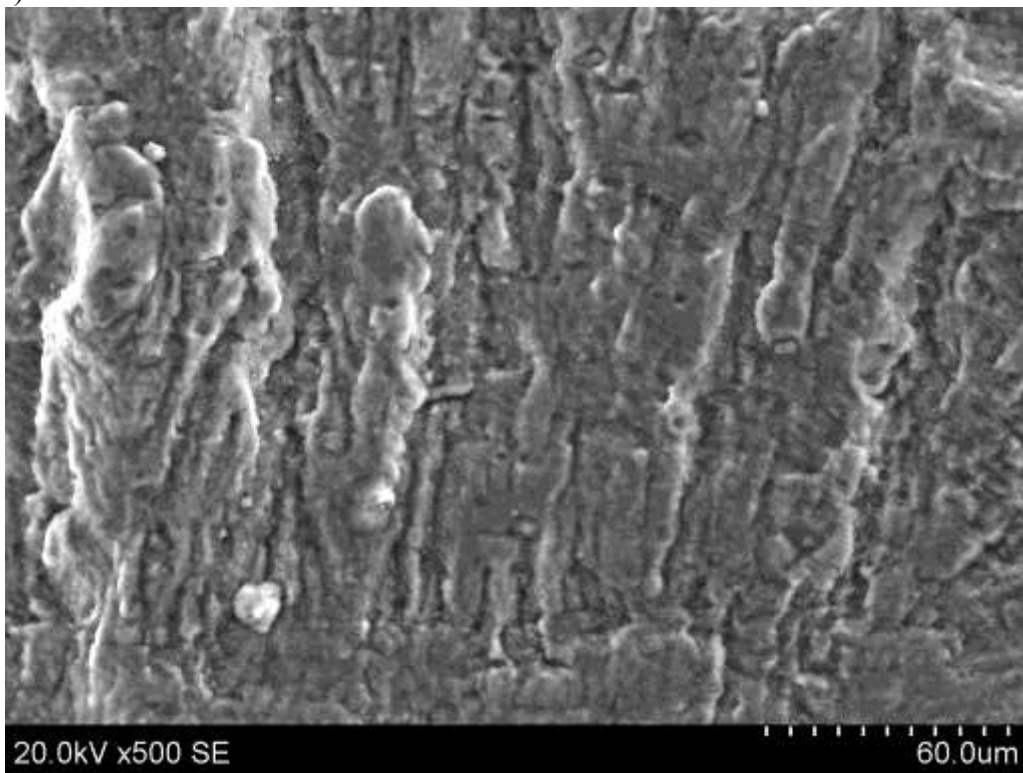


(b) Boxed region in (a)

Figure 59 SEM micrographs of the sample S042-D1 interpass leak parting sheet crack face. Arrows in (b) indicate oxidized fatigue striations.

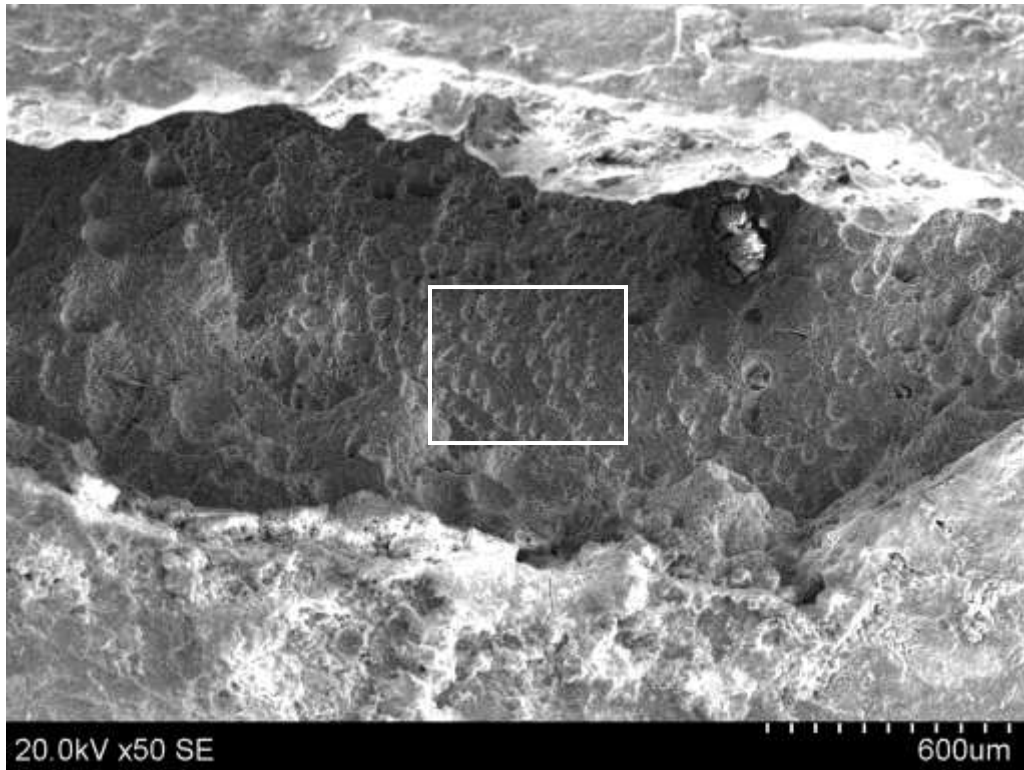


(a)

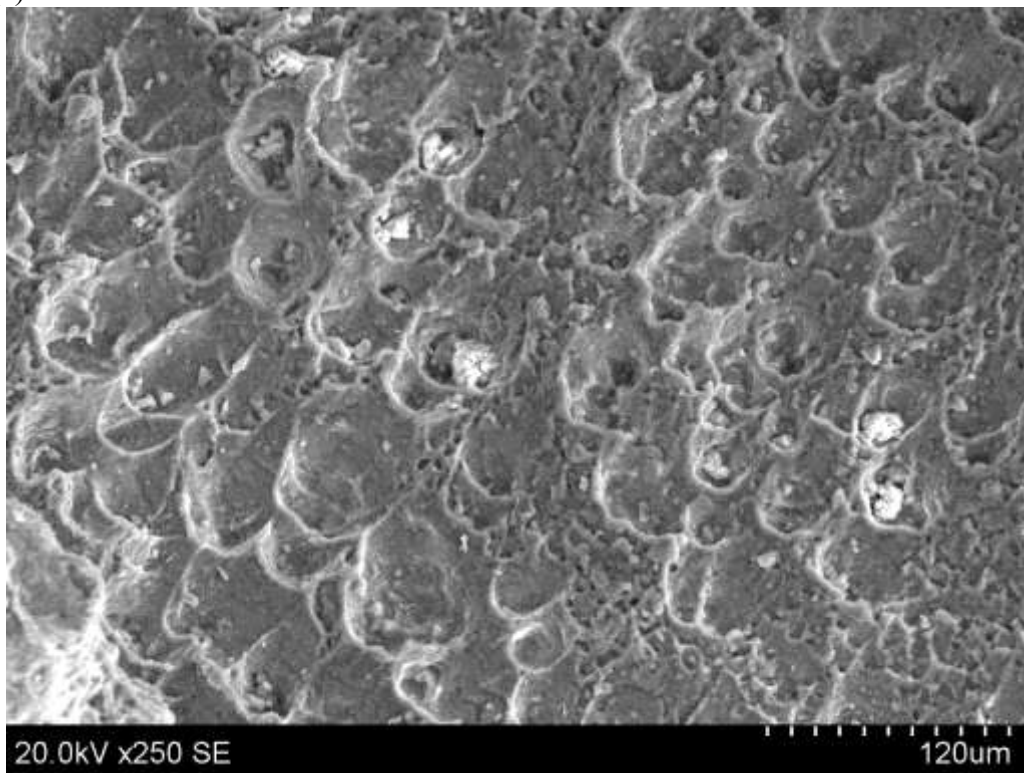


(b) Boxed region in (a)

Figure 60 SEM images of the cap sheet crack face.

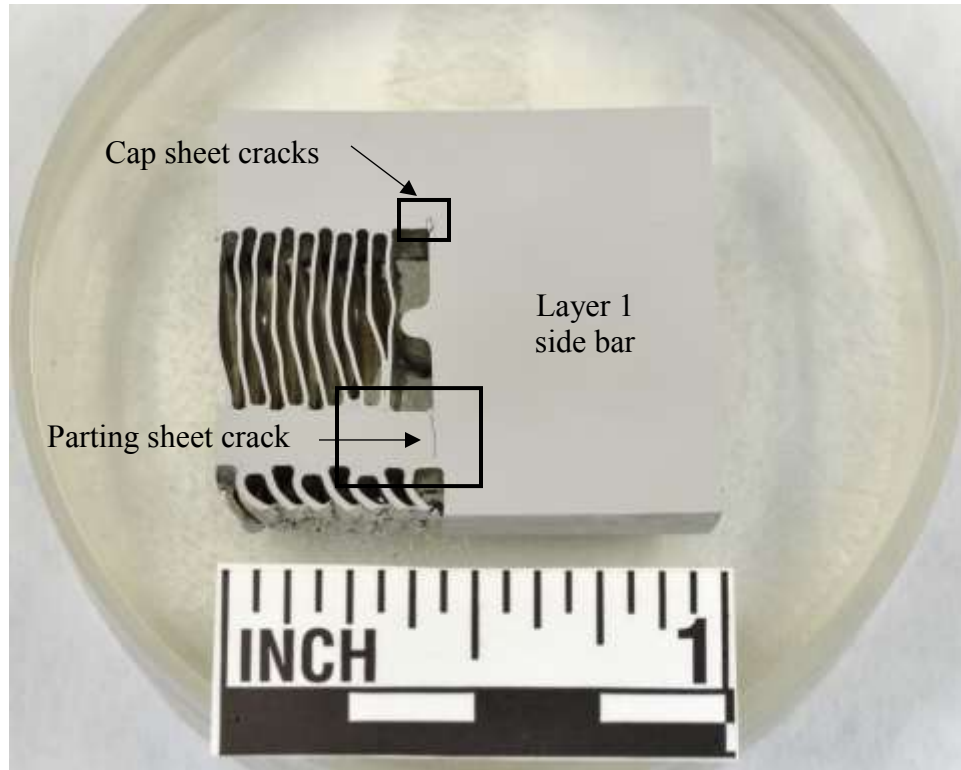


(a)

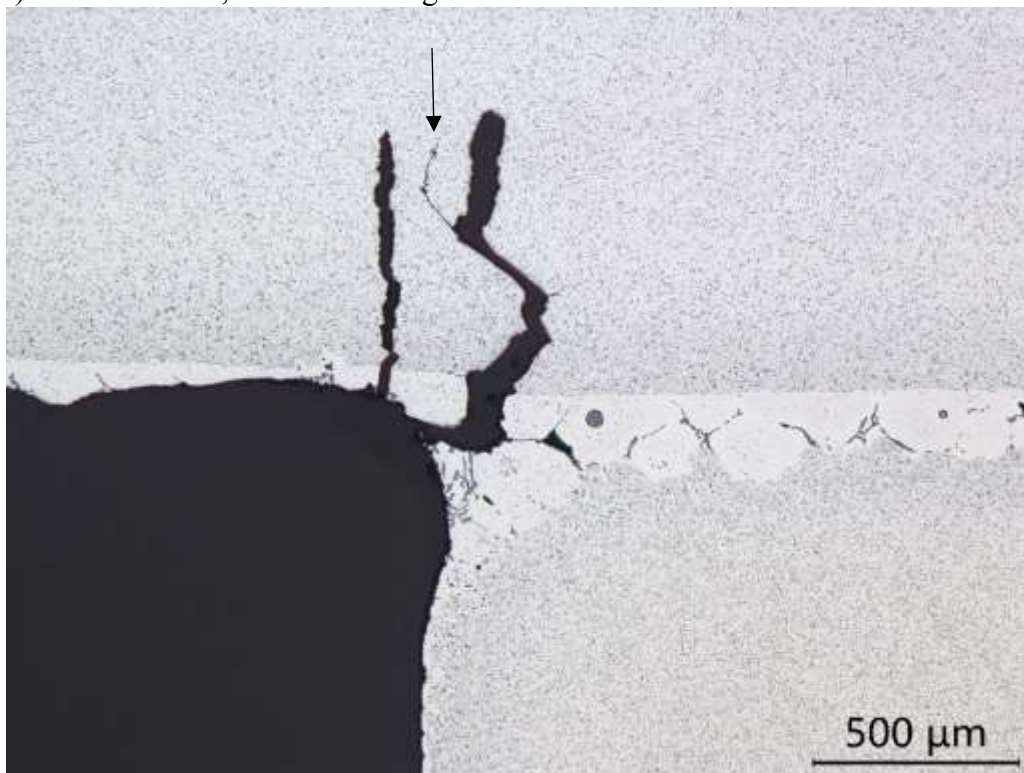


(b) Boxed region in (a)

Figure 61 SEM micrographs of the S042-D1 attachment plate fillet weld crack, taken through the open crack. Elongated dimples indicate ductile shear overload crack growth.

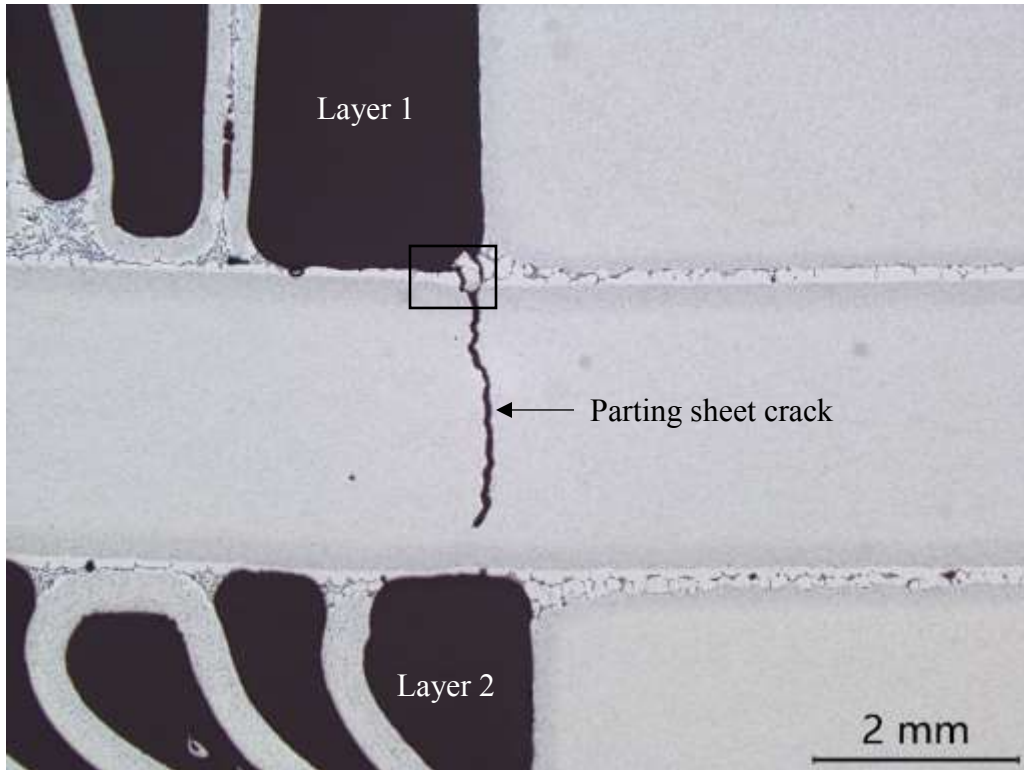


(a) S042-D1-1C1, indicated in Figure 52a



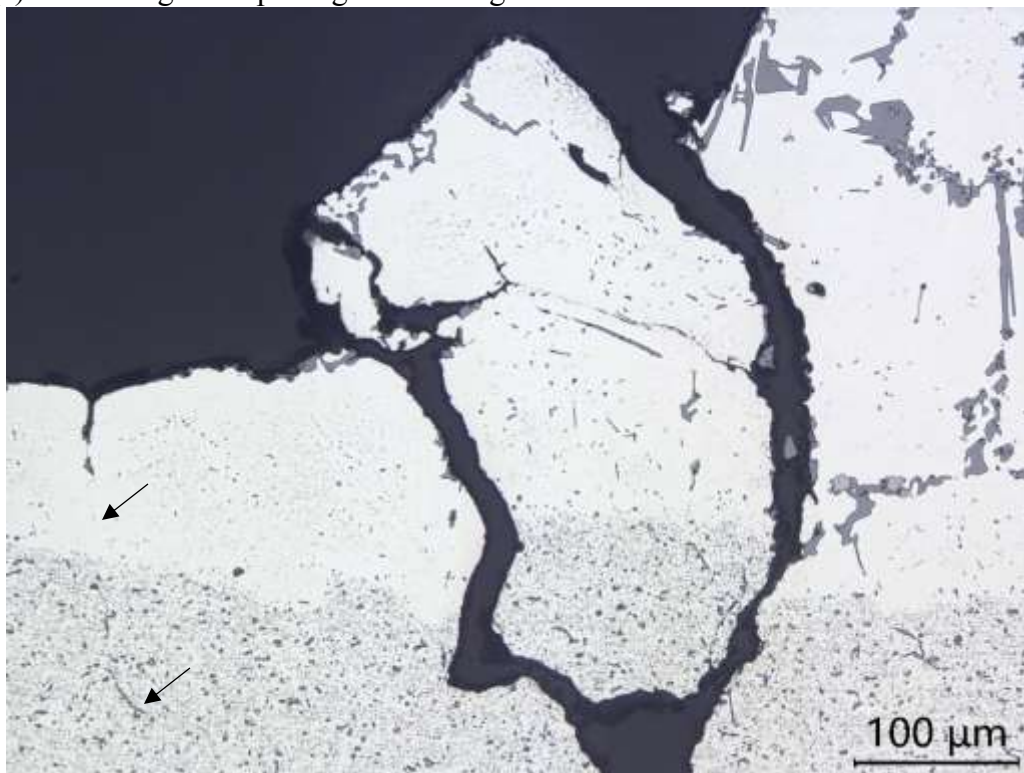
(b) 50X

Figure 62 Photograph and micrograph section S042-D1-1C1 cap sheet crack. In (b) the arrow points to a narrow crack that represents the condition of the other two cracks before they were blunted by plastic deformation.



(a) Boxed region of parting sheet in Figure 62a

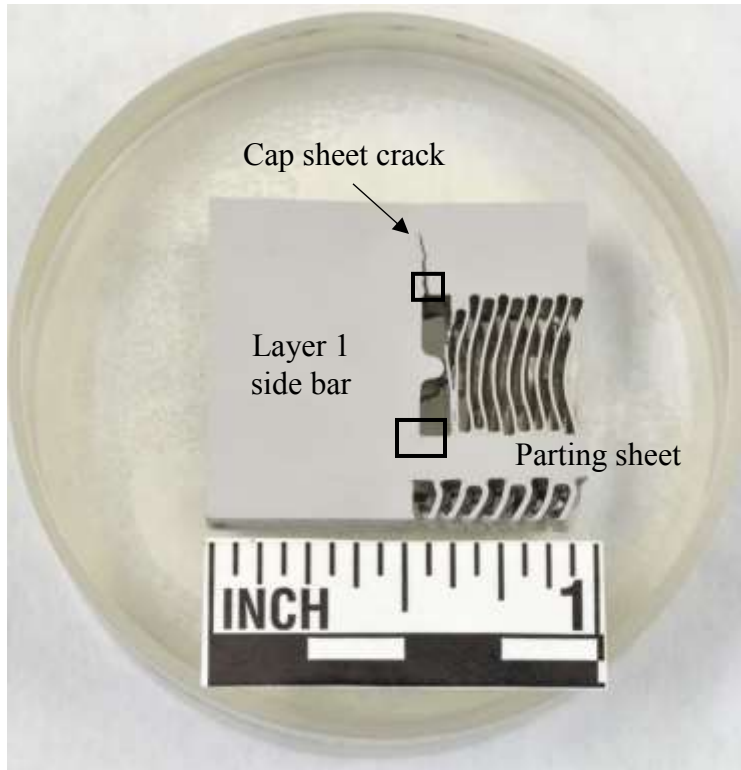
13X



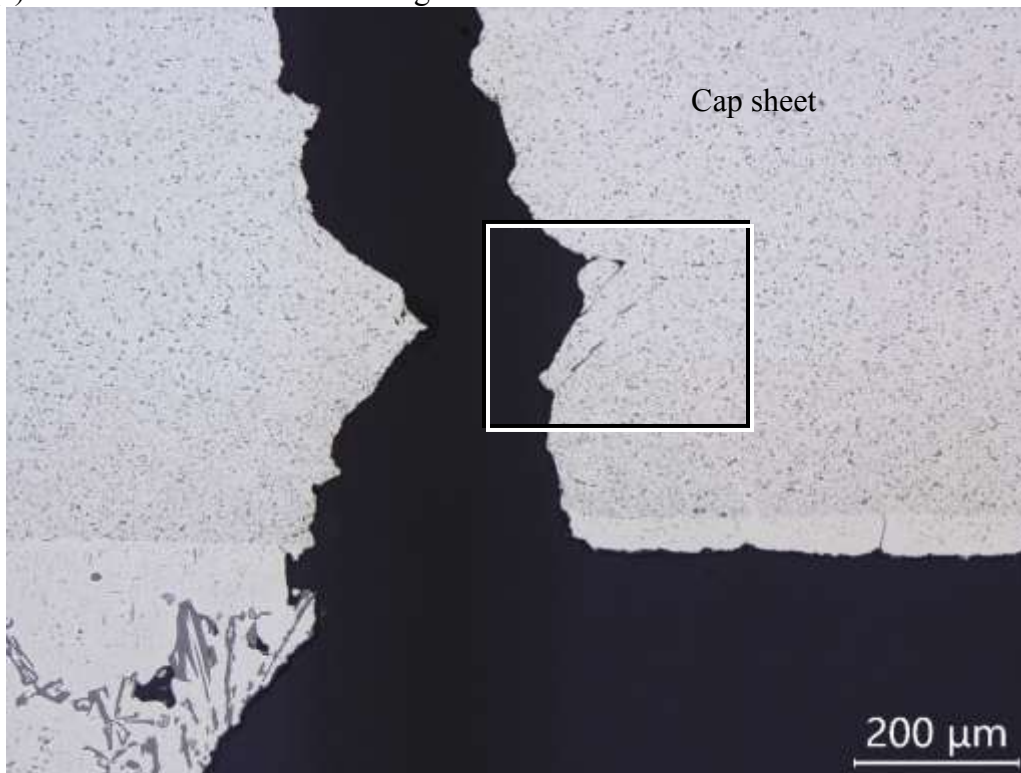
(b) Boxed region in (a)

200X

Figure 63 Optical micrographs of a layer 1 and 2 parting sheet crack, specimen S042-D1-1C1. In (b), arrows indicate a small, narrow crack next to the large blunted crack.



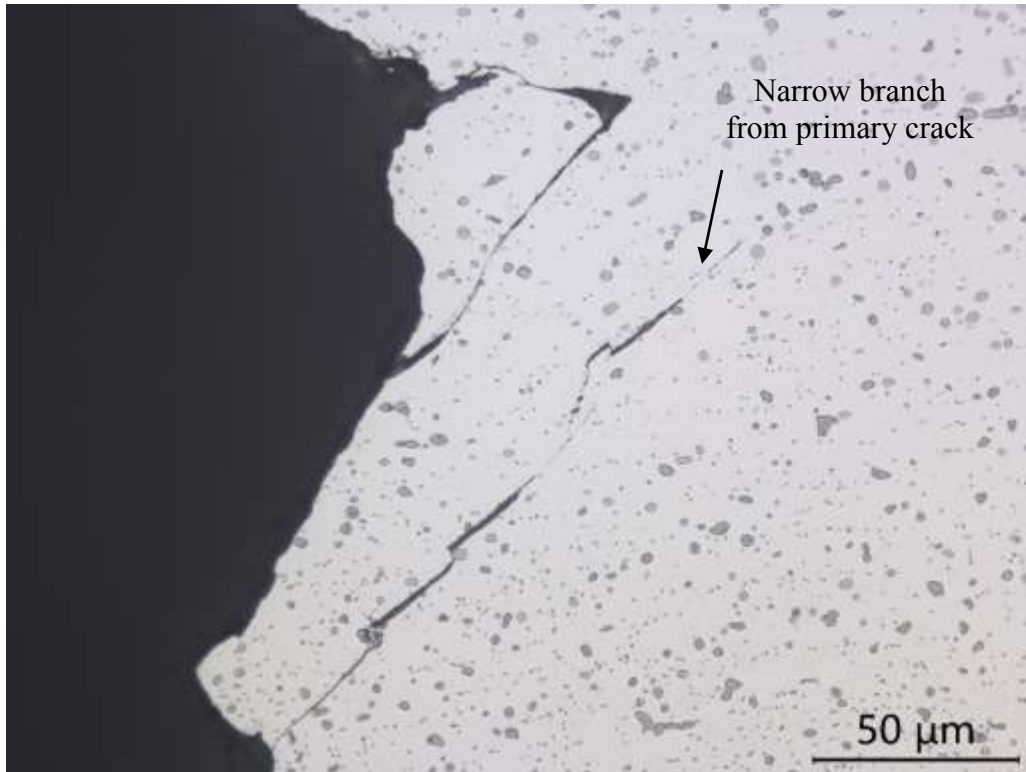
(a) S042-D1-1C2 indicated in Figure 52a



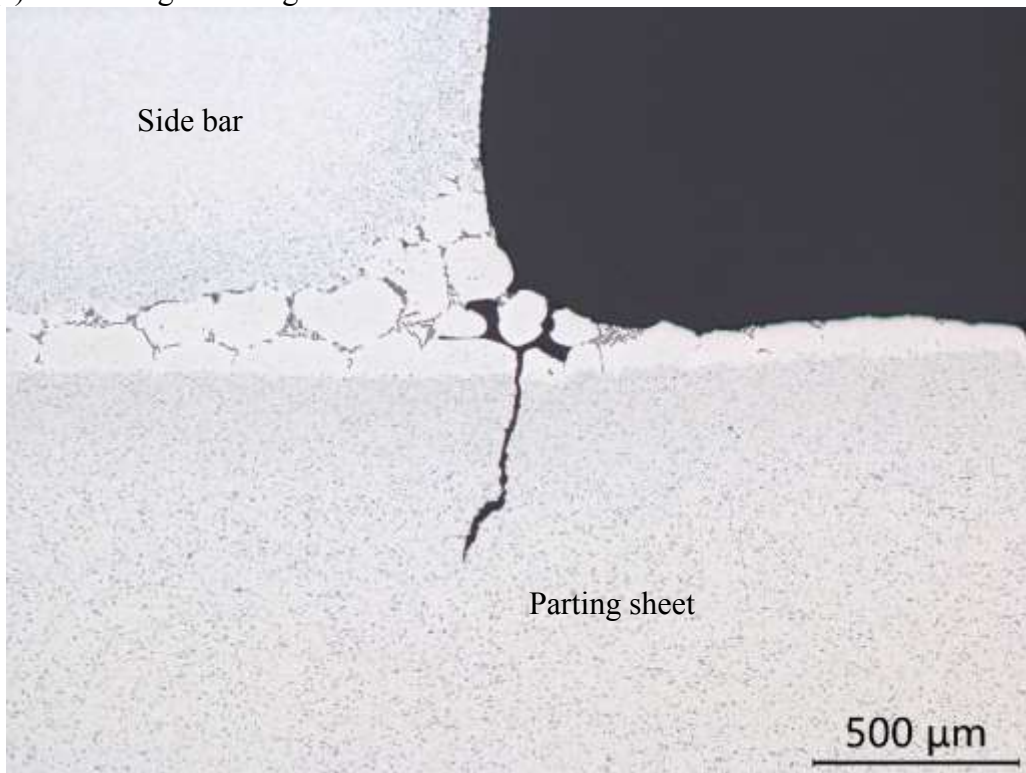
(b) Boxed region of cap sheet crack in (a)

100X

Figure 64 Photograph and micrograph section S042-D1-1C2 indicated in Figure 52a. The cap sheet crack initiated on the inside of the cap sheet and the parting sheet crack initiated on the layer 1 side of the parting sheet.

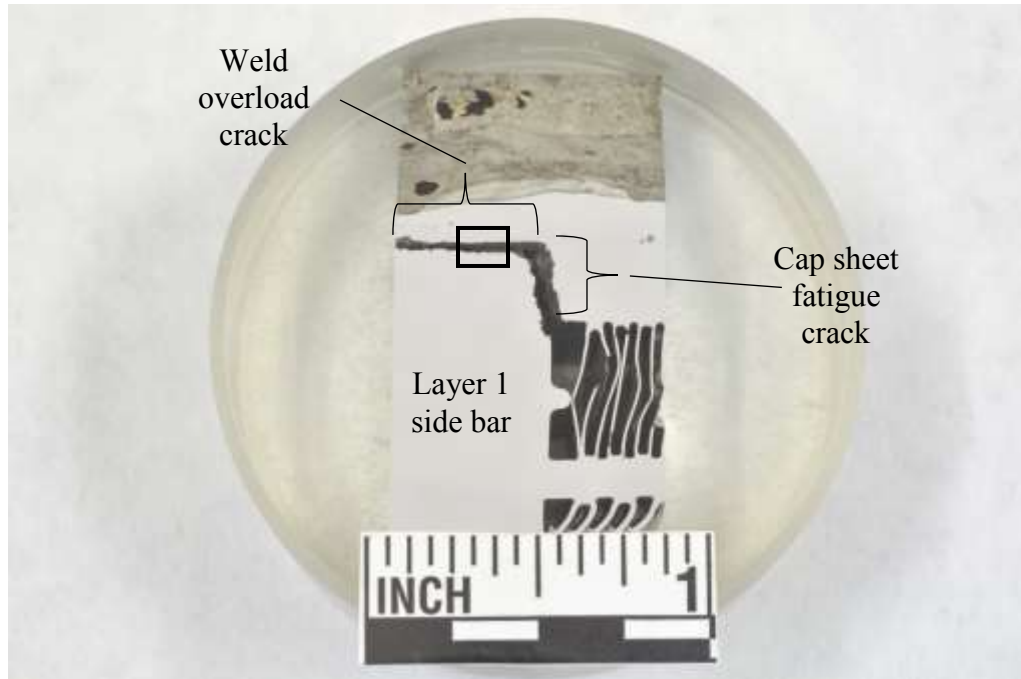


(a) Boxed region in Figure 64b 500X

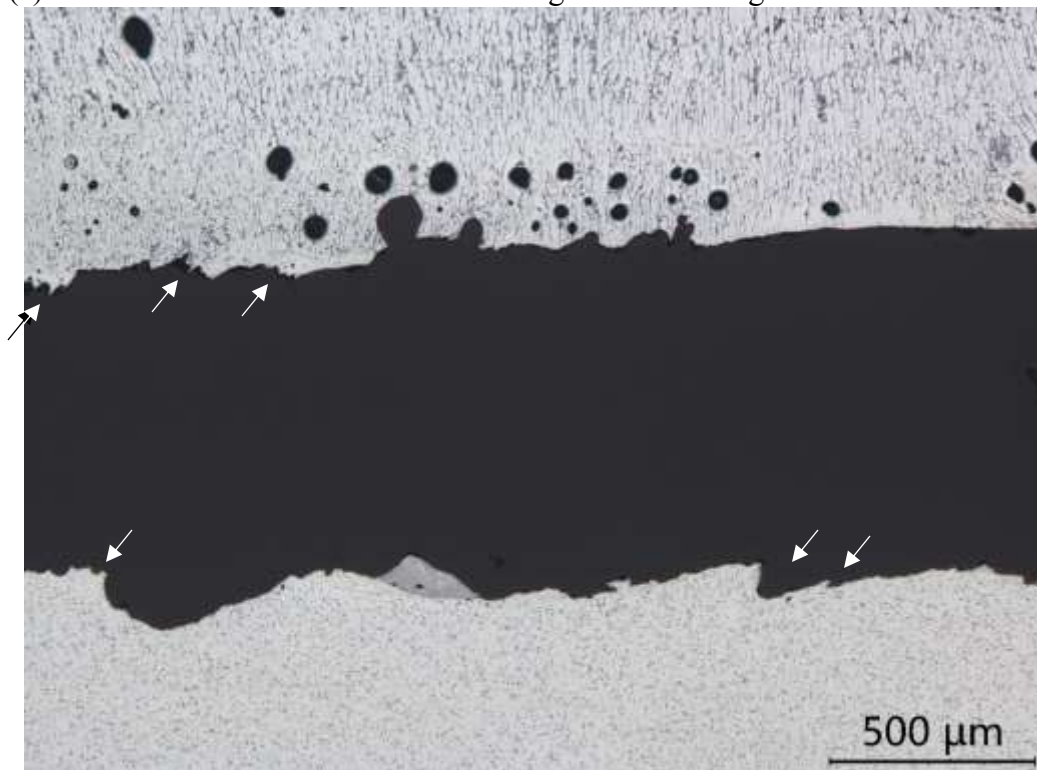


(b) Boxed region of parting sheet in Figure 64a 50X

Figure 65 Micrographs of the section shown in Figure 64a.



(a) Section S042-D1-1D-3 indicated in Figure 52a and Figure 58b



(b) Boxed region in (a) 50X

Figure 66 Photograph and micrograph section S042-D1-1D-3, cap sheet crack and attachment plate fillet weld crack. Section indicated in Figure 52a and Figure 58b.



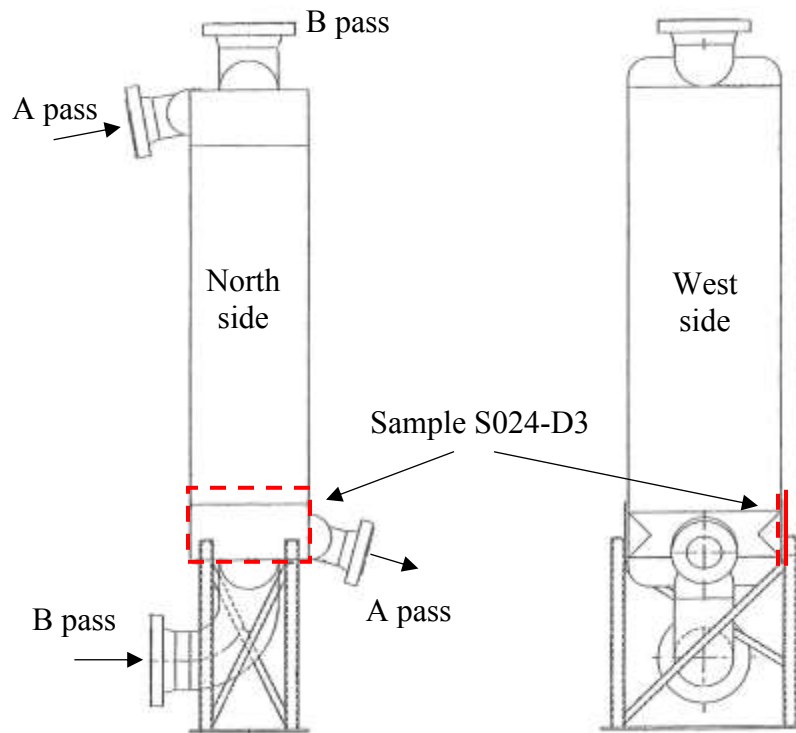
### **3.13. ACSR Sample S042-D3 Visual Examination**

Sample S042-D3 was cut from the ACSR bottom, south side. The sample spanned the full width of the reboiler, extended from the level of the B inlet header welds to above the attachment plate, and included layer 1 and the parting sheet between layer 1 and 2. A drawing with the location of the sample indicated and a photograph of the sample are shown in Figure 67.

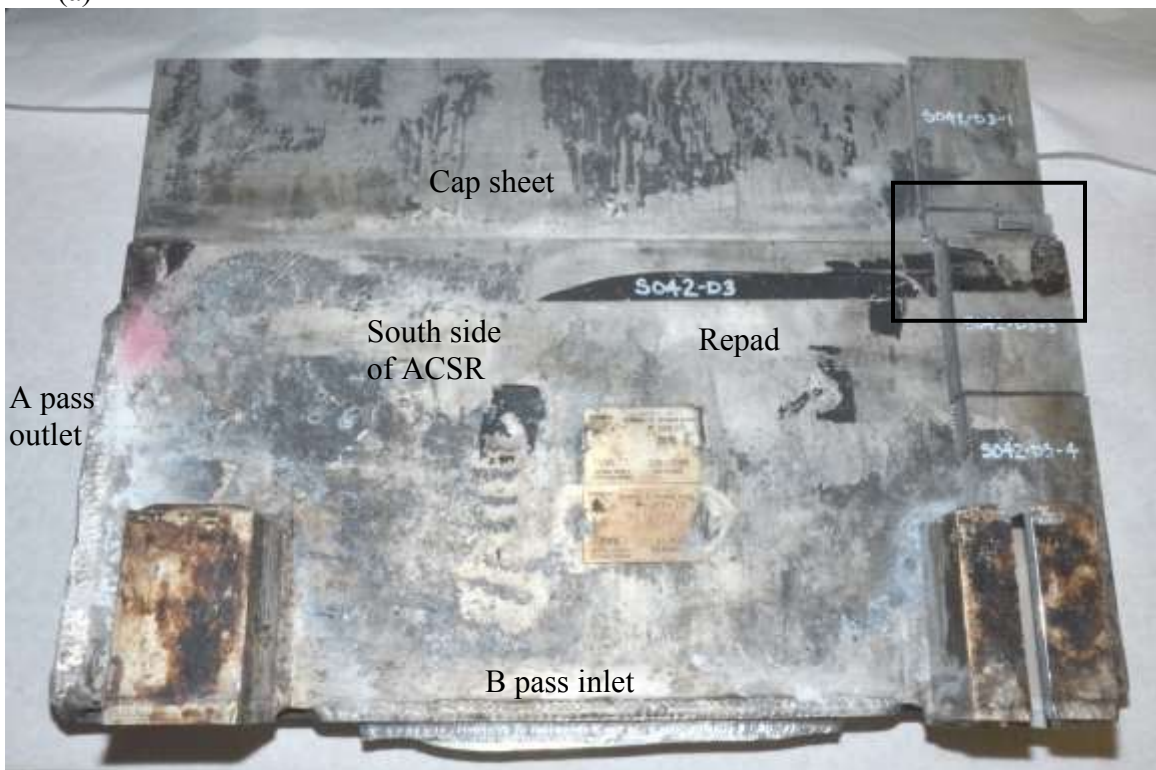
A depression was visible in the cap sheet at the upper east corner of the attachment plate. In the other samples, similar depressions were found to be associated with cap sheet fatigue cracks that initiated on the inside surface in the corner formed by the side bar. The sample was cut through the depression, resulting in section S042-D3-2 indicated in Figure 68a. The attachment plate was removed from this region by cutting near the edge with a circular saw. No cracks in the cap sheet under the attachment plate or in the depression above the attachment plate were detected.

### **3.14. ACSR Sample S042-D3 Metallography**

Section S042-D3-2, indicated in Figure 68a, was prepared for metallography using the same techniques as described in previous sections of this report. A photograph and micrographs of the section are shown in Figure 69 and Figure 70. A short, wide crack that had initiated on the inside surface of the cap sheet was present under the depression visible on the outside surface. A shorter, narrow crack was present next to the larger wide crack. Based on the examination of other similar crack faces, the two cracks initiated and grew by fatigue. The narrow crack indicates the two cracks initiated at the same general time, but the larger crack grew faster, eventually shielding the smaller crack from cyclic stresses. When a large strain/stress event occurred, likely caused by the fire, the longer crack blunted, but because the smaller crack was shielded by the larger crack, it remained narrow. Therefore, the smaller crack represents the typical width of fatigue cracks that grew in the ACSR during normal service conditions.



(a)



(b)

Figure 67 Simplified drawing of the ACSR annotated with the location of sample S042-D3, and a photograph of the sample.

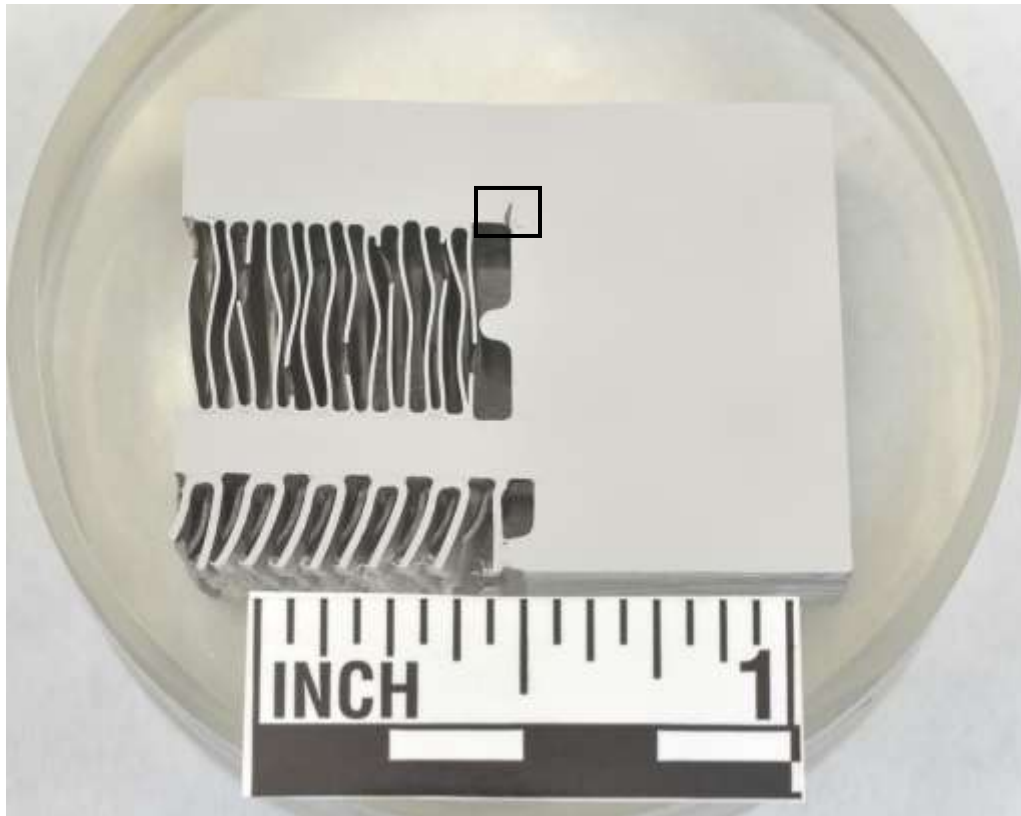


(a) Boxed region in Figure 67b

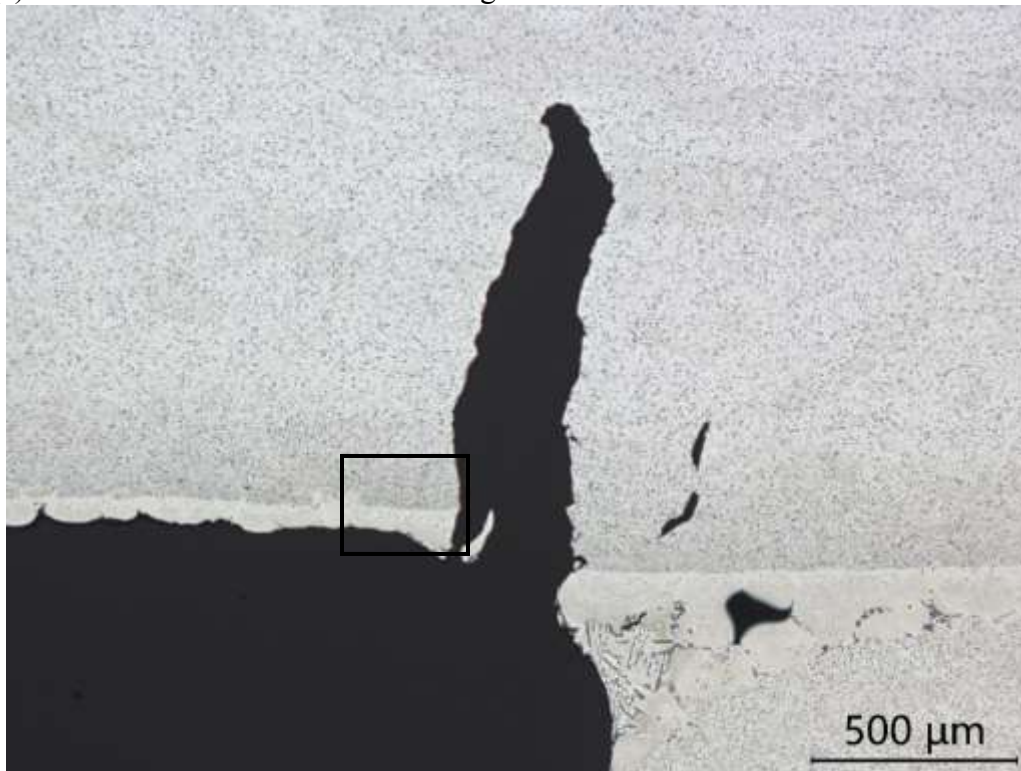


(b) Attachment plate removed from corner

Figure 68 Photographs of the sectioned corner of sample S042-D3.



(a) Section S042-D3-2 indicated in Figure 68a



(b) Boxed region in (a)

50X

Figure 69 Photograph of section S042-D3-2 indicated in Figure 68a, prepared for metallography and micrograph of a cap sheet crack in the section.



Figure 70 Micrograph of a narrow crack next to the larger wide crack in the section S042-D3-2, from the boxed region in Figure 69b. Arrows indicate the crack.



#### 4. DISCUSSION

Visual examination and metallography indicated fire damage in the form of localized melting and partial melting of the B pass inlet nozzle, B pass inlet header, and sample S042-C. If a pressure boundary breach in these regions had preceded the fire, evidence of such a breach was destroyed by the fire.

Thermal stresses are a recognized concern and recognized cause of failure in brazed aluminum plate-fin heat exchangers such as the ACSR.<sup>3</sup> Much of the discussion about thermal stresses involves temperature fluctuations that cause thermal stresses which exceed the yield strength or tensile strength of exchanger components. However, the recognition of both thermal stresses and temperature fluctuations in these exchangers means that thermal fatigue is a potential degradation mechanism. The presence of fatigue cracks in the subject ACSR confirms that thermal fatigue can compromise the pressure boundary of brazed aluminum plate-fin heat exchangers.

Fatigue, whether driven by applied loads or temperature fluctuations, is commonly divided into high-cycle or low-cycle regimes. High-cycle fatigue is often described as occurring over greater than  $10^4$  cycles and low-cycle fatigue occurs below  $10^4$  cycles. The demarcation of  $10^4$  cycles is arbitrary. A more accurate distinction is that high-cycle fatigue occurs under conditions of predominantly elastic loading while low-cycle fatigue occurs under conditions of cyclic stresses that generate significant plastic strain. Furthermore, high-cycle fatigue failure is dominated by the time required to initiate a growing fatigue crack, rather than the number of cycles required to advance a growing crack.

Based on SEM examination of the ACSR fatigue cracks during this evaluation, the crack surface morphology, which includes the spacing of visible fatigue striation remnants, suggests that most of the crack growth occurred in the lower frequency range of high-cycle fatigue. The metallographic evidence of narrow small cracks and crack branches supports the conclusion that high-cycle fatigue dominated the crack growth and, therefore, likely dominated the initiation stage of fatigue.

One relevant question regarding the findings of this evaluation is whether fewer high amplitude thermal cycles or more frequent low-amplitude thermal cycles dominated the thermal fatigue life. The combination of low-amplitude and high-amplitude cycles is referred to as variable amplitude loading and has been studied extensively in laboratory conditions. One consistent result of variable amplitude loading tests is that higher amplitude events leave progression marks on the surface and often retard the crack growth rate immediately after the event. The cracks examined during this evaluation had progression marks indicative of higher stress amplitude events, separated by regions of relatively uniform fatigue striation spacing, indicative of lower amplitude higher frequency fatigue cycles. Unfortunately, thick oxide that likely grew on the cracks during the fire, destroyed fine details of the crack surfaces. Consequently, we can conclude that variable amplitude thermal stresses contributed to the fatigue crack growth, we do not have a good record that indicates the low-amplitude range of the thermal stresses which caused crack growth.

---

<sup>3</sup> ALPEMA, The Standards of the Brazed Aluminum Plate-Fin Heat Exchanger Manufacturers' Association, 2010, [www.alpema.org](http://www.alpema.org).



## 5. CONCLUSIONS

The following conclusions are based upon the submitted samples and the evidence gathered:

1. Evidence of a pressure boundary breach that could have led to the fire was destroyed by melting and partial melting on the north side of the ACSR, B pass inlet header, and B pass nozzle.
2. Fatigue cracks were found in the cap sheets of three samples, S042-B, S042-D1, and S042-D3.
3. One of the cap sheet cracks had propagated through the sheet, but may not have presented a leak path until the fire caused enough thermal strain to rupture the final ligament. This crack was located under the attachment plate on the south side, at the top of the ACSR.
4. Fatigue cracks were found in parting sheets of samples S042-B and S042-D1. In sample S042-B, cracks were found in parting sheets between layers 99 and 98, and between layers 98 and 97. Both of these parting sheet cracks were located below the through-cap sheet crack.
5. A through-parting sheet crack presented an interpass leak path between layers 99 and 98 in sample S042-B.

---

Prepared by:

A handwritten signature in black ink that reads "SMF" followed by a long horizontal stroke.

---

Sam McFadden, Ph. D.  
Associate Director of Laboratories

---

Reviewed by:

A handwritten signature in black ink that reads "Audrey A Fasching" in a cursive style.

---

Audrey A. Fasching, Ph.D., P.E.  
Senior Materials Engineer